Structural and functional studies concerning human N-acetyl mannosamine kinase

Dissertation zur Erlangung des akademischen Grades

Doktor der Naturwissenschaften (Dr. rer. nat)

Eingereicht im Fachbereich Biologie, Chemie, Pharmazie der Freien Universität Berlin

von

Jacobo Martínez Font

aus Barcelona, Spanien

Berlin, August 2011

Die vorliegende Arbeit wurde in der Zeit von März 2008 bis August 2011 unter Anleitung von Prof. Dr. Saenger am Institut für Chemie und Biochemie/Kristallographie der Freien Universität Berlin im Fachbereich Biologie, Chemie, Pharmazie durchgeführt.

1. Gutachter: Prof. Dr. Wolfram Saenger

2. Gutachter: Prof. Dr. Udo Heinemann

Disputation am:

10.11.2011

Abbreviations

Å	Angstrom (10^{-10} m)
ADP	Adenosine diphosphate
AMPPCP	5'-adenylyl (beta,gamma-methylene)diphosphonate
AMPPNP	Adenylyl Imidodiphosphate
ATP	Adenosine triphosphate
bp	base pair
C-terminal	Carboxyl terminal
CCD	Charged coupled device
CD	circular dichroism
CTP	Cytidine triphosphate
CV	Column volume
DANN	Deoxyribonucleic acid
DNAse	Deoxyribonuclease
EDTA	Ethylenediaminetetraacetic acid
GlcNAc	N-acetyl glucosamine
GNE	glucosamine (UDP-N-acetyl)-2-epimerase/N-acetylmannosamine kinase
HIBM	human inclusion body myopathy
hMNK	human N-acetyl mannosamine kinase
IPTG	Isopropyl β-D-1-thiogalactopyranoside
ITC	Isothermal titration calorimetry
kDa	Kilodalton
LB-Media	Luria Bertani media
M	Molarity (mol/l)
ManNAc	N-acetyl mannosamine
ManNBut	N-butyl mannosamine
ManNProp	N-propyl mannosamine
mRNA	messenger ribonucleic acid
M_w	molecular weight
N-terminal	Amino terminal
NeuNAc	N-acetyl neuraminic acid
Ni-NTA	Ni^{2+}-nitrilotriacetic acid
OD	Optical density
PAGE	polyacrylamide gel electrophoresis
PCR	polymerase chain reaction
PDB	*Brookhaven Protein data bank*
PEG X	Polyethylene glycol (mean molar mass X g / mol
rmsd	root mean square deviation
RNA	ribonucleic acid
ROK	Repressor, Open reading frame, kinase
SDS	Sodium dodecyl sulfate

TEMED	N,N,N',N'-Tetramethylethylenediamine
TEV	Tobacco etch virus
Tris	tris(hydroxymethyl)aminomethane
UDP	Uridine diphosphate
UTP	Uridine triphosphate
UV	Ultraviolet
wt	wild type
% (v/v)	volumen of solute with respect to the final volume of the solution
% (w/v)	x % (w/v) means x grams of solute per 100 ml solution

Acknowledgments

First and foremost, I am heartily thankful to my advisor Prof. Wolfram Saenger for giving me the opportunity to work on such an interesting project, allowing me to work independently and develop my own ideas but guiding and supporting me continuously with patience. I kindly appreciate the fruitful discussions with him and his ability to make science, and more generally life, easy.

I also want to thank Dr. Eva Tauberger, who carefully helped me to make the first steps on the way to this thesis. She has been always ready to help me in the lab and answering multitude of questions about molecular biology. Working together with her, preparing and supervising practical courses, has been a pleasure.

I am very grateful to Dr. Sebastien Moniot for his incredible patience to answer all kind of crystallographic questions and for waking me up with good music every time I fell asleep during the night on our long beamtime measurements at the synchrotron.

I say thank you to Sofia Banchenko, Dr.Sebastian Geibel, Alessandra Beltrami, Haydar Bulut, Traudy Wandersleben, Dr. Quingjun Ma, Dr. Albert Guskov, Dr. Ardeschir Vahedi, Dr. Azat Gabdulkhakov, Clemens Langner, Claudia Alings and Carsten Jakob who together with the above cited persons formed the AG Saenger and with whom I had great times that I will miss.

Further, I am very thankful to Long Duc Nguyen, who realized most of the enzymatic and binding tests, for the nice and open cooperation. I acknowledge ditto Dr. Hua Fan and Prof. Dr. med. Werner Reutter, who started the project and developed the idea behind this thesis.

I am grateful to all the members of the AG Wahl, AG Hauke and AG Scharf for their help during the hard laboratory move and reconstruction time.

I am indebted to Dr. Chris Weise, who helpfully measured the MALDI-TOF spectra for different proteins and to Dr. Reinhold Zimmer for the synthesis of the hMNK Inhibitor.

I am also thankful to Prof. Solioz, Dr. Helge Abitch and Dr. Steffano Mancini from the Swiss Copper Group for the good teamwork on the copper homeostasis project.

Finally, I will always be thankful to my parents, family and friends for their unconditional support.

INDEX

1. INTRODUCTION

1.1. Contextualization of glycan and sialic acids

Cricks „Central Dogma of Molecular Biology", first published in 1956 and renewed in 1970 [1], stated that biological information flows from DNA to RNA to protein. This concept, even if valid and necessary, is insufficient to completely explain the make-up of cells, tissues, organs, physiological systems and organisms. Indeed, there are other two major classes of molecules apart from DNA, RNA and proteins that are required to form a cell, namely lipids and carbohydrates. These molecules play a crucial role in energy storage, as signaling effectors, as recognition markers and as structural components [2].

The completion of the human genome sequencing revealed an unexpectedly small number of genes. [3, 4] Carbohydrates can covalently bind to the lipids (glycolipids) and proteins (glycoproteins or proteoglycans) as single monosaccharides or as sugar chains (also referred as glycans), providing an enhanced structural diversity and allowing one protein to act as many, depending on the carbohydrate or glycan inventory. This offers, at least partially, an explanation for the small number of genes identified [5]. Glycosylation (the enzymatic attachment of glycans to lipids or proteins) is a tissue-specific and developmentally regulated process [6, 7] that involves around 2% of the human genes [5].

The surfaces of all mammalian cells are covered by a dense sugar coating or glycocalyx, whereas glycans can also exist as freestanding entities or as a part of secreted molecules (Figure 1.1). Due to their surface location glycans are involved in cell-cell, cell-matrix, and other cell-molecule interactions. The outermost monosaccharide position on glycan chains is usually occupied by a sialic acid molecule. As the terminal sugar of membrane-associated glycoconjugates, sialic acids play a dual role: they are required for protection and adaptation of life, and they serve as recognition sites for pathogenic microorganisms.
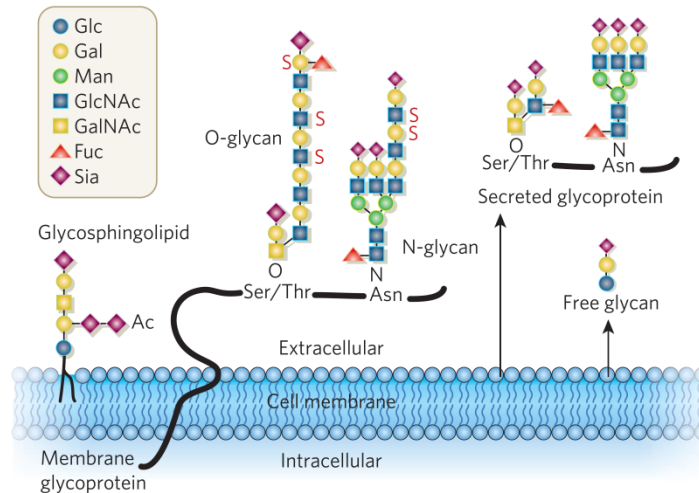
Figure 1.1 Schematic representation of the glycoconjugates diversity. Sialic acids (Sia) can be found at the terminal position of N- or O- bonded glycans attached to membrane glycoproteins and glycolipids, to secreted proteins, as freestanding entities. Figure extracted from [8]

1.2. Sialic acids history and definition

The term sialic acid (Sia) was first used by Gunnar Blix, who in 1936 isolated several such species from bovine submaxilary mucin [9]. In 1941 Enst Klenk called "neuraminic acid" (Figure 1.2) a substance that he isolated after methanolysis of brain gangliosides [10]. It was not until 1957 that Alfred Gottschalk, together with Blix and Klenk, found a consensus and christened the new monosaccharide family as "sialic acids" because of its discovery in salivary mucins (the Greek term for saliva is sialos). [11]
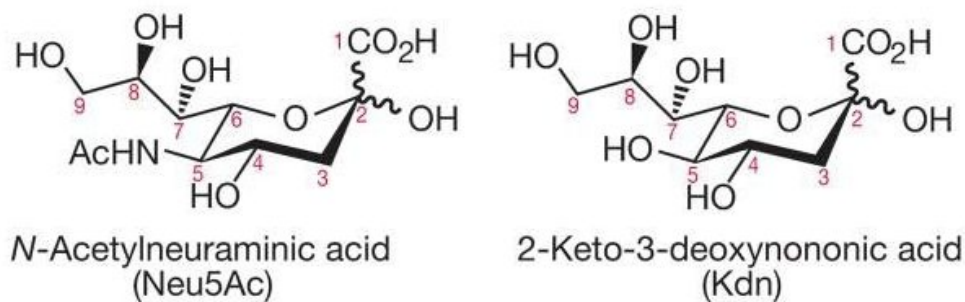
Figure 1.2 Most common sialic acids. N-acetyl neuraminic acid and Kdn differ only by the substitution at the C-5 position and are the precursors for virtually all other sialic acids, metabolically derived from these two. In vertebrates, Neu5Ac and its derivatives are more common than Kdn. The mutarotation between the α- and β- anomers is indicated by ondulated lines at the anomeric center C-2. Figure extracted from [2]

Sias were originally defined as "neuraminic acid" and its derivatives. [11, 12] before the discovery of Kdn (2-Keto-3-deoxynononic acid) extended this definition. The inclusion of Kdn and its derivatives in the Sias family is not only based on the high structural similarity but also on its occurrence [13] and biosynthetic pathway [14].

Sias are the only nine-carbon backbone keto sugars known in nature (apart from the bacterial pseudaminic and legionaminic acid [15]). They are characteristically hydrophilic and the only sugar type that bears a net negative charge (the carboxylic group at the C-2 position is deprotonated at physiological pH). In solution, Sias form a pyranose ring by intramolecular hemiketal condensation adopting a $^2C_5$ chair conformation. As components of glycoconjugates, Sias exist only in the α- configuration (C-1 carboxyl in trans orientation with respect to the C-7 carbon). Interestingly, the activated donor form, Cytidine monophosphate (CMP)-sialic acid, adopts always the β-configuration [15].

1.3. Differential features of the sialic acid family

- Vertebrate glycoconjugates are composed mainly of five and six carbon-backbone sugars, whereas Sias are exceptionally the only nine-carbon α-keto sugars.

- Due to their hydrophilicity and negative charge Sias occupy the most terminal position in the glycan chains, which allows them to mediate interactions with other cells and with the environment.

- Diversity: the multitude of possible modifications (see section 1.4) creates a family with over 50 structurally different molecules. This feature combined with the different glycosidic linkage possibilities to the underlying monosaccharides in the glycan chain generates hundreds of ways in which Sias are present in nature.

- Contrary to the other vertebrate monosaccharides, Sias seem not to be ubiquitous in nature. They are mainly present in vertebrates and certain bacterial forms and generally not found in plants, prokaryotes or invertebrates. However there are many reports of Sias in mollusks [16] or insects like *Drosophila* [17].

- The characteristic biosynthetic pathway implies the condensation of a neutral six carbon sugar with a pyruvate molecule.

- Monosaccharides are transferred to the nascent glycans from an activated nucleotide sugar or "donor" by enzymes called glycosyltransferases. Syaliltransferases are a subclass of glycosyltransferases that catalyze the transfer of Sias. Interestingly, the donor form for Sias transfer is CMP-sialic acid, a higher energy donor form than the donors used by all other vertebrate monosacharides (uridine or guanidine diphosphates).

1.4. Sialic acids diversity

As the terminal monosaccharides on glycan chains, Sias are involved in many biological recognition processes. The great variation of ways, in which sialic acids can present themselves (Figure 1.3), makes this family especially suited to assume such a function. This diversity potential results from the variety of possible covalent linkages to the underlying sugar chains (over the C-2 position) in combination with the high diversity of natural modifications within the monosaccharide itself.

Linkages

The linkage of Sias to the underlying sugars of the glycan chains is performed by specific sialyltransferases using the high energy donors CMP-sialic acids. The most common linkages are between C-2 of Sias and C-3 or C-6 of galactose or the C-6 position of N-acetyl galactosamine. Less common is the presence of Sias in an internal glycan position, usually attached to another Sia over the C-8 position.

Natural modifications

The modification of the C5- position with an N-acetyl group or a hydroxyl group produces the two main precursors of all Sias members, respectively, N-Acetyl neuraminic acid (Neu5Ac) and 2-Keto-3-deoxynononic acid (Kdn). There are two other possible modifications at C-5: a hydroxylated N-acetyl group (producing N-glycolyl neuraminic acid- Neu5Gc) or just an amino group (producing neuraminic acid, Neu). These four C-5 modifications (Neu5Ac, Kdn, Neu5Gc and Neu) can undergo one or more additional substitutions at the C-4, C-7, C-8, C-9 hydroxyl groups by acetate, lactate, sulfate, phosphate or methyl esters. The carboxyl group at position C1 is usually in its anionic form and free (not substituted) at physiological pH. However, intra- or intermolecular lactonization involving the C1 carboxylate and adjacent hydroxyl

groups and intramolecular lactamization with a free amino group at C-5 in the case of Neuraminic acid have been described.
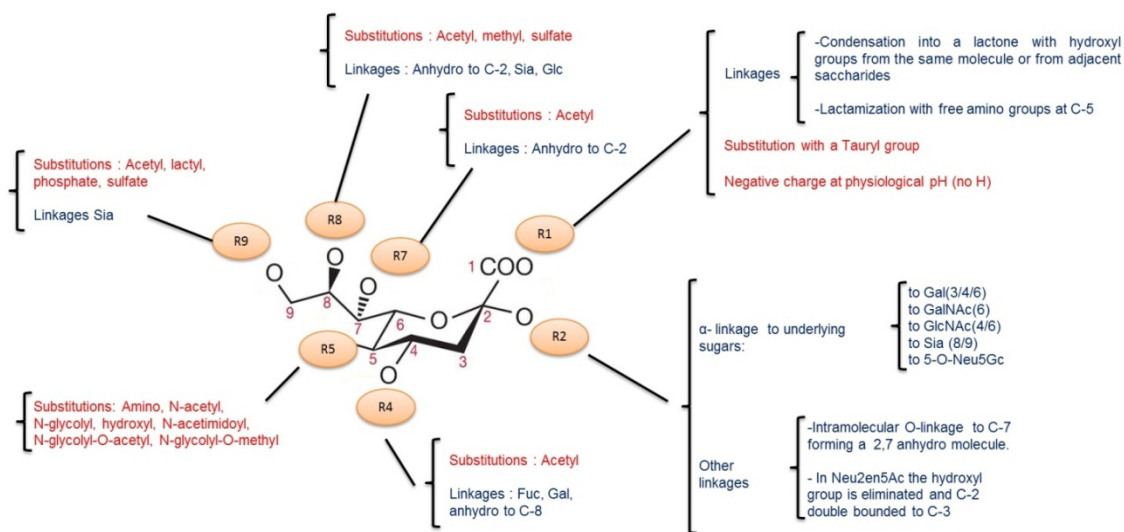
Figure 1.3 Sialic acids diversity. The elementary building stone common to all sialic acids, a nine-carbon backbone, is shown in the α-configuration. The different substitutions and linkage possibilities have been listed in red and blue, respectively, for clarity. The combination of all subtitutions results in a family with more than 50 variants. Moreover, this issue combined with the different linkage possibilities produces the great diversity in which sialic acids can present themselves. Figure extracted from [2] and modified.

1.5. Sias general biological functions

Roland Schauer, one of the most prolific authors in the sialic acid field, speaks about the role of Sias in nature in these terms: *"It is not easy to describe a general role of Sia because these monosaccharides participate directly or indirectly in multiple and diverse cellular events"* [18]. Indeed, their chemical and structural diversity, variety of linkages and ubiquity as part of complex glycoconjugates of animals and microorganisms classify Sias as one of the most versatile function regulators in cell biology.

In awareness of the intricacy of the topic I try here to describe some of the Sias functions known to date:

- As a part of glycoconjugates, Sias play an important role for the expression and structural stability of some glycoproteins like acetyl choline receptors, whose susceptibility to be degraded by proteases increases in its non-glycosylated form [19]. Another clear example of this effect has been found in Erythropoietin

(EPO). Recombinant EPO with increased sialylation showed increased serum half-life and activity [20].

- The carboxylic group, deprotonated at physiological pH, confers Sias a strong electronegative charge, making them well suited for the binding and transports of ions and drugs [21, 22] or to enhance the viscosity of mucins [23, 24].

- Another general property of Sias seems to be an antioxidative effect and free radical scavenging as proposed elsewhere [25, 26].

- Sias can also regulate the ligand binding affinity of some receptors [2] like somatostatin [27]. The TrKa Tyrosine kinase receptor, a signaling receptor for neurotrophin grow factors, is only activated after Sias are removed and the underlying galactose residues therefore unmasked [28].

- *Antirecognition effect* as biological masks of antigenic sites, receptors and penultimate galactose residues. (1.6)

- Contrary to their antirecognition effect, Sias can be part of many recognition processes as ligands for hormones, toxins, antibodies and specific proteins (mainly lectins) of vertebrate cells, bacteria and viruses [18, 29]. (1.6)

1.6. Sias recognition/antirecognition duality function

The two latter functions of Sias described in chapter 1.5 deserve an own section, due to their biological relevance and extension.

Antirecognition effect (Figure 1.4)

This effect is based on the hydrophilic and bulky nature of Sias combined with their negative charge. There are many ways in which Sias can perform this function. The electrostatic repulsion with other cells and molecules, the masking of penultimate sugars (in most cases galactose), which otherwise can be recognized by specific receptors (like the galactose receptor), the shielding of antigenic sites of macromolecules, the antiproteolytic effect in glycoproteins or the inhibition of the action of some endoglycosidases are some of them [30].

The uptake by hepatocytes of desialylated serum glycoproteins was the first report of this phenomenon [31]. Indeed, the desialylation demasks galactose letting this residue exposed for a Gal-recognizing receptor. In the same way, it was observed that rat erythrocytes, threated with sialidase and reinjected, disappeared within hours from the

bloodstream (even if their normal life time is circa 120 days) as a consequence of phagocytosis by liver and spleen macrophages [32]. Interestingly, thrombocytes and lymphocytes are similarly sequestered but reappear after several hours. In this case macrophages bind the cells but do not phagocyte them, and they are released after resialylation. In addition, the binding of macrophages to the blood cells could be inhibited by galactose [33]. Since old erythrocytes expose more galactose residues than young ones, it has been suggested that the trapping of desialylated cells could be a mechanism to sequestrate aged red cells [34].

Tumor cells present an increased sialylation level. The malignancy and the metastatic potential increases with oversialylation. In this case, both effects, antirecognition and recognition, play a role simultaneously: increased sialylation offers tumor cells a protection in front of the humoral and cellular defense systems (antirecognition) and at the same time Sias, especially a Sias-rich carbohydrate called sialyl Lewis X, are bound by lectins located on the surface of platelets and endothelial cells (recognition). This binding enables cell spreading and metastasis [30, 35-37].
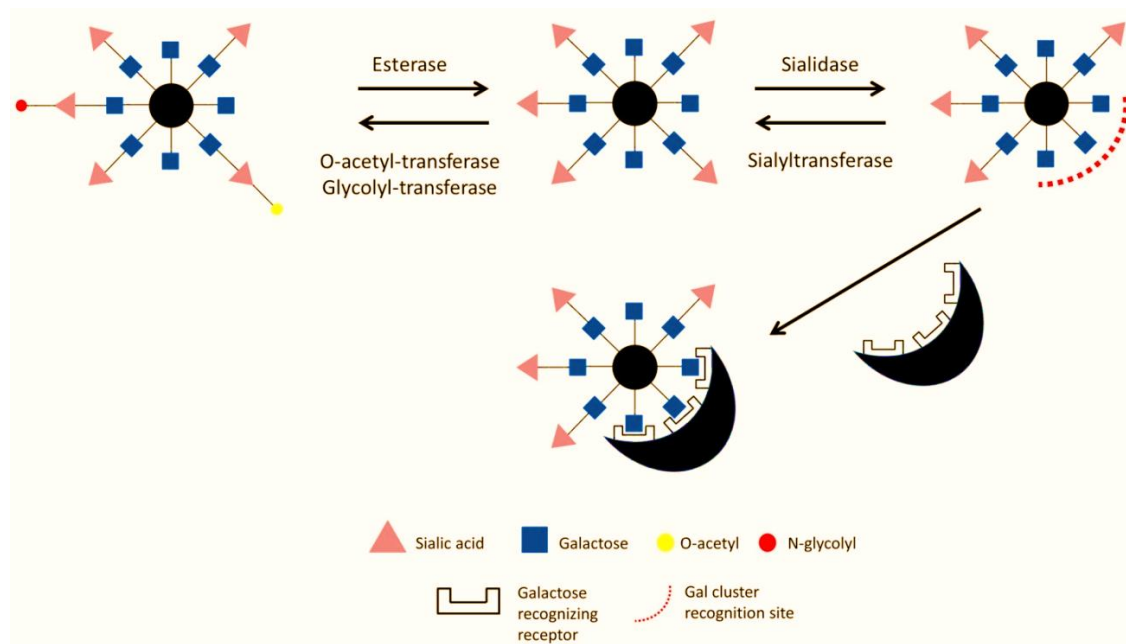
Figure 1.4 Model of the antirecognition effect. Sias degradation by sialidases or modifications by other specific enzymes can modulate the interaction between cells. Some galactose-recognizing receptors like the galectins on macrophages can identify and bind a cluster of unmasked galactose residues. An O-acetylation or an N-glycolyl group can inhibit Sias digestion and consequently its interaction with Sias recognizing receptors, bacteria or viruses. Some bacteria use O-acetylations to mask immunogenic epitopes and evade the host immune defense.

Many pathogenic viruses and bacteria secrete sialidases to unmask Gal residues on the host endothelia and attach to them via galactose-recognizing lectin [18]. Carbohydrates can be an antigenic determinant. Desialylation caused by a viral or bacterial infection can unmask one of them and provoke the production of autoantibodies.

Sias as ligands

Some of the roles of Sias commented before are: provide hydrophilicity and negative charge to vertebrate cell surfaces, mask antigenic sites or penultimate galactose residues or act as binding sites for pathogens and toxins. However, all those listed functions are "extrinsic" ones. Sias are essential for embryonic development in vertebrates but not in insects suggesting the idea that they are involved in some "intrinsic" functions. In fact, there are Sias-recognizing proteins mediating specific recognition events [8, 38]. Microorganisms use in most cases the carbohydrates attached to the host cell surface for binding. The binding of influenza virus A to erythrocytes and respiratory tract mucins, whose surface is strongly sialylated, was the first documentation of this phenomenon in 1942 [39]. But not only microorganisms possess Sias-binding proteins. Several vertebrate proteins have been found that mediate recognition events via sialic acid binding. The most extensively studied and biggest families are described below:

- Factor H: This was the first vertebrate Sia-binding protein to be discovered. It is a glycoprotein present at high concentrations in blood plasma that plays a crucial role as negative regulator of the alternative complement pathway. This pathway is constantly active and acts without antibodies. The first product of the pathway is the protein complex C3bBb, which will bind indistinctly to the surfaces of host cells and pathogens. Factor H specifically recognizes sialic acids and certain sulphated glycosaminoglycans on the cell surfaces of the host vertebrates via anion binding domains and contributes to the dissociation of the complex C3bBb-cell, which inhibits the remainder of the cascade. Since pathogens are not recognized by Factor H, the complex C3bBb-pathogen will not be dissociated, and the terminal complement components will be activated [40, 41]. Pathogenic microbes that express Sias are therefore better prepared to evade the immediate alternative complement pathway and tend to be more virulent. [42]

- Selectins: Lectins are proteins that specifically recognize and bind carbohydrates. The subfamily of the selectins is composed of three C-type lectins (defined by a common structural motif and by calcium requirement for sugar binding), which recognize two specific structures composed of sialic acids that are α-1-3 linked to fucose. These ligand structures are called sialyl Lewis X and are required but not sufficient for the binding [43, 44]. Selectins are involved in the immune response by mediating cell-cell interactions. The first one to be discovered, L-selectin, is constitutively expressed on leukocytes and involved in the homing of this type of cells into the lymph nodes.[45] E-selectin is present on activated endothelial cells and involved in the adhesion of leukocytes to them. E-selectin is not constitutively expressed but transcriptionally induced under certain conditions [46]. P-selectin is stored in granules of platelets and endothelian cells and transported to the cell surface if required, where together with E-selectin it will initiate the localization of leukocytes at sites of inflammation by recognizing sialic acid containing ligands on the cell surface [47, 48].

- Siglecs: The sialic-acid binding Ig like lectins (Siglec) superfamily is the largest family of Sias recognizing lectins. Siglecs are membrane proteins that display common functional and structural features. The extracellular domain is composed by an N-terminal (variable) V-set like subdomain and repeated units (from 1 to 16) of a (constant) C2-set like domain. A single transmembrane pass connects the extracellular and the cytosolic domains, where many phosphorylation sites are involved for intracellular signal transduction [49, 50]. The recognition of Sias by Siglecs is dependent on many structural features. Indeed, not only the negative charge is recognized but also the side chain (C7-C8-C9), the N-acetyl moiety and the underlying sugar moiety or even the whole glycan chain [8, 15].

1.7. The biosynthetic pathway of Sias in vertebrates

As commented before, from a biosynthetic point of view Neu5Ac and Kdn are the precursors for all Sias. The here described production pathway of Neu5Ac takes place in vertebrates (the bacterial pathway is very similar). The initial substrates for the Neu5Ac biosynthesis are either fructose-6-phosphate (Frc-6-P, obtained from glycolysis) or N-acetyl glucosamine (GlcNAc, obtained by degradation of endogenous or exogenous glycans). For better understanding of the process, it is useful to divide it in two main parts: the formation of UDP-GlcNAc and the synthesis of Sias and the respective activated forms CMP-Sias.

From Frc-6-P to UDP-GlcNAc

Glucosamine-6-phosphate synthase catalyzes the amination of Frc-6-P using glutamine as NH_2-donor [51]. The final product Glucosamine-6-P (GlcN-6-P) will then be irreversibly N-acetylated using acetyl-CoA as an acetyl donor to produce GlcNAc-6-P [52]. These two first reaction steps can be alternatively substituted by the phosphorylation of GlcNAc by GlcNAc kinase (both ubiquitous) [53].

GlcNAc-6-P is then rearranged into GlcNAc-1-P and activated by UTP to form the final product UDP-GlcNAc [54]. The biosynthesis of UDP-GlcNAc is regulated by a feedback inhibition mechanism involving GlcN-6-P synthase and UDP-GlcNAc itself.

In addition UDP-GlcNAc is also the precursor for the formation of UDP-N-acetyl-galactosamine and the substrate for the attachment of GlcNac to Serine or Threonine residues on cytosolic and nuclear glycoproteins.

From UDP-GlcNAc to CMP-sialic acid (Figure 1.5)

In vertebrates, the first two steps of this second half of the biosynthesis of Neu5Ac are performed by the bifunctional enzyme UDP-GlcNAc-2-Epimerase/ManNAc-Kinase (GNE/MNK) [55]. The epimerase GNE converts UDP-GlcNAc into N-acetyl Mannosamine (ManNAc) by anti-elimination of UDP in a stepwise E1 mechanism and formation of acetamidoglucal as intermediate [56]. Then, ManNAc kinase phosphorylates ManNAc to afford ManNAc-6-phosphate. In mammals the direct epimerization of GlcNAc-6-P into ManNAc-6-P does not occur but some microorganisms possess enzymes to perform this reaction.

The next step, an aldol condensation between the ManNAc-6-P and phosphoenolpyruvate (PEP), is catalyzed by Neu5Ac-9-P synthase [57] and the product, NeuNAc-9-P, is thereafter dephosphorylated by NeuNAc-9-phosphate phosphatase to yield NeuNAc [58]. The newly created NeuNAc needs to be activated before being added to the corresponding glycan. This reaction is performed by CMP-NeuNAc synthetase [59] in the nucleus. [60] This feature is unique for sialic acid, since all other naturally occurring carbohydrates are activated in the cytosol and use UTP or GTP for activation instead of CTP.

The CMP-Neu5Ac molecules are finally transported from the nucleus to the Golgi apparatus by a specific protein of the Golgi membrane [61], where they will be attached to nascent glycans by specific sialyltransferases. The numerous modifications of NeuNAc producing the great diversity of Sias are performed by Golgi-resident enzymes. [62]
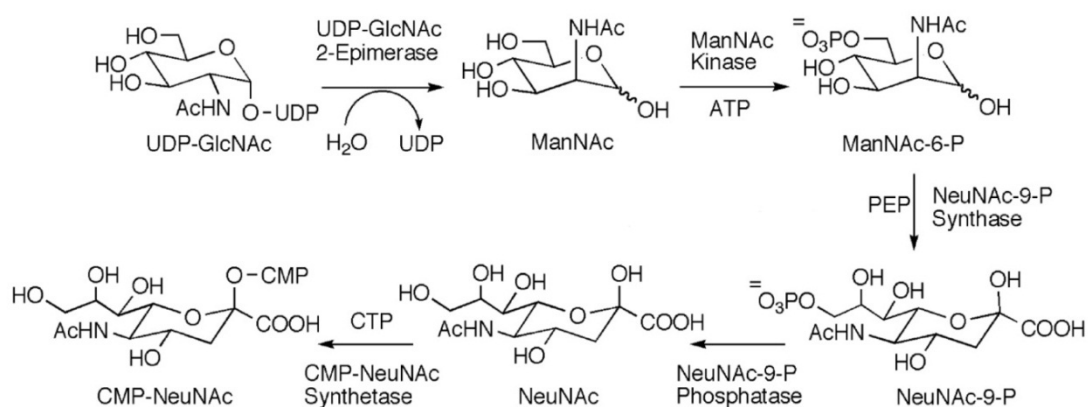
Figure 1.5 Schematic overview of the biosynthesis of CMP-NeuNAc starting from UDP-GlcNAc. All the enzymes and cofactors involved in the second half of NeuNAc biosynthesis are listed and the substrates of the catalyzed reactions represented. All reactions take place in the cytosol but the NeuNAc activation, which interestingly is performed in the nucleus. CMP-NeuNAc regulates its own biosynthesis by feedback inhibition of the enzyme responsible for the first reaction, the UDP-GlcNAc-2-Epimerase (GNE). Figure extracted from [63]

1.8. The UDP-GlcNAc-2-Epimerase/ManNAc Kinase (GNE/MNK or GNE)

Genetics

The human GNE gene, coding for the bifunctional enzyme GNE/MNK, consists of 14 exons localized on chromosome 9p12-13. All of them but one are located in close proximity in one gene. The last one, a 90 bp exon called A1, is localized 20000 bp upstream of exon 1 [64]. Three different isoforms have been described for hGNE: hGNE1, hGNE2 and hGNE3 [65]. hGNE1 encodes a 722 amino acids protein, whereas in hGNE2 the N-terminus is prolonged by 31 addictional residues and in hGNE3 the same N-terminus is 41 amino acids shorter with respect to hGNE1. GNE1 is ubiquitously expressed reaching its highest concentrations in the liver and placenta and at lower concentrations in the muscle, brain, kidney and pancreas. On the other side, GNE2 and GNE3 show a tissue-specific expression pattern. The present work focuses on the hGNE1 isoform.

Primary structure, domains, multimerization state and function

GNE is a highly conserved protein found throughout the animal kingdom [52]. The human GNE (from now on, only the isoform hGNE1 is referred- see above) is a 722 amino acids long protein with two clearly differentiated functional domains: an N-terminal domain (amino acids 1-378) containing the UDP-GlcNAc 2-Epimerase and a C-terminal domain (amino acids 410 to 722) containing the N-acetyl Mannosamine kinase. These two consecutive enzymatic reactions (epimerization and phosphorylation) are pivotal steps on the biosynthetic pathway of NeuNAc and consequently on all other sialic acid variants (1.7).

The epimerase activity of GNE was first described in 1958 [66] and the ManNAc Kinase activity in 1961 [67] but it was not until 1983 that Van Rinsum et al. co-localized both activities. [68] In 1997 it was demonstrated that the enzymes catalyzing these two reactions are co-expressed in a single polypeptide chain [55].

Biochemical characterization of GNE showed that it exists as dimer or tetramer. In its tetrameric form GNE is fully active but the dimer shows only kinase activity. At physiological concentrations of UDP-GlcNAc the tetrameric state is maintained [55, 69].

Activity regulation

Many mechanisms regulate the activity of GNE. The main one is a feedback inhibition process induced by the endproduct, the CMP-sialic acid (Figure1.6) [70]. Moreover GNE possesses eight conserved motifs for protein kinase C. The interaction between protein kinase C and GNE with the subsequent phosphorylation of the latter has been shown in mouse liver. GNE activity is enhanced upon phosphorylation [71]. In some cancer cell lines (such as Morris hepatoma [72]) or HIV-infected lymphocytes [73], an epigenetic regulation has been observed. In these cases, the mRNA expression is downregulated by methylation of the promoter region which leads to a drastical decrease of the cellular sialylation.
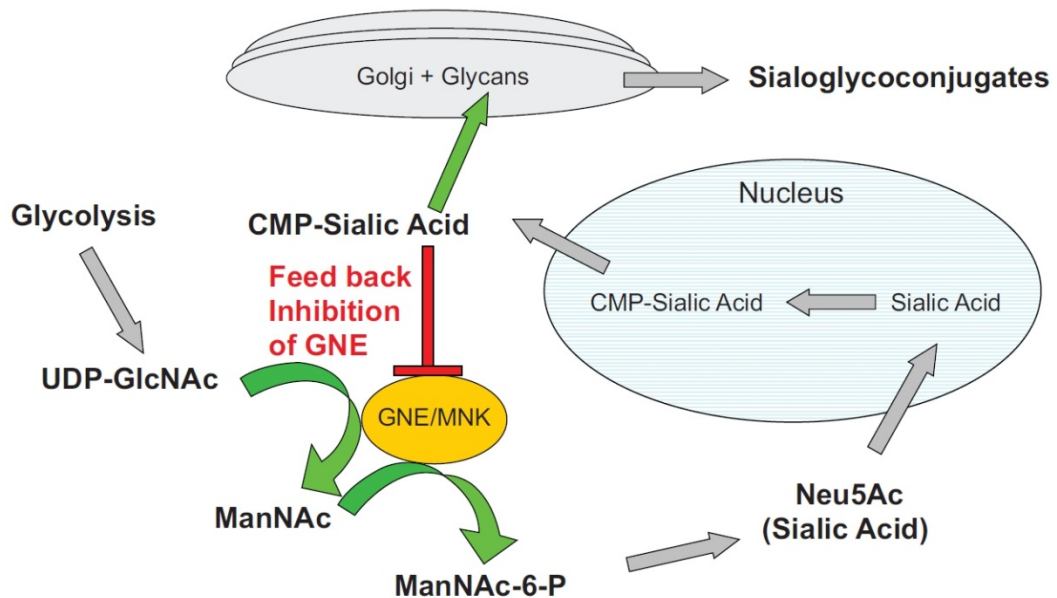
Figure 1.6 GNEregulation by feedback inhibition in the context of the sialic acid biosynthetic pathway. Because GNE is the rate limiting step of the pathway, its activity is regulated by allosteric inhibition via the downstream product, the CMP-sialic acid. Figure extracted from [74]

1.9. Alternative roles of GNE

The role of GNE in sialic acid biosynthesis has already been described in this introduction. However, there are many reasons to speculate with the possibility of some other putative functions of GNE. On the one side, there is the enigma of the hereditary inclusion body myopathy (HIBM), a human disease that gives rise to muscle dystrophy in humans and is caused by different point mutations of GNE. Interestingly, all the mutants produce the disease and most of these GNE variants show a reduced enzymatic activity but not all (see GNE related diseases). The connection between muscle dystrophy and a mutation in the key enzyme of sialic acid biosynthesis is not trivial and suggests that GNE could be involved in some growth and differentiation processes. Moreover Krause et al. found that GNE is not only localized in the cytosol but also in the nucleus and in association with the cytoplasmatic side of the Golgi membrane, two parts of the cell not primarily involved in sialic acid metabolism. [75] The unexpected localization of GNE within the cell could be explained by multienzyme complex formation of GNE with other enzymes involved in the sialic acid biosynthetic pathway [52].

On the other side, three interaction partners have been found for GNE. Weidermann et al. (2006) found by two-hybrid screen that the promyelotic leukemia zinc finger (PLZF) and the collapsing response mediator protein 1 (CRMP-1) interact with GNE [76]. PLZF is a transcription factor that interacts with Cullin3, a component of E3-ligases involved in ubiquitinylation of proteins, a process that is linked with proteasome degradation. In this context, the impairment of the binding between GNE and PLZF induced by point mutations could disturb the normal proteasome degradation processes. This is in line with the accumulation of proteins in muscles found in HIBM patients. The connection between GNE and CRMP-1 remains still unclear. Also α-actinin 1 has been found to interact with GNE and could be related to the muscle specificity of HIBM.

Interestingly, overexpression of GNE in HEK cells produced increased mRNA levels for ST3Gal5 and ST8Sia1 (coding for the gangliosides GM3 synthase and GD3 synthase, respectively) [77]. This suggests a regulatory function and could also explain the localization of GNE in the nucleus.

1.10.   GNE related diseases

GNE knock-out mice die at embryonic day 8.5, demonstrating that the impairment of sialylation of glycoconjugates induces cell death [38].This can be either caused by the consequent loss of antigen antirecognition masks or by the prevention of cell migration and differentiation (1.6). In humans, missense mutations of GNE can result in two different disorders of sialylation that are compatible with post-embryonic development. In *Sialuria*, a mutation of either Arg263 or Arg266 (Figure 1.7) provokes a lack of feedback inhibition of GNE by the downstream product CMP-sialic acid. This dysfunction gives rise to a massive overproduction of free NeuNAc and its consequent accumulation in the cytoplasm and excretion into body fluids [78, 79]. Patients suffering from this autosomal dominant disorder show different degrees of involvement of organ systems like hepatomegaly and mental retardation [80].
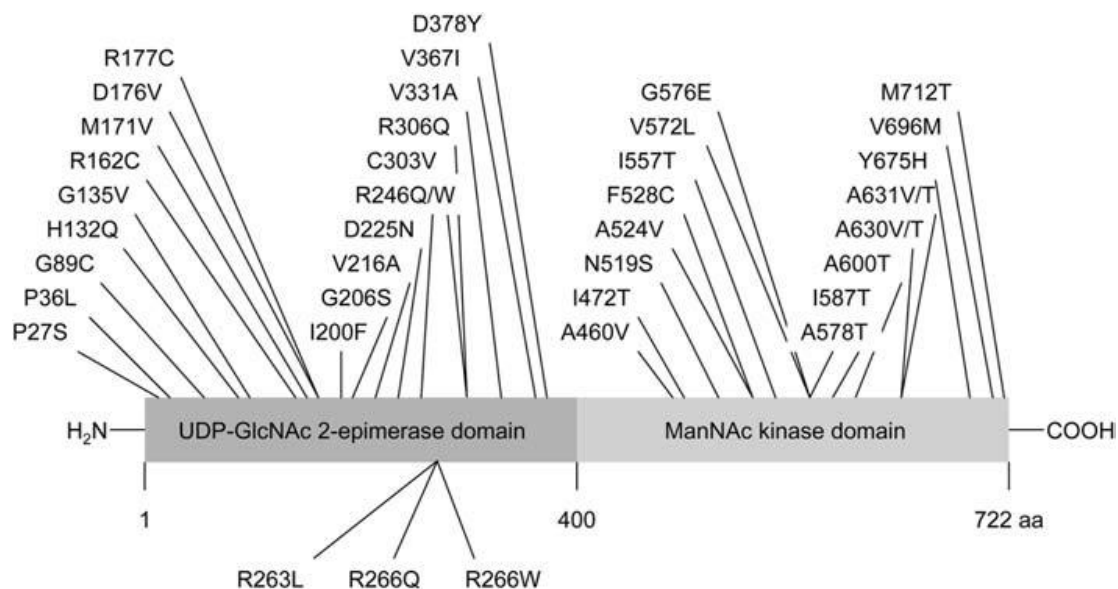
Figure 1.7 Schematic representation of the distribution of many of the HIBM (above) and Sialuria (below) associated GNE point mutations. Figure extracted from [52]

The *hereditary inclusion body myopathy* (HIBM) is also caused by mutations in GNE. It is an autosomal recessive neuromuscular disorder that appears late in life and spares some muscle groups [81]. There are more than 50 described point mutations producing HIBM described, affecting both functional domains [82] (Figure 1.7). Most of the analyzed mutants display reduced activity for both GNE and MNK, suggesting that mutations in one domain can also influence the function of the other one. The different variants show different enzymatic activities but the same disease phenotype, which

suggests that the disease mechanism is probably not related to the enzymatic functions (epimerase and kinase) of GNE [83]. Furthermore, in agreement with this hypothesis, HIBM patients do not show any other defect apart from the commented skeletal muscle dystrophy, and no pathological feature could be assigned to a sialic acid defect to date [52].

1.11.   Previous available structural information on hGNE

The structure of hGNE has been tried to determine in our laboratory previously without success. Therefore, in this work, efforts have been invested in solving the structure of both enzymatic domains separately by creating constructs of the epimerase and kinase domains.

In case of the hGNE epimerase domain, the instability of the protein made it unsuitable for crystallization. To date (May, 2011) only 6 structures of proteins sharing between 21 and 24% identity with the epimerase domain of hGNE have been deposited in the protein databank. (http://www.pdb.org)   All of them are annotated as UDP-N-Acetylglucosamine 2-Epimerase and were obtained from bacterial sources (PDB codes: 3OT5,1VGV,1F6D,3BEO,3DZC,1V4V).

The structure of the MNK domain of hGNE was recently solved (published in October 2009) in its apo- form by Tong et al. at 2.8 Å resolution [84]. The elucidation of this structure was sufficient to derive the overall folding of the enzyme and to speculate on the substrate binding site, based on structural comparisons with other similar known sugar kinases. Also a mapping of disease related mutations on the MNK structure was done to predict possible structural effects of the mutations [85]. However, due to the relatively low resolution, the absence of ligands and the lack of electron density of some loops in the structure some questions remained open.

The crystallization of proteins is a laborious work, often unthankful and capricious. A point mutation or a shortened construct can dramatically change the crystallization properties of a protein. It was therefore decided to design a construct for the MNK domain of hGNE similar to the one used by Tong et al. [84], since it proved to be prone to crystallize.

1.12.   The MNK domain of GNE belongs to the ROK family

The elucidation of the hMNK apo-structure (Figure 1.8), revealed that hMNK belongs to the **R**epressors, **O**pen reading frames, **K**inase (ROK)-family, a functionally diverse enzyme family that was first described in 1994 by Titgemeyer et al. [86] encompassing transcriptional regulators, uncharacterized open reading frames and several sugar kinases. Comparing the primary structures of different ROK family members (the hMNK domain of GNE was included among them), Hanson et al. proposed two consensus sequences as a specific signature common to all family members [87]. The consensus motif 1 is a glycine rich 28 amino acids sequence with four glycines conserved among all the compared structures. The second motif is 14 amino acids long and contains 2 conserved cysteine residues and a histidine or another cysteine at the third position. In 2005, Schiefner et al. [88] presented the first structure of a ROK family member, the transcriptional regulator Mlc.
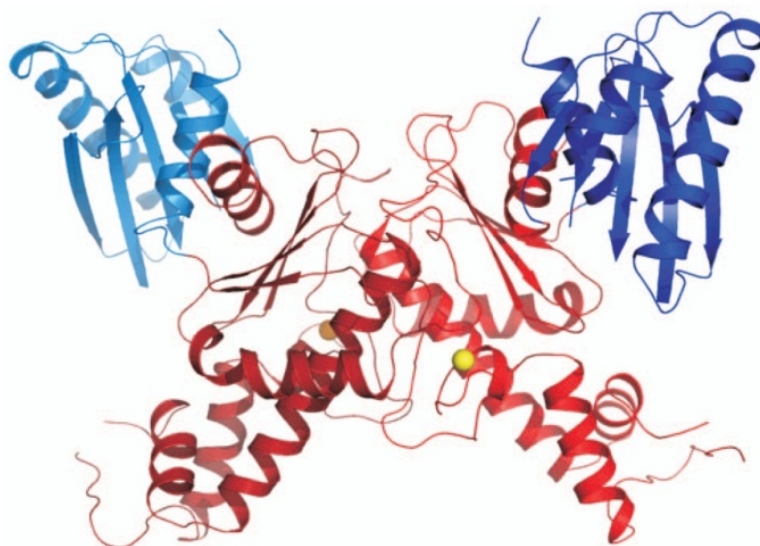
Figure 1.8. Representation of the homodimeric GNE kinase domain (PDB code: 3EO3). hMNK displays two clearly differentiated lobes: an N-terminal lobe (in blue) and a C-terminal one (in red), linked by a hinge region. This architecture is typical of sugar kinases and allows the enzyme to trap the sugar substrate between both lobes. Upon substrate binding, both lobes move closer to each other over the hinge region. The yellow spheres represent the Zinc cations, a characteristic feature of the ROK family. The displayed apo-structure of MNK was solved at 2.8 Å resolution and some essential loops for substrate and ATP binding are missing. This can be explained either by the flexibility of the loops in the ligand-free form or by the presence in the crystallization conditions of chymotrypsin that could have chopped the disordered protein regions. Figure extracted from [84].

Using the novel structural information combined with a renewed sequence comparison of the ROK family members they merged the two consensus motifs to a single one, which contains a zinc (Zn^{2+}) binding motif. There are two variations of this motif: $G\underline{H}X_{9-11}\mathbf{C}X\mathbf{C}GX_2G(\mathbf{C/H})X\underline{E}$ and $G\underline{H}X_{11-17}\mathbf{C}X_2\mathbf{H}X_2\mathbf{C}X\underline{E}$ (the metal binding amino acids are printed in bold and the underlined residues are conserved in many sugar kinases inside or outside of the ROK family. X can be any amino acid and the underscore specify the length number of amino acids separating the conserved motifs). hMNK contains the first Zn^{2+} binding motif (G568-E588), and a Zn^{2+} is coordinated by three cysteines and one histidine.

1.13.   Starting point and aims of this thesis

As exposed in the introduction, Sias are involved in many biological recognition processes due to their terminal position on glycan chains. The increased sialylation of tumor and especially of metastatic cells renders Sias highly relevant in pharmacology and medicine [89]. In the same way, the key role of the bifunctional enzyme GNE on the biosynthetic pathway of Sias and on the regulation of the sialylation of the cell surface glycoconjugates [90] have been also described here.

When this project was started, the structure of the full length GNE had been unsuccessfully tried to solve, and only the structure of the apo-form of the kinase domain had been determined (1.11). However, the published MNK structure had only a resolution of 2.8 Å, no substrate bound, and was lacking electron density for some loops, that were presumably necessary for substrate and ATP binding. The presence of chymotrypsin in the crystallization conditions or the flexibility of the loops in the absence of a ligand could be an explanation for this issue.

The main motivation has been therefore to solve the crystal structure of the MNK domain at higher resolution and in complex with its native substrate, N-acetyl mannosamine (ManNAc) and ADP, ATP or a non hydrolyzable ATP analogue to understand the catalytic mechanism of the enzyme and open possibilities to design specific inhibitors, which could be a very valuable tool in Sias research. In addition, this new structural information could be used to judge wether the HIBM related mutants produce the disease based on structural changes or even disruption.

2. MATERIALS

2.1. Instrumentation

Molecular biology work

Electroporator	Easyject Prima	EquiBio
Thermocycler	Tpersonal, Trio Thermoblock	Biometra
Gel Imager		INTAS

Electrophoresis

Electrophoresis chamber	Biometra	Biometra
Power supply	EPS 600, EPS 3500	Amersham Pharmacia
Power supply	E452	Consort

Cell culture

Incubator	Innova 4230	New Brunswick Scientific
Shaker	G25	New Brunswick Scientific
Shaker	Multitron	Infors HAT

Centrifugation

Table centrifuges	5804R	Eppendorf
	5417R	Eppendorf
Centrifuges	RC-5B,RC-5C	Sorvall
	Avanti J-26 XP	Beckman-Coulter
Ultracentrifuge		Beckman-Coulter
Rotor	60Ti, JLA 8.1	Beckman-Coulter
	GS3,GSA,SS34	Sorvall

Protein purification

Homogeneizer	Emulsiflex-C5	Avestin
Sonicator	Sonoplus	Bandelin
FPLC	ÄKTA purifier Basic	GE Healthcare
Äkta software	Unicorn 4.00	GE Healthcare
Affinity column	Histrap^{TM} 5 ml	GE Healthcare
Gelfiltration column	HiLoad^{TM} Superdex75 (26/60)	GE Healthcare

Spectroscopy

UV/Visible Spectrophotometer	Ultrospec 3100pro	Amersham Pharmacia
Photometer	Gene Quant	Amersham Pharmacia
Spectrophotometer	Nanodrop-ND 2000c	PEQLAB Biotechnologie
CD-Spectrometer		JASCO
quartz cuvette	45 µl, 3mm	Hellma
Plastic cuvette	Plastibrand	Brand

Other

Autoclave	Varioklav	H&P Labortechnic
Autoclave	VX-150,VX-95	Systec
pH-meter	761 Calimatic	Knick
Pipettes	10µl - 1 ml	Gilson
Weights	XS002S-Delta range	Mettler Toledo
Weights	XS205-Dual range	Mettler Toledo
Weights	Acculab	Sartorius
Vortex mixer	Genie 2	Bender and Hobein
Thermomixer	5436	Eppendorf
Microcalorimeter	ITC200	Microcal

2.2. Crystallization

Crystal-Screen I		Hampton Research
Crystal-Screen II		Hampton Research
Index-Screen		Hampton Research
Crystal Screen Lite		Hampton Research
Natrix Screen		Hampton Research
PEG/ION-Screen		Hampton Research
JBScreen 8		Jena Bioscience
JBScreen 9		Jena Bioscience
Anion Screen		Nextal Biotechnologies
JCSG Core suite I-IV		JCSG
PACT Screen		Qiagen
Liquidator		Steinbrenner lab systems
12-well plattes		Nelipak bv
96-well plattes		Greiner Bio-one
Microplate sealer	AMPLIseal^{TM}	Greiner Bio-one
Nylon loops		Hampton Research
Cover glass	22 x 22 mm	VWR international
Microscope	SZ60	Olympus

Other

Concentrator	Amicon Ultra- 15ml	Millipore
Tipps		Greiner Bio-one
Filters	0.22 µm	Millipore
Acupuncture needle		B-braun

2.3. Chemicals buffers and media

Ammonium persulfate (APS)		Merck
Bromophenol blue		Serva
Dithiothreitol (DTT)		AppliChem
Glycerin		Merck
Isopropyl thiogalactoside (IPTG)		
Protease inhibitor cocktail	Complete	Roche
N,N,N',N'- Tetramethylethane - 1,2 diamine (TEMED)		Merck
Agar		Roth
Peptone (casein)		Roth
NaCl		Roth
Yeast extract		AppliChem

Protein Purification

Breaking buffer	500 mM NaCl, 50mM Tris/HCl (pH 8)
Histrap Buffer A	500 mM NaCl, 20mM Tris/HCl (pH 8)
Histrap Buffer B	500 mM NaCl, 20mM Tris/HCl (pH 8), 500 mM Imidazol
Gelfiltration Buffer	150 mM NaCl, 10mM Tris/HCl (pH 8 8)

Electrophoresis

TAE Buffer (1X)	40 mM Tris 20 mM Acetic acid ,10 mM EDTA (pH 8)
TBE Buffer (1X)	89 mM Tris, 89 mM Boric acid, 2mM EDTA (pH8)

Media

Luria Bertani (LB) - Medium	Peptone	10 g/l
	Yeast extract	5 g/l
	NaCl	5 g/l
LBKC-Medium	Peptone	10 g/l
	Yeast extract	5 g/l
	NaCl	5 g/l
	Kanamycin	50 µg /ml

	Chloramphenicol	34 µg/ml
LBKC-Agar	Agar-Agar in LB-Medium	16 g/l
	Kanamycin	50 µg/ml
	Chloramphenicol	34 µg/ml

2.4. Plasmids and bacterial strains

pET28 a (+) (Novagen)	lac Promoter, lac Repressor, Km^R
pUMVC3-hGNE1	CMV promoter, intron A, KmR

Strain	Phenotype
E.coli-BL21 Codon plus (DE3)-RIL (Stratagene)	*E. coli B F⁻ ompT hsdS(rB⁻ mB⁻) dcm⁺Tetr gal I (DE3)* *endA Hte [argU ileYleuW Camr]*
E.coli-XL10Gold (Stratagene)	*endA1 glnV44 recA1 thi-1 gyrA96 relA1 lac HteΔ(mcrA)183Δ (mcrCB-hsdSMR-mrr)173 tetR F'* *[proABlacIqZΔM15 Tn10(TetR Amy CmR)]*

2.5. Primers

Sequencing primers

FW primer	5'- taatacgactcactata- 3'
RV primer	5'- gctagttattgctcagcgg- 3'

Amplification primers

FWMNK_NdeI primer	5'-gtaccatatggaaaacctgtattttcagggcactctaagtgccttggccgttg-3'
RVMNK_XhoI primer	5'-gtacctcgagttattacctgcgtgttgtgtagtccag-3'

Mutaganesis primers

FWD517N	5'-ccctgtgtgtgggtagacaat**aat**ggcaactgtgctgccc-3'
RVD517N	5'-gggcagcacagttgcc**att**attgtctacccacacaggg-3'
FWD517A	5'-ccctgtgtgtgggtagacaat**gct**ggcaactgtgctgccc-3'
RVD517A	5'-gggcagcacagttgcc**agc**attgtctacccacacaggg-3'

The mutations with respect to the hmnk sequence are displayed in blue. The other two nucleotides corresponding to the mutated codon are displayed in red.

2.6. Enzymes, kits and ladders

NdeI		NEB
XhoI		NEB
T4-ligase		NEB
Vent-Polymerase		NEB
2-log DNA ladder	(0.1 - 10 Kilobases)	NEB
Protein ladder- p7702L	(6.5- 212 Kda)	NEB

Kits

Wizard Plus SV Minipreps DNA Purification System	Promega
Wizard SV Gel and PCR Clean-Up System	Promega
Quick change II XL Site-Directed Mutagenesis Kit	Stratagene

3. METHODS

3.1. Cloning

The DNA fragment coding for the N-acetyl mannosamine kinase domain (hMNK) of human GNE1 (amino acids 406 to 720) was amplified by PCR from the plasmid pUMVC3-hGNE1 (Reinke et al. 2009) using the primers FwMNK-NdeI and RvMNK-XhoI. The PCR product was loaded into a 1% agarose gel. A band of 945 bp, corresponding to the amplified *hmnk* was extracted from the gel and digested with the restriction enzymes NdeI and XhoI for 3 hours. After digestion the sample was loaded into a 1% agarose gel and extracted again. The overexpression plasmid pET28a (+) was digested with the same enzymes and purified in the same way. Finally, the digested and purified plasmid and PCR product were ligated overnight using the enzyme T4-ligase. The chemically competent overexpression strain *E.coli BL21 Codon Plus (DE3) RIL* was transformed with the ligation mixture (3.1.4) and the transformation reaction was streaked out on an LBKC agar platte. The resulting plasmid pET28a-MNK was extracted from cultures inoculated with the colonies that appeared in the selection plates and verified by sequencing.

3.1.1. Polymerase chain reaction (PCR)

A PCR from the DNA fragment coding for amino acids 406 to 720 of hMNK was performed using a Tpersonal Thermocycler from Biometra. The primers used for the reaction are specified on section 2.5, and the reaction program and mixture are specified below:

Reaction mixture (100µl):	PCR program:		
20 ng Template (pGNE)	1.Denaturation	5s at 94 °C	
10 pmol FW primer (2.5)	2.Annealing	30s at 58 °C	
10 pmol RV primer (2.5)	3.Elongation	60s at 72 °C	
1 X Thermopol Buffer (NEB)	4.Denaturation	30s at 94 °C	
0.2 mM dNTP	5.Annealing	30s at 62 °C	30 x
2 U Vent polymerase	6.Elongation	60s at 72 °C	
2 %(v/v) DMSO	7.Pause	4°C	

3.1.2. Agarose gel DNA extraction

The complete PCR product mixture was loaded into a 1% agarose. The DNA band corresponding to the desired amplified *hmnk* fragment was visualized with a Gel imager (INTAS) under UV-light (312 nm), cut and extracted using the PROMEGA kit "Wizard SV Gel and PCR Clean-Up Systems" following the kit instructions.

3.1.3. DNA digestion

The purified DNA and the plasmid pET28a(+) were then digested with restriction enzymes NdeI and XhoI (NEB). The digestion reaction was set up to a final volume of 100 µl and contained 80 units of each restriction enzyme and 2-5 µg of plasmid or PCR product. The digestion reaction was carried out under the conditions suggested by NEB for four hours and at 37 °C.

3.1.4. DNA ligation

The digestion reaction created a plasmid and an insert with cohesive ends that were ligated using the enzyme T4-DNA-ligase (NEB) and following the instructions of the manufacturer. The ligation mixture was set up to a final volume of 20 µl. Prior to the ligation, an aliquot of both, insert and plasmid, was loaded into an agarose gel and visualized to estimate the relative quantity. Based on this visual observation, the plasmid/insert ratio used for the reaction was 3:1.

3.1.5. Preparation of chemically competent cells

200ml LBC medium were inoculated with 0.5 ml *E.coli*-BL21 Codon plus (DE3)-RIL (Stratagene) overnight culture and incubated by shaking and 37°C until a $OD_{600nm}= 0.4$ was reached. The cells were centrifuged (3000 rpm, 10 minutes, GSA-Rotor, 4°C) and resuspended in 20 ml ice-cold sterile $CaCl_2$ solution (100 mM CaCl2, 20% Glycerol). After 20 minutes further incubation on ice, the cells were centrifuged and resuspended with the $CaCl_2$ solution once again. Finally, the cells sere centrifuged once again, and

resuspended in 1ml CaCl2 solution. The resulting chemically competent cells were aliquoted in 50 or 100 µl portions, shock frozen in liquid nitrogen and stored at -80°C.

3.1.6. Transformation (Heat shock)

A 100 µl aliquote of chemical competent *E.coli*-BL21 Codon plus (DE3)-RIL (Stratagene) cells was thawed on ice. 5 µl of the ligation mixture (3.1.4) were added and gently mixed with the cells. After 30 minutes incubation on ice, the mixture was warmed in a water bad at 42°C for 30 seconds and again 2 minutes on ice. Then, 400µl LB-Medium were added to the mixture and this was incubated in the shaker (200rpm) at 37°C for 45 minutes. The cells were finally streaked out on LBKC-agar plates and incubated overnight at 37°C.

3.1.7. Colony PCR

The colony PCR allows to quickly screen newly transformed clones in order to find a positive one. Twelve colonies were selected and used to simultaneously inoculate 3 ml of LBKC, an LBKC-agar plate and a PCR reaction mixture prepared as described before (3.1.1) but omitting the template.

The PCR reaction was carried out under the already described conditions (3.1.1), loaded on a gel and visualized under UV-light (312nm). The 3 ml liquid LBKC-medium inoculated with positive clones (clones showing the corresponding amplified band on the gel after the PCR) were incubated overnight in a shaker (200 rpm) at 37°C.

3.1.8. Plasmid preparation

The plasmids were prepared using the Wizard Plus SV Minipreps DNA Purification System from Promega following the manufacturers protocol.

3.1.9. DNA Sequencing

Plasmid sequencing was performed by Eurofins MWG Operon (Ebersberg) or Seqlab (Göttingen) following the cycle sequencing method, a modification of the traditional Sanger sequencing method (www.eurofinsdna.com). For every reaction 2 µg plasmid DNA were prepared (3.1.2). The sequencing primers (2.5) were synthesized by Eurofins MWG Operon. The resulting sequences were analyzed and compared with the wild type sequence using the SDSC biology work bench portal (http://workbench.sdsc.edu).

3.1.10. Clone and plasmid storage

The *E.coli* overexpression strains were prepared for long time storage as follows: 20 ml LBKC were inoculated with a single colony of the clone to be stored and incubated in a shaker (200 rpm) at 37°C until an OD_{600} of 0.8 was reached. The bacterial suspension was then gently mixed with Glycerol (1:1), shock frozen in liquid nitrogen and stored at -80°C.

A backup of the plasmids was also prepared (3.1.8) and stored at -20°C.

3.1.11. *In vitro* DNA-Mutagenesis

The *hmnk* mutants D517N and D517A were prepared with the kit Quick change II XL Site-Directed Mutagenesis (Stragagene) prepared following the instructions of the manufacturer. The primers were designed (2.5) according to the provider indications. 20 ng template plasmid (pET28a-MNK) and 200 ng of every primer were used for the PCR reaction that was performed using the Thermocycler Tpersonal from Biometra.

HIBM mutants were prepared similarly to wild-type MNK using the same PCR primers and conditions. MNK mutants N519S, F528C, I587T, A631T, A631V were cloned using pFastBac-hGNE1 mutants, with the respective *gne* mutation, as templates [83]. For the M712T mutant the template used was the pBluescript-hGNE1 construct [91].

3.2. Protein expression and purification

3.2.1. Expression test (small scale expression)

To find the optimal conditions for protein overexpression, the variables temperature (18°C, 37°C), time (3h, overnight) and concentration of inducing agent, IPTG were tested. 3ml LBKC-Medium were inoculated with 3µl of a pre-culture (3.2.2) and at OD_{600}=0.6 induced with IPTG to the final concentration of 0.1 mM or 1mM and incubated at 37°C in the shaker (200rpm). Prior to the induction and after 3h growth of a cell culture samples (1ml each) were extracted, centrifuged (13000 rpm, 5 minutes), the supernatant was discarded and the remaining cell pellet was resuspended in SDS-sample buffer (3.3.2) and heated at 95 °C for 5 minutes. The rest of the culture was incubated overnight and then, a 1 ml aliquot was collected and treated in the same way after 18h. The same experiment was repeated at 18°C. All the samples were then loaded into a 17.5 % SDS- polyacrylamide gel (3.3.2), stained, and the expression pattern of the protein obtained under the different conditions was evaluated.

3.2.2. Pre-culture

Pre-cultures were prepared by inoculating 200 ml LBKC- medium with a single colony of the overexpression strain *E.coli* pET28a-MNK (3.1) or with 50 µl of glycerol stock (3.1.10) and the cells were incubated at 37°C in the shaker at 200 rpm.

3.2.3. Protein overexpression

Eight 1 liter flasks with fresh LBKC-medium were inoculated 1:100 with the pre-culture of the corresponding *E.coli* overexpression strain and incubated at 37 °C by shaking (200rpm) until an absorbance of approximately 0.6 at 600 nm was reached. The cultures were cooled to 18 °C, and the protein expression was induced with IPTG supplied to a final concentration of 1 mM. The incubation was continued for additional 20 hours at 18 °C in a shaker. The cells were harvested by centrifugation at 6000 x g for 15 min at 4 °C, resuspended in 50 ml breaking buffer (50 mM Tris HCl pH 8, 500 mM NaCl), frozen and stored at – 20 °C.

3.2.4. Cell disruption

The thawed cell suspension was placed on ice and complemented with a tablet of EDTA-free complete protease inhibitor cocktail (Roche) and 10 µg/ ml DNase I prior to cell disruption. The cells were broken by three pressure cycles at 1000-1500 bar at 4 °C using an Emulsiflex C5 homogenizer (Avestin, Germany).

3.2.5. Ultracentrifugation

Cell debris were removed by centrifugation at 38,000 rpm for 1 h at 4 °C (Beckman, Ti45 rotor). The supernatant was sterile filtered (Steriflip 0.22 µm, Millipore, Germany) before loading it on a Nickel-NTA affinity column.

3.2.6. Chromatographic purification

The strategy designed for the purification of hMNK and all the variants included a two steps purification process, one Ni-NTA affinity (3.2.6.1) and one size exclusion chromatography (3.2.6.2). All chromatographic steps were performed at 4°C using an ÄKTA purifier (GE Healthcare) and monitored at 280and 260nm.

3.2.6.1.   Ni-NTA affinity chromatography

The filtered cell lysate was added onto a Histrap 5ml column (GE Healthcare, Germany). The column was washed with 20 column volumes (CV) of Histrap buffer A (2.3). To elute the protein the column buffer was slowly exchanged by Histrap buffer B (containing 500 mM Imidazol) using a gradient of 15 CV. The collected fractions were analyzed by SDS-PAGE in a 17.5 % sodium dodecylsulfate (SDS) polyacrylamide gel that was stained with Coomassie-Blue as described (Laemmli *et al*., 1973). The MNK-containing fractions were pooled and concentrated using an Amicon-Ultra-30k centrifugal filter (Millipore, USA) by centrifugation at 4000 rpm (Eppendorf, Germany) to a final volume of 2 ml for size exclusion chromatography.

3.2.6.2.   Size exclusion chromatography

Size exclusion chromatography was carried out with a preparative Superdex S-75 26/60 column (GE Healthcare, Germany). The sample was injected with a final volume of 2 ml to the column and eluted with 10 mM Tris-HCl pH 8, 150 mM NaCl with a flow rate of 2.5 ml/ min. The eluted fractions were monitored by measurement of the OD at 280 nm and checked for purity by SDS-PAGE in a 17,5 % SDS-polyacrylamide gel that was stained with Coomassie-Blue. Fractions containing pure MNK were pooled and concentrated using an Amicon-Ultra-30k centrifugal filter (Millipore, USA) to a final concentration of 15 mg/ml and used for crystallization setups.

3.2.7.   hMNK digestion with TEV or Thrombin

Initially, the designed purification strategy included the digestion of hMNK after the Ni-NTA column with TEV protease, and posterior repetition of the Ni-NTA chromatography collecting the digested protein on the flow-through to finally perform a gel filtration chromatography. For this procedure, a TEV protease cleaving site was introduced with the primers during the cloning process, at the N-terminus of the protein (3.1 and 4.1). However, the cleavage of the hexa-histidine tag either with Thrombin of TEV protease resulted in protein precipitation and this step was omitted.

For the proteolytic digestion, the pooled fractions after Ni-NTA chromatography were concentrated to a final volume of 10 ml, the enzyme was added, the mixture was loaded into a dialylsis bag (10 KDa pore size) and overnight digested and dialyzed against buffer histrap A.

3.3. General biochemical methods

3.3.1.   Agarose gel electrophoresis of DNA

The agarose gels were prepared mixing 1% (w/v) agarose with 1 X TAE buffer (40 mM Tris, 20 mM acetic acid, 10 mM EDTA (pH 8)) and heating the mixture until the agarose was completely dissolved. Subsequently, the mixture was slowly cooled down until a temperature of approximately 50 °C was reached, ethidium bromide was added to a

final concentration of 50 µg/ml and poured into a gel chamber (10 cm x 7 cm x 1cm) where it was let for circa 20 minutes to polymerize.

The samples were prepared by mixing the DNA with DNA-Sample buffer (5x) in a 5:1 volume ratio and loaded into a gel. The electrophoresis was performed applying a voltage of 12V/cm for 1 hour in 1X TAE buffer. The DNA bands on the gel were finally visualized under UV-light (312nm) using a gel imager (INTAS).

DNA-Sample buffer (5x)
0.25 % Bromophenol blue (w/v)
0.25% Xylen Cyanol (w/v)
40 % D(+)-Saccharose (w/v)

Electrophoresis buffer (1x)
40mM Tris
1.142 % Acetic acid (v/v)
1mM EDTA, pH 8.0

3.3.2. Discontinuous denaturing sodium dodecyl sulfate polyacrylamide gel electrophoresis (SDS-PAGE) of Proteins

The SDS polyacrylamide gels (11 cm x 8.5 cm x 0.2 cm) are composed of a stacking gel (4% polyacrylamide) and a separating gel (17.5 %). The gel polymerization was induced by addition of 0.05% (v/v) ammonium persulfate (APS) and 0.05 % (v/v) N, N, N', N' –tetramethyl diamine (TEMED). The samples were prepared by mixing 20 µl of protein solution with 20 µl of sample buffer 5x, and heated to 95°C for minutes. The electrophoresis was performed applying a voltage of 20 V/cm.

The gels were immersed in Coomassie blue staining solution for 20 minutes for staining and finally destained with boiling water for 15 minutes.

Sample buffer (5x):
50 mM Tris/Hcl, pH 7.0
10 % Lauryl sulfate (w/v)
0.1 % Bromophenol blue (w/v)
1 % 2-Mercaptoethanol (v/v)
14% Dithiothreitol (DTT) (w/v)
10 % Glycerol (v/v)

Electrophoresis buffer:
25 mM Tris/HCl, pH 8.3
1.44 % Glycin (w/v)
0.1 % Lauryl sulfate (w/v)

Coomassie Staining solution:
0.5 % Coomassie Brilliant-Blue G250 (w/v)
6.25 % Ethanol (v/v)
4.25 % Perchloric acid (v/v)

3.3.3. DNA concentration determination

The determination of the DNA concentration was performed measuring the absorption of the DNA containing solution at a wavelength of 260 nm with a Nanodrop-ND 2000c (PEQLAB Biotechnologie). 1μl sample was used for every measurement. The concentration was calculated using the Beer–Lambert law:

$$A = \mathcal{E} \times c \times l$$

where:

A= Absorption of the sample at 260 nm

ε = Molar extinction coefficient of the sample

c= Concentration of the sample

l= Path length (1mm for the Nanodrop 200c machine)

The extinction coefficients of the DNA-primers were determined by the manufacturer (TIB molbiol). For plasmid-DNA the concentration was calculated assuming that for a path length of 1 cm, the absorption at 260 nm of 50μg/ml is equal to 1.0.

3.3.4. Protein concentration determination

3.3.4.1. UV-absorption

The concentration was calculated measuring the absorption of the protein sample at 280 nm and applying the Beer-Lambert law as described in section 3.3.3. The extinction coefficient for hMNK was calculated using the program ProtParam (http://www.expasy.org/tools/protparam.html).

3.3.4.2. Bradford test

Alternatively, the protein concentration was photometrically determined (Ultrospec 3100pro, Amersham Pharmacia) by Bradford [92] at a wavelength of 595nm following the instructions of the manufacturer (BioRad).

3.4. Protein characterization

3.4.1. Kinase activity test

The kinase activity tests were realized by Long Duc Nguyen (Charité Universitäts Medizin- AG Fan). The kinase activity of recombinant MNK was determined spectrophotometrically, using a coupled enzyme ATPase assay. The reaction was initiated by addition of hMNK (0.1-1 µg) to the kinase assay reaction mixture (final volume of 200µl), incubated for 20min at 37°C and stopped by adding 800µl of 10 mM EDTA. The decrease of NADH was monitored at 340mM.

Kinase assay reaction mixture
60 mM Tris.HCl pH 8.1
10 mM $MgCl_2$
5 mM ManNAc
10 mM ATP
0.2 mM NADH
2 mM phophoenolpyruvate
2 U pyruvate kinase
2 U lactate dehydrogenase

To determine the Km, the kinase activity was measured at different substrate concentrations of ManNAc and ATP, respectively. The obtained activity was graphed double reciprocally, and Km was determined from an average of 4 independent measurements.

MNK kinase activity was measured for different substrates ManNAc, GlcNAc, ManNProp and GlcNProp. The highest affinity (hMNK for ManNAc) was set to 100 %. The specificity of the cited substrates is given relative to the ManNAc activity.

The effect of the inhibitors was determined measuring the kinase activity of hMNK at 250 µM ManNAc and 5 mM of the inhibitors GlcNProp, 3OMeGlcNAc, 6OAcManNAc.

3.4.2. Circular Dichroism Spectroscopy (CD-Spectroscopy)

Using CD-Spectroscopy it is possible to determine the secondary structure content (far UV) and the changes in the tertiary structure (near UV >250nm) of proteins [93]. The CD-Spectrum is based on the difference in extinction coefficients of a chiral molecule for left and right circularly polarized light. This difference is measured in the form of ellipticity (Θ_λ).

The measurements have been performed in the far UV Spectrum using a JASCO J-810 CD-Spectrometer under a constant nitrogen gas stream of 3 l/min. All measured samples were in gelfiltration buffer (2.3), the path length of the cuvette was 1 mm and the ellipticity for the spectrum range (195 nm to 240 nm) was monitored. The mean residue molar ellipticity was calculated with the following equation:

$$[\Theta_\lambda] = (0.1 \times \Theta_\lambda) / (c \times d \times n)$$

Where Θ_λ is the ellipticity in degrees, c the protein concentration in mol/l, d the path length in cm and n the number of amino acids in the protein. The units of the mean residue molar ellipticity are (deg x cm^2)/dmol.

To determine the secondary structure content, the data between 195 nm and 240 nm was loaded into the program CDSSTR [94] using the DichroWeb-Server [95] platform (http://dichroweb.cryst.bbk.ac.uk/html/home.shtml).

3.4.3. Isothermal Titration calorimetry (ITC)

The protein concentrations (432 µM for wt-hMNK and 110 µM for the variant D517N) were determined by UV spectroscopy using as absorpion coefficient 18450 M^{-1} cm^{-1}. The protein and the ManNAc solution (1 mM) were prepared in gelfiltration buffer (2.3). The experiments were performed using an ITC 200 (Microcal). 280 µl protein solution were placed in the calorimeter cell and the injection syringe was loaded with ManNAc solution. After thermal equilibration at 30°C and 1 minute initial delay, 20 consecutive injections of 2 µl ManNAc solution were made into the calorimeter cell under continuous stirring (1000 rpm). The injection spacing was 150 seconds, which allowed complete reequilibration. The data was fitted to a one-site model and the corresponding K_D calculated using the software Origin 7 (Microcal).

3.5. Crystallographic methods

3.5.1. Crystallization

Crystals of the binary complex hMNK/MNK were obtained by co-crystallization using the vapor diffusion method [96]. All the samples were centrifuged for 5 minutes at 13000 rpm before initiating the crystallization experiments. The first screenings were performed using 96-well sitting drop plates and diverse commercial screenings (2.2). 100 µl crystallization solution was added in each reagent well. Every reagent well contained three sample drop wells, which were used to test different ratios between protein solution (P) and the precipitating agent (W). In each well three different drops were set up by mixing 2µl P + 1 µl W, 1µl P + 1 µl W and 1µl P + 2 µl W. The plates were sealed and incubated at 18°C and the growth of crystals periodically examined (daily during the first week and once a week the following 2 months).

Once initial crystallization conditions were found by the screening method described above, the crystals were optimized by the hanging drop method. To this extent, 12-well plates were used. 500µl precipitant agent were added to every well, and the drops were set up by mixing equal volumes (2 µl) of complex solution (15 mg/mL protein in gelfiltration buffer and 2 mM ManNAc) and reservoir solution (0.2 M calcium acetate, 0.1M sodium cacodylate pH 6.5 and 40% PEG 300) on a cover glass. The wells were sealed by placing the cover glasses upside-down on Vaseline-greased plates.

3.5.2. Soaking experiments

To obtain the ternary complexes crystals of the binary hMNK/ManNAc complex were soaked with ADP or ATP or AMPPCP. The cover glass containing the crystals was turned and the mother liquor stepwise replaced by the soaking solution containing 0.1 M sodium cacodylate pH 6.5, 50 % PEG 300 and 20 mM ADP or ATP or AMPPCP. The stepwise replacement was made by adding 1µl soaking solution, mixing and removing 1µl mother liquor (4 times).

3.5.3. Data collection and processing

Given the high PEG 300 concentration present in the mother liquor, no further cryoprotectant was required to avoid ice formation. Crystals were mounted on Nylon loops (Hampton research) and directly flash-frozen in liquid nitrogen prior to data collection. During the data collection, the crystals were rotated in the X-ray beam and cooled using a nitrogen gas stream at 100°K. Previous to data collection two images were collected at 0° and 90°. Using the program MOSFLM [97] the images were indexed and the crystal system determined. MOSFLM offers also an interface called STRATEGY that was used to predict the optimal oscillation angle, the best orientation to start the data collection and the rotation angle necessary to obtain a complete data set. The exposure time was chosen to take account of two main directives: on the one side the exposure time should be long enough to become a good intensity signal for the higher resolution reflexes and on the other side short enough to avoid overloaded reflectionss (the intensity is too high, the detector pixels are oversaturated and the reflection is not measured correctly) and crystal radiation damage.

All data sets were collected from single crystals at beam line BL 14.2 at BESSY, Berlin at 100°K and 0.918 Å wavelength with a fast scanning MX-225 ccd-detector from Rayonics (Evanston, USA). The data was integrated, reduced and scaled using XDS [98].

3.5.4. Solving the phase problem

The structure of the MNK/ManNAc complex was solved by molecular replacement using the program MOLREP of the CCP4 program suite [99]. A monomer from the previously published dimeric structure of the apo-form from MNK (PDB code 3EO3) was used as search model. The first solution located one kinase monomer in the asymmetric unit.

3.5.5. Model refinement and validation

The solution obtained by molecular replacement (3.5.4) was subjected to rigid-body refinement, followed by iterative cycles of TLS and restrained-maximum likelihood refinement, including isotropic temperature factor adjustment with REFMAC [100] and

by manual rebuilding using COOT   [101]. During this process, 5% randomly selected reflections have been used to calculate Rfree to monitor bias during model building and refinement. Water molecules were added using COOT and the model was validated using MOLPROBITY [102]. The refined structure of the MNK/ManNAc was used as search model to solve the structures of the other three complexes (MNK/ManNAc/ADP, MNK/ManNAc-6P/ADP and MNK/ManNAc/AMPPCP). The refinement of the latter complexes was performed as described above. The atomic coordinates and structure factors have been deposited in the Protein Data Bank under accession codes 2YHW (hMNK/ManNAc), 2YHY (hMNK/ManNAc/ADP) and 2YI1 (hMNK/ManNAc-6P/ADP). The coordinates and data for the model for the complex hMNK/ManNAc/AMPPCP have not been deposited in the databank, since the data quality was not good enough to guarantee the reliability of the model as explained in section 4.13.

3.5.6. Structural comparison and picture preparation

The superimposition of the protein structures was performed with the programs COOT [101], DALI [103] and PYMOL [104]. This latter one was also used for pictures preparation. The DALI server compares the positions of the $C\alpha$-atoms of the amino acids between a query model and the proteins present in the PDB databank and calculates the root mean-square deviation for them.

3.6. Preparation of 6-O-Acetyl ManNAc

The synthesis of the 6-O-Acetyl ManNAc was developed and performed by Dr. Reinhold Zimmer (Institut für Chemie und Biochemie-Organische Chemie, FU Berlin) as follows. ManNAc (442 mg, 2 mmol) was dissolved in pyridine (10 mL). *O*-Acetylpropanon-oxime (207 mg, 1.8 mmol), 4 Å-molecular sieves (100 mg) and lipase AY30 (1.1 g) were added, and the suspension was stirred vigorously at 50 °C. After 5 days additional lipase AY30 (1.1 g) was added and the suspension stirred for additional two days at the same temperature. The lipase was removed by filtration and the precipitate was washed with MeOH (10 mL). After addition of toluene (15 mL) the solvents were removed by a rotary evaporator, this process was repeated with another 10 mL of toluene and the resulting crude product was purified by flash chromatography (silica gel, EtOAc:MeOH:H_2O= 25:4:1) to yield 6-*O*-acetyl ManNAc (18 mg, 4%).

4. RESULTS

4.1. Cloning and protein purification

First trials with a clone expressing hMNK as GST fusion protein yielded no crystals, suggesting that the polypeptide length plays a crucial role in protein crystallization. An addition or deletion of one single amino acid can drastically change the physicochemical properties of a protein and consequently its ability to form crystals. Therefore, a new construct was designed based on the length of the published apo-structure [84], that proved to be prone to crystallize. The plasmid was prepared as described in materials and methods and transformed into the *E. coli* strain BL21-Codon plus-(DE3)-RIL (Stratagene). Even if a bacterial host was used to express a human protein, no codon usage optimization at DNA level was necessary. Nevertheless, protein expression could be only obtained using the above cited *E coli* strain, which is modified with additional tRNA genes that are otherwise rare in *E. coli*.
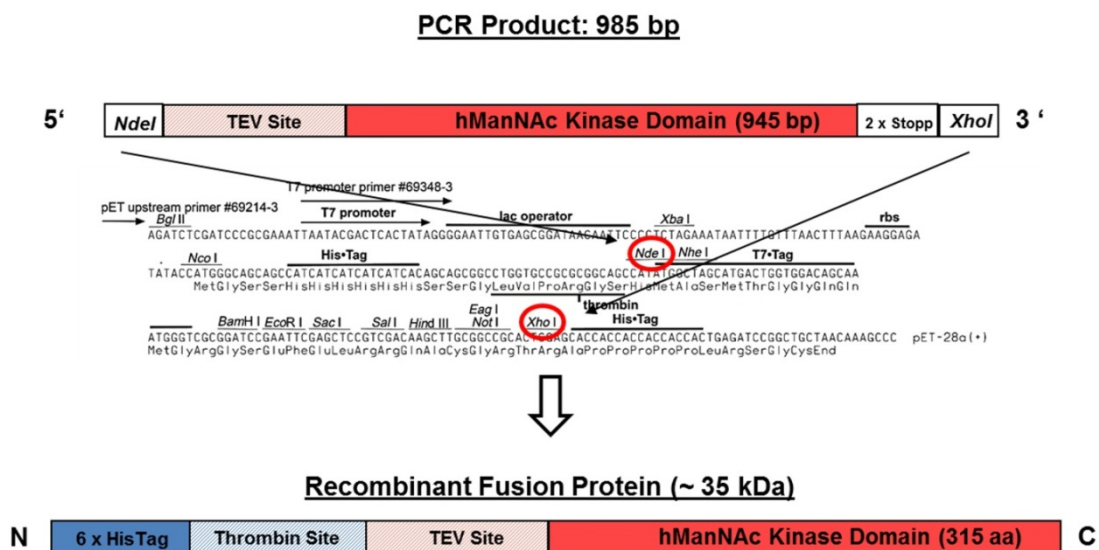
Figure 4.1 Schematic view of the cloning strategy and the resulting recombinant protein. The PCR product was ligated between the restricted sites indicated by arrows and in a red circle. The corresponding DNA fragment beween the two circled enzymes was removed by digestion (3.1.3).

After the culture conditions were optimized we could obtain a very good expression yield (over 26 mg pure protein per liter culture) by cultivating cells at 18°C and

overnight in LB medium. The expressed protein was a fusion of the MNK domain of GNE (amino acids 406 to 720-Uniprot code Q9Y223) to a hexa-histidine (N-terminal) linked by a thrombin site (from the original vector) and an additional TEV protease site that was introduced with the primers (Figure 4.1)

After cell disruption and centrifugation of cell debris, His_6-hMKN was present in the supernatant fraction. A two steps purification process (Histrap column –GE Healthcare-followed by size exclusion chromatography- S75, GE Healthcare) was sufficient to obtain His-hMNK with the purity required (>95 %) to perform crystallization trials.

Removing of the His-tag, either with thrombin or TEV, resulted in hMNK precipitation at concentrations higher than 10 mg/ml. For this reason and since the undigested protein yielded high quality crystals (see sections 4.3.2 and 4.3.3) the His-tag was not removed.

The size exclusion chromatography was monitored at 280 nm and shows mainly a single peak, indicating monodispersity for hMNK in solution. The retention time of the eluted protein corresponds to a molecular weight (M_W) of 70 KDa, which suggests that hMNK exists as a dimer in solution and correlates with the dimeric form found in the crystal structure (see section 4.5).
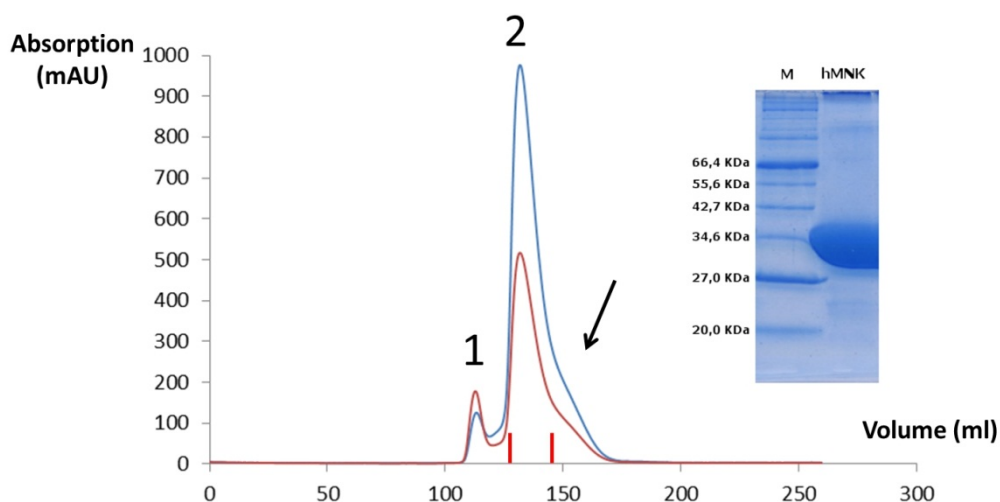
Figure 4.2 Size exclusion elution profile and SDS-PAGE of hMNK. hMNK was monitored at 280 nm (blue curve) and 260 nm (red curve). Peak #1 corresponds to aggregates. The elution volume for the main peak (#2, 132.5 ml) corresponds to a M_W of 70 KDa (S75 26/60-GE Healthcare). The small Peak shoulder (arrow) could be attributed to an equilibrium in solution between the monomer and dimer. The fractions between the red lines were pooled. The purity and correct size of hMNK was checked by SDS-PAGE. hMNK migrates at the expected M_W for a monomer under denaturing conditions.

The cloning of the HIBM mutants presented in this work was performed in the pET28a (+) vector (Novagen), as described in section 3.1.11. They were also purified as described for hMNK-His$_6$.

	Pure protein yield (mg Protein/ L culture)	Oligomerization
wtMNK	26	dimer
D517A	25,5	dimer
D517N	25,7	dimer
N519S	11,5	dimer
F528C	3,7	dimer
I587T	16,9	monomer
A631T	11,2	dimer
A631V	6,6	dimer
M712T	18,5	dimer

Table 4.1 Comparison of the protein expression yield and the oligomerization state (based on Gel filtration retention times) of wt-hMNK-His$_6$ and its HIBM related variants

4.2. Protein Characterization

4.2.1. Circular dichroism spectroscopy

The secondary structure content of wt-hMNK, the variants D517A and D517N, and the HIBM related variants were determined by CD-spectra. The aim of the experiments was to offer a structural basis to compare all MNK variants, since the attempts to determine the crystal structure of one of the HIBM related variants were unsuccessful. The case of D517A and D517N is slightly different. Based on the crystal structure of hMNK in complex with ManNAc, the residue D517 was presumed to play a catalytic role (4.8). In order to verify or deny this presumption, both variants were prepared and their enzymatic activity tested (4.2.3). However, a change in the enzyme activity after a point mutation could be either due to a loss of the specific catalytic activity or to a general tertiary structure disruption, which would surely impair the enzymatic activity. CD-spectroscopy aroused as the easiest and fastest method to answer this question. Figure 4.3 shows the normalized spectra of the wt-MNK and variants, D517A and

D517N and Table 4.2 shows the percentages of secondary structure determined for all variants.
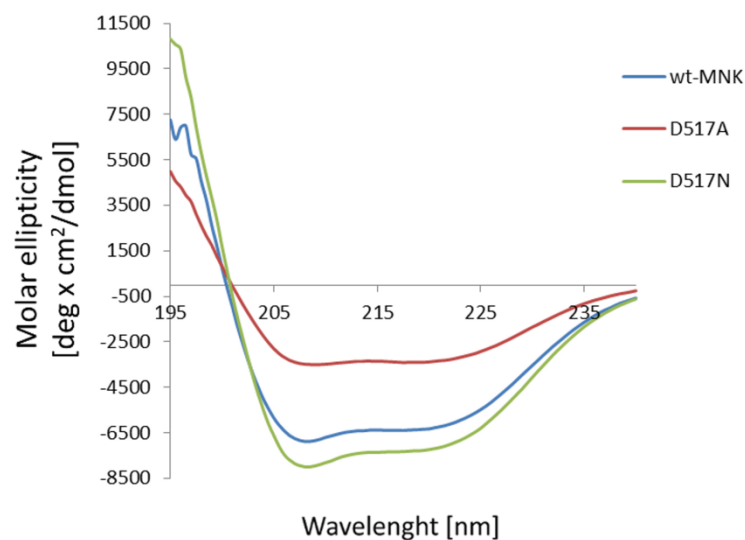
Figure 4.3 CD spectra for MNK and the two inactive variants D517N and D517A. CD-spectra for all the variants listed in Table 4.2 were measured, their molar ellipticity calculated and used to elucidate the secondary structure content. The curve graphically shows how a point mutation can affect the protein folding. This is especially evident for the α-helix content (with minimum at 222 nm) of D517A relative to the wild type and D517N.

	α-helix	β-sheet	Beta-turn	Random coil
Wt-MNK	20	24	18	38
D517A	16	26	18	40
D517N	23	22	18	37
N519S	15	27	18	40
F528C	10	31	18	41
I587T	11	30	18	41
A631T	10	31	17	42
A631V	12	29	17	42
M712T	11	30	17	42

Table 4.2 Secondary structure content for MNK and its variants

Furthermore, CD-spectroscopy was used to calculate a rough melting temperature for wt-hMNK in its apo form and in complex with its native substrate ManNAc. To this end the molar ellipticity was monitored at 222 nm while the temperature of the cuvette

containing the sample was continuously increased from 10°C to 80°C. The melting temperature for wt-MNK (15µM) was 44,60°C. After addition of 1mM ManNAc, the melting temperature decreases to 43,07°C, contrary to the expected stabilization of proteins upon substrate binding. However, such a variation is not significant and the addition of ManNAc in a 100-fold excess concentration might have changed the buffer conditions and be a reason for destabilization of this variant.

4.2.2. Isothermal titration calorimetry (ITC)

After it had been proven, that both variants were inactive (4.2.3) and that the secondary structure content of D517N and wt-hMNK did not differ significantly (4.2.1), it was important to determine whether the variants still retained the ability to bind ManNAc.
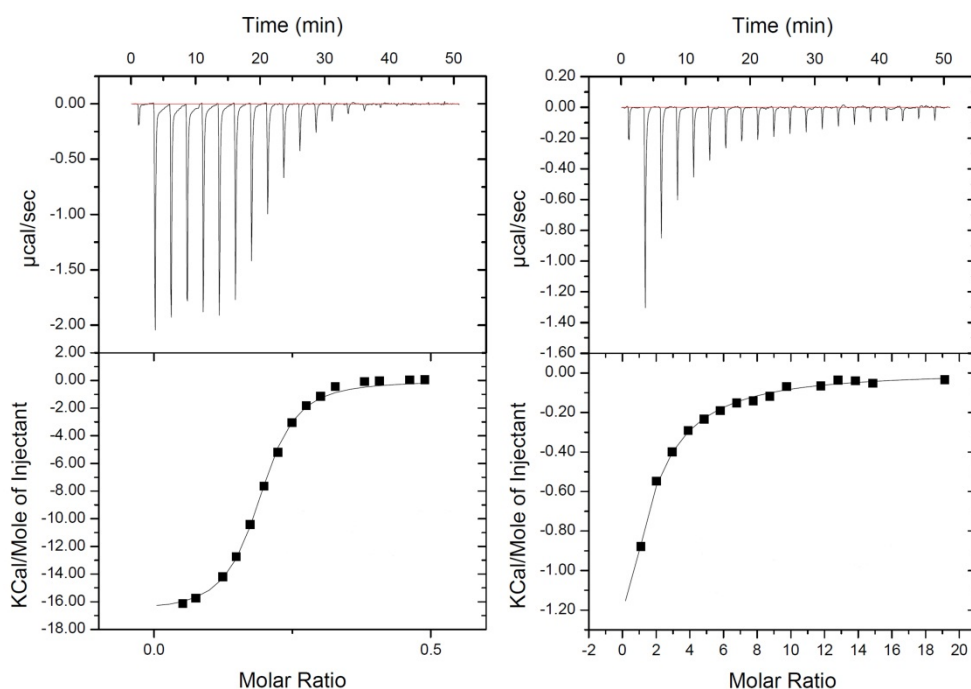
Figure 4.4   Isothermal titration calorimetry (upper part) for wt-MNK/ManNAc (left) and D517N/ManNAc (right) and their derived binding isotherm (lower part) . The titrations were performed as described (3.4.3). Binding isotherms were prepared by integrating the raw ITC data. The solid line in the binding isotherm graphic results from the nonlinear least-squares fitting to a one-site model.

The binding affinities of wt-hMNK for ATP and ManNAc had been previously determined based on the enzymatic reaction (in the form of Km). Though, given the complete enzymatic inactivation of the variants D517A and D517N, their binding affinity

for ManNAc could not be determined using the same technique. ITC offered the possibility to determine the binding affinity (in form of K_D) independently of the catalytic reaction.

The dissociation constants (K_D) determined for WT-MNK/ManNAc (2.5µM) and D517N/ManNAc (259µM) show that the mutation of D517 to an asparagine clearly diminishes (100-fold) the binding affinity of hMNK for ManNAc, as was expected given its direct implication in sugar binding. Upon mutation, the affinity has been two orders of magnitude reduced but not abolished. Finally, ITC experiments with D517A and ManNAc showed a very low (or non-existent) affinity and no K_D could be determined.

4.2.3. Enzymatic activity and specificity.

The specific activity of recombinant hMNK for its native substrate ManNAc (2.4 U/mg protein), was determined using a coupled enzyme ATPase assay monitored spectrophotometrically (3.4.1). The results correlate with the kinase activity of the full length GNE found in previous studies [83]. The relative specificity of hMNK for different ManNAc-related substrates was also checked. hMNK shows highly specific activity for ManNAc and almost no activity for GlcNAc or ManNBut (4 and 6 %, respectively). About 30% activity was observed for ManNProp. The activity of the different mutants (HIBM related, D517A and D517N) was also compared and the results of the comparison relative to the wild-type are shown in Table 4.3. Furthermore, kinetic experiments based on the enzymatic activity of hMNK made it possible to determine the Km for ManNAc (95 µM) and for ATP (4.4 mM).

Protein	Activity [%]
wt-hMNK	100
D517A	0
D517N	0
N519S	25
F528C	78
I587T	24
A631T	4
A631V	26
M712T	40

Table 4.3 Relative activity of wt-MNK and its mutants.

4.3. Crystal structure of the complex hMNK-ManNAc

The apo-hMNK structure was solved by Tong et al. [84] before we started this project. Therefore, we concentrated our efforts in improving the resolution (2.8 Å) and to solve the structure of hMNK in complex with its natural substrate ManNAc.

4.3.1. Crystal reproduction and soaking

First, we tried to reproduce the previously published crystallization conditions (15% PEG 4000, 0.2M ammonium acetate, 0.1 sodium citrate pH 6.0, [84]) and improve them using the fine screening method and the Additive Screen from Hampton research. The addition of additives produced no improvement. The quality of the crystals was slightly increased by fine-screening (12-16% PEG 3350, 0.2M ammonium acetate, 0.1 sodium citrate pH 5.4) and we could obtain a dataset at 2.6 Å resolution with the same space group P3$_1$21 and comparable unit cell constants (a=b=130.0, c=127.0) as published.
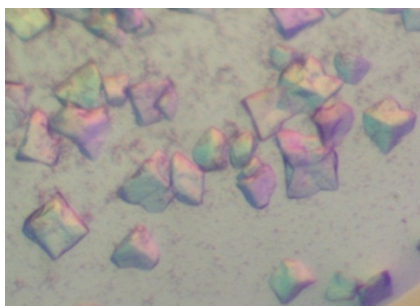
Figure 4.5. Apo-hMNK crystals The following conditions were used: Protein solution: 40 mg/ml hMNK, 5mM ADP, 1:100 (w:w) chymotrypsin. Reservoir: 12-16% PEG 3350, 0.2M ammonium acetate, 0.1 sodium citrate pH 5.4

This small upgrade was not significant for our aims, and these crystallization conditions yielded no crystals for the complex (hMNK at 40 mg/ml and 2mM ManNAc incubated at room temperature for 1 hour), but we could achieve a small success by soaking native hMNK crystals with 5mM ManNAc. This treatment significantly decreased the diffraction quality of the crystals. We could collect a complete dataset to a final resolution of 3.68 Å and solved the structure by molecular replacement using the apo-MNK as search model (PDB code 3EO3). Inspection of the final electron density revealed a clear peak in the difference map (Fo-Fc) that could be attributed to a ManNAc molecule. In this way, we could locate the substrate binding site but at this

resolution, the orientation of the sugar could not be assessed with reliability. (Figure 4.6c.
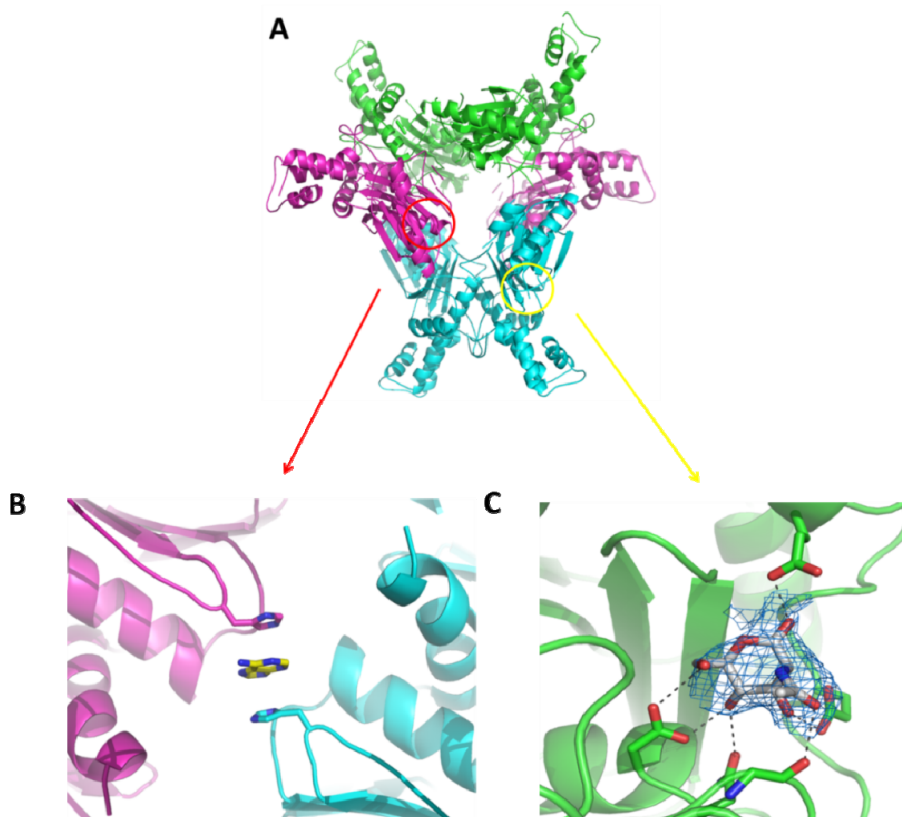
Figure 4.6 (A) Crystallographic hexamer. The hMNK apo-crystals contain three monomers per asymmetric unit (in green, blue and lila). Two of them (green with lila) form a natural dimer whereas the third one forms the dimer with one of the symmetry related mates. It has been previously hypothesized that this hexamer could have a biological relevance. Indeed, GNE multimerization has been described elsewhere before [55]. However, the interaction beween dimers in the crystal involves their respective N-terminal lobes. MNK is the C-terminal domain of the bifunctional enzyme GNE, and the epimerase domain is located at its N-terminus. Therefore, it seems sterically improbable that such an interaction could occur and we rather consider it a crystallographic artifact. **(B) Adenine mediates crystal contacts between symmetry mates.** The crystals were obtained when 5mM ADP was added to the protein solution. Surprisingly, no electron density attributable to ADP had been found in the former published structure [84]. A patch of electron density between the histidines 554 (displayed as sticks) of two symmetry related hMNK molecules could be ascribed to an adenine molecule (as sticks in yellow backbone). Either the flexibility of the unbound ribose and pyrophosphate makes these moieties invisible or the adenine ring is a trace product of ADP degradation. **(C) Localization of the ManNAc binding site.** Soaking of the apo-hMNK crystals with 5mM ManNAc allowed us to locate the sugar binding site and consequently the active site of the enzyme. Upon soaking, the crystal diffraction quality decreased (final resolution of 3.68 Å). The 2Fo-Fc map contoured at 1.0 σ (blue grid) can be attributed to a ManNAc molecule but the orientation cannot be unambiguously assigned. We modeled it based on the most plausible hydrogen bond contacts (black dots) with the surrounding residues.

We also tried to soak native apo-hMNK crystals with ATP, ADP and the not hydrolysable ATP analogues AMPPNP and AMPPCP but, after solving the structure, no electron density for the respective nucleotides could be found. We had been using chymotrypsin in our protein solution and we could not find any electron density for the residues 485 to 497 (the former structure missed residues 475 to 498 [84]). We initially assumed therefore, that the chopping of these residues allowed crystallization and that the missing residues were involved in nucleotide binding but not in sugar biding.

4.3.2. Co-crystallization of the complex hMNK-ManNAc

The complex was formed by gently mixing 5mM ManNAc with a 15 mg/ml hMNK purified solution in Gel filtration buffer. After incubation on ice no further separation or purification steps were performed. Diamond shaped crystals grew by mixing equal volumes (2 µl) of MNK in 0.2 M calcium acetate, 0.1M sodium cacodylate pH 6.5 and 38-46 % PEG 300 at 18°C and reached their maximal size within 4-5 days. These crystals were obtained without using chymotrypsin.

Figure 4.7 hMNK-ManNAc crystals

4.3.3. X-ray data collection and processing

The X-ray diffraction data for the co-crystallized complex was collected from a single crystal at beam line BL 14.2 at BESSY (Berlin) at 100°K and 0.918 Å wavelength using the fast scanning MX-225 ccd-detector. The data was integrated, reduced and scaled using XDS. [98] The resulting data set was complete to 1.65 Å resolution. After data processing we could assess that the crystals belong to the primitive tetragonal crystal system. The screw axes were then assigned looking for serial extinctions along the crystal axis h00 and 00l. In this way we could reduce the space group possibilities to the enantiomorphs $P4_12_12$ or $P4_32_12$. The discrimination between the two

enantiomorphs was only possible after solving the phase problem (4.3.4). The unit cell constants were a=b=90.73 c=100.78 α=β=γ=90°.

4.3.4. Determination of the hMNK-ManNAc structure

To solve the phase problem we used the molecular replacement method. Using the program PHASER [105] a rotation search followed by a translation search in the resolution range 30-3.0 Å was performed using the apo-MNK structure (PDB accession code 3EO3) as search model. A solution was found in space group $P4_12_12$ with only one kinase monomer in the asymmetric unit. The initial solution was then subjected to rigid-body refinement and to an iterative process of manual model rebuilding using the 2Fo- Fc and Fo-Fc electron density maps in COOT [101] and restrained-maximum likelihood refinement, including isotropic temperature factor adjustment with REFMAC. [106]

The refined 1.65 Å structure contains one MNK monomer in complex with one single molecule of ManNAc and 424 water molecules per asymmetric unit. High quality electron density allowed the building of the model with reliability for the major part of the kinase domain of human GNE and its native substrate. Only residues 601-625, corresponding to a loop, were poorly defined in the electron density maps, and no electron density could be attributed to residues 617-620 that are consequently missing in the final model. The stereochemical quality of the structure has been checked with PROCHECK [107]. Data collection and refinement statistics for the binary complex hMNK-ManNAc is shown in Table 4.4.

	MNK /ManNAc
Data collection	
Beamline	BESSY MX 14.2
Space group	P 41 21 2
Unit Cell (Å)	a= b= 90.7; c= 100.8
	α= β= γ= 90°
Nominal resolution (Å)	45.3 – 1.64
Outermost resolution shell (Å)	1.73-1.64
Unique reflections	52083 (7584)
Completness (%)	100 (100)
Redundancy	12.9 (12.9)
Rmerge	5.8 (72.5)
Rmrgd-F	5.9 (39.5)
Mean I/σ(I)	30.66 (4.37)
Refinement	
Rwork / Rfree (%)	14.8/17.0
r.m.s.d. From ideal geometry	
Bond lengths (Å)	0.026
Bond angles (°)	2.068
Dihedral angles (°)	6.637
Chiral center restraints	0.157
Mean B-factor (Å2)	
Overall model	25.7
Protein atoms	25.2
Sugar	12.5
ADP	-
Ramachandran Plot statistics	
Most favored regions(%)	91.3
Additional allowed regions (%)	8.3
Generously allowed regions (%)	0.0
Disallowed regions (%)	0.4
PDB ID	2YHW

Table 4.4 Data collection, refinement and Ramachandran plot statistics for the hMNK/ManNAc structure. The highest resolution shell values are indicated in parenthesis. $R_{merge}= \Sigma h \Sigma i\ |I(h,i)-\langle I(h)\rangle| / \Sigma h \Sigma i\ I(h,i)$, where $I(h,i)$ is the intensity value of the *i*th measurement of an equivalent reflection with indices h,k,l and $\langle I(h)\rangle$ is the corresponding mean value of I(h) for all i measurements. R_{mrgd-F} evaluates the quality of the amplitudes of a dataset and and has been listed as an alternative to R_{merge}, since R_{mrgd-F} is redundancy independent whereas R_{merge} is flawed in data with higher redundancy [108]. $R_{work}= \Sigma\ |F_O-F_C| / \Sigma\ |F_O|$, where F_O and F_C are the observed and a calculated structure factors, respectively. R_{free} is the R factor calculated using 5% of the reflections that are otherwise not used in the refinement. R.m.s.d (root mean-square deviation). The Ramachandran plot shows only one residue located in disallowed region, the Glutamate

612. This residue forms part of a region with poorly defined electron density and can therefore be considered as a modeling problem rather than a real feature of the protein.

4.4. The overall structure of the hMNK-ManNAc monomer

As displayed in Figures 4.8A and 4.8B, the secondary structure of hMNK is composed of two clearly differentiated domains: the N-terminal domain is composed of residues 406-528 and 703-717 (colored cyan and yellow respectively) and the C-terminal domain (red) contains residues 536-699. Both domains are connected by two flexible loops or hinges (colored green) allowing the hMNK to change from an open conformation to a closed one upon substrate binding.

The N-terminal domain is composed of a central 5-stranded mixed β-sheet ($\beta7$, $\beta4$, $\beta1$, $\beta2$, $\beta3$ - where $\beta2$ is antiparallel to the other strands) flanked by $\alpha1$ and $\alpha2$ on one side and by $\alpha11$ and $\alpha3$ (yellow) on the other side, protruding from the C-terminal domain. Two further β strands ($\beta5$ and $\beta6$) form a hairpin β-sheet in the loop connecting $\beta4$ with $\alpha2$.

The C-terminal domain is composed of a 4-stranded beta-sheet ($\beta9$, $\beta8$, $\beta11$, $\beta12 - \beta9$ is antiparallel to the other β-strands). The β-sheet is located on an α-helix cluster formed by ($\alpha4$-$\alpha10$). The presence of a well-coordinated zinc cation (Figure 4.10) between $\alpha4$ and $\alpha5$ was confirmed by an anomalous difference map. The two domains define a large cavity containing the active site, where ManNAc (gray in Figure 4.8A) and the nucleotide (Figure 4.13) bind.

4.5. Multimeric state

Only one monomer is present in the asymmetric unit of the MNK-ManNAc crystals. However, an examination of the crystal structure using PISA [109] revealed that every monomer is sharing 13% of its solvent accessible surface with a symmetry related mate. The monomer-monomer shared interface area measures 1760 Å^2 per monomer, and these findings correlate with the retention times obtained in analytical gel filtration experiments, which indicate a M_W of 75 kDa and consequently a homodimer.

All amino acids implied in dimerization belong to the C-terminal domain of the protein. A total of 30 hydrogen bonds stabilize this interaction. The N-terminal domain is not implicated in dimerization and possesses therefore more freedom, which allows it to undergo the necessary conformational change to bind ManNAc (Figure 4.12).
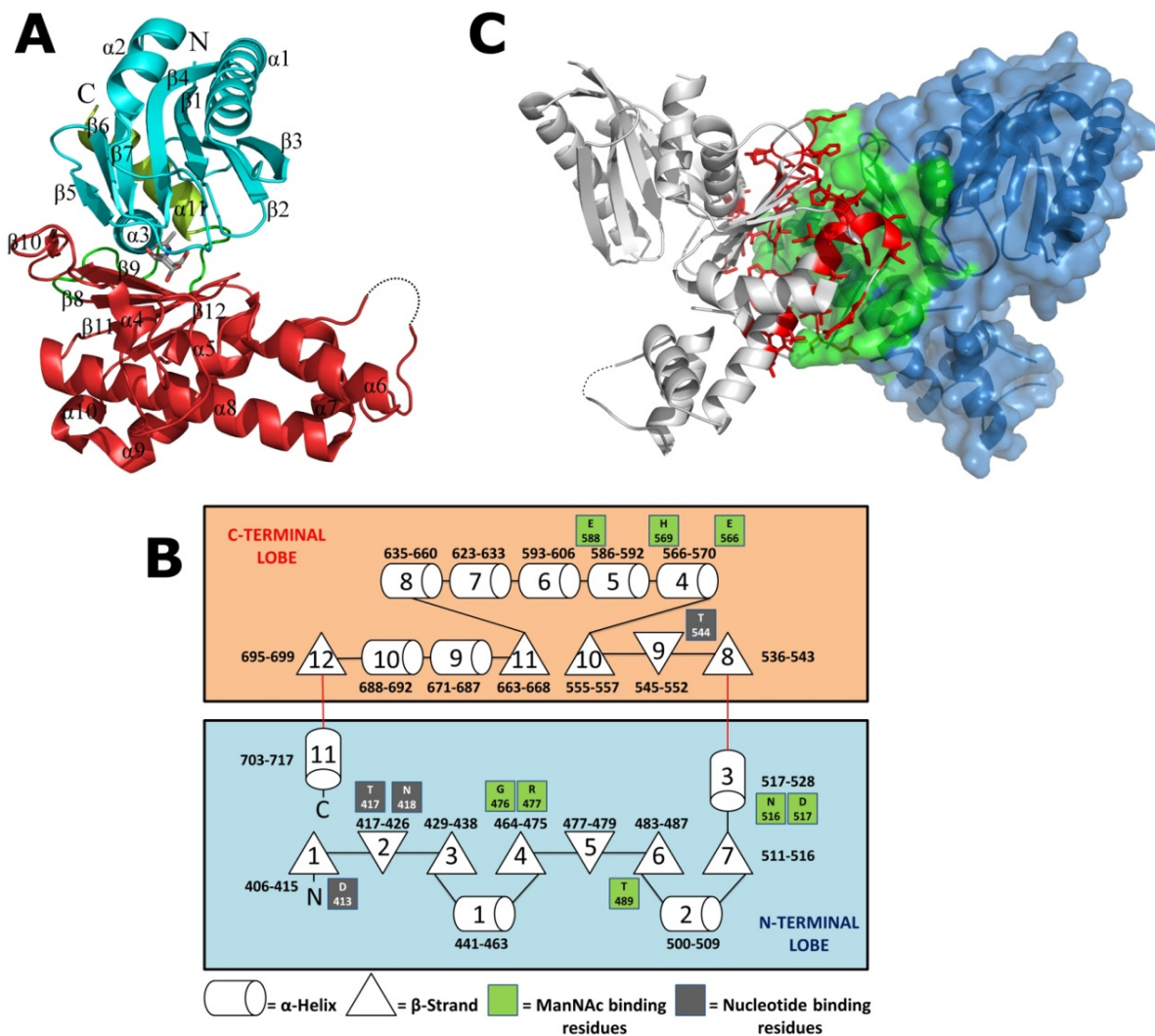
Figure 4.8 (A) Ribbon representation of the hMNK monomer in complex with its natural substrate ManNAc. The N-terminal lobe is shown in blue, while the C-terminal lobe is colored in red. The sugar molecule is depicted as sticks in grey. The secondary structures are labeled as α (helices) or β (strands) followed by a number indicating their occurrence in the primary structure. The last α-helix (α11) protrudes out of the C-terminal lobe into the N-terminal domain and is colored green for clear orientation. The dashed line in the loop connecting α6 with α7 indicates a flexible unmodeled region. **(B) Schematic representation of the MNK topography.** The two lobes are boxed and colored according to (A) and connected by two red lines indicating the hinge regions. The numbers close to each secondary structure indicate the first and last amino acid of the element. The residues forming the ManNAc and the ADP binding site are in green and grey rectangles, respectively. **(C) Dimeric representation of hMNK**. The

physiological dimer of hMNK was reconstituted from monomer A using the crystallographic 2-fold axis. Monomers A and A' are displayed in white (ribbon) and blue (ribbon and surface) with their interfacing residues (1760 Å²) colored in red and green, respectively.

Comparison of the dimerization area between the hMNK-ManNAc structure and the apo–MNK structure [84] shows an increment of the contact interface and the number of hydrogen bonds upon binding of the substrate. The apo-MNK structure has a monomer-monomer interface area of 1587 Å^2 with 22 hydrogen bonds stabilizing the dimer whereas for theh MNK-ManNAc crystals these values are increased to the already mentioned 1760 Å^2 and 30 hydrogen bonds, respectively.

The apo-MNK structure featured a crystallographic hexamer (see Figure 4.6A), which has been discussed by the authors to be biologically relevant. This hexamer is formed by interactions between the N-terminal domains of symmetry related mates. Nonetheless, our findings suggest that this interaction is a crystallographic artifact rather than a naturally occurring multimer, since this would reduce the flexibility of the N-terminal domain that is required for substrate binding.

4.6. Sequential and structural homology search and family classification

A primary sequence analysis identified the GNE homolog proteins of sus scrofa (pig-Q30E20), Ailuropuda melanoleuca (Giant panda-D2HAM4 Uni-Prot accession number), Mus musculus (mouse-Q91WG8), Rattus norvegicus (rat-O35826), Crisetulus griceus (chinese hamster-Q7TQ49), Gallus gallus (Chicken-Q5F3V7) as the first hits sharing a very high sequence identity with the MNK domain of hGNE (98%,98%,97%,97%,96% and 88% respectively). The first hits from bacterial sources share between 35 and 30 % identity with the MNK domain from GNE and are listed as uncharacterized ROK family proteins (see definition below), sugar kinases or transcripitional regulators (NagC and Mlc-like).

A structure-based similarity search was performed using the DALI server [103] and revealed in first place an uncharacterized putative glucokinase from *Enterococcus faecalis* (PDB accession code: 2QM1, 26 % amino acid sequence identity with respect to the MNK domain from hGNE and 3.5 Å rms deviation of superimposed C α-atoms), in second place a putative N-acetyl mannosamine kinase from *Escherichia coli* (2AA4,

26% and 2.3 Å), in third place a putative N-acetylglucosamine kinase from *Thermotoga maritima* (2HOE, 20% and 2.3 Å), in fourth place a putative fructokinase from *Bacillus subtilis* (3LM9, 22% and 2.3 Å) and in fifth place and MLC-like transcriptional regulator (1Z05, 24% and 3.0 Å). It is important to note, that from all the above cited proteins, only the fructokinase from *Bacillus subtilis* has been biochemically characterized so far and the annotated functions for all other are just putative ones assigned only on the basis of sequential and structural homology. One of the first characterized enzyme to find is, interestingly, the MLC protein from Escherichia coli (1Z6R, 22% and 2.8Å), a ROK-family-transcriptional repressor controlling the expression of a number of genes coding for enzymes of the phosphotransferase system (PTS) like ptsG and manXYZ, the specific enzyme II for glucose and mannose PTS transporters as well as regulating the transcription of malT, coding for the global activator of the mal regulon [88].

From these structural and sequential comparisons we can infer that human MNK belongs to the sugar-kinase/HSP70/actin superfamily that features a common ATPase domain characterized by five common structural motifs. Three of them, Phosphate1 (G416, T417), Phosphate2 (G543,T544) and Adenosine are implied in ATP binding. The other two, Connect1 and Connect2 (helix α3 and helix α11, respectively), bridge from one domain to the other in opposite directions making close helix-helix contacts and defining the interdomain hinge region [110]. All these characteristic sequence conserved motifs have been found for the hMNK as well (see information in parentheses above). Furthermore, hMNK can be included more specifically into the ROK family, a functionally diverse enzyme family that encompasses transcriptional **R**egulators, uncharacterized **O**pen reading frames and several sugar **K**inases (1.12). The Phosphate1 and Phosphate 2 Gly-Thr-motifs are perfectly conserved in all compared sequences but two: the MLC protein from *E. coli* and the N-acetyl glucosamine kinase from *Thermotoga maritima.* Those two share an N-terminal extension of about 80 amino acids length. A multiple alignment of many ROK family protein sequences showed that all ROK-transcriptional regulators possess an N-terminal extension of approximately 80 amino acids containing a helix turn-helix motif responsible for DNA binding, whereas the ROK-kinases lack such an extension [86]. This suggests that the N-acetyl glucosamine kinase from *T. maritima* has been false annotated as a kinase, and should be rather considered as a transcriptional regulator. The evolutionary change is also remarkable: either the ROK-transcriptional regulators lost the ability to bind phosphate (and per extension ATP) or the ROK-sugar kinases received it and simultaneously lost the capacity to bind DNA.
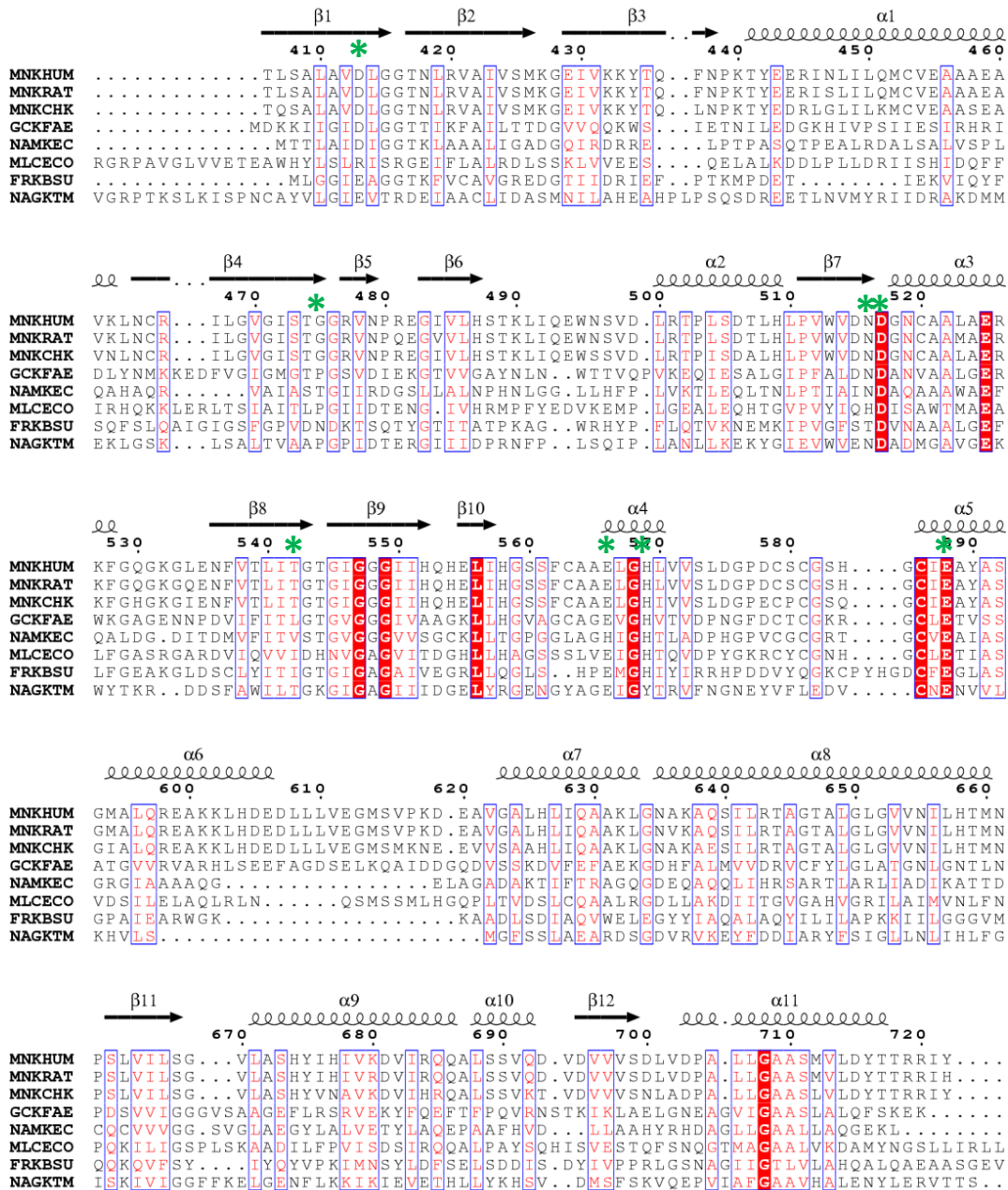
Figure 4.9. Multiple sequence alignment of hMNK with sequential and structural homologs. The sequence identities are highlighted in red background and similarities are displayed as red letters. The secondary structures corresponding to hMNK are labeled on top. Helices appear as spirals and β-strands as arrows. The residues are numbered according to the hMNK primary sequence and no other numbering has been included for clarity. The green asterisks indicate the active site residues. The sequence corresponding to hMNK (Uni-prot code Q9Y223) has been abbreviated as MNKHUM, the MNK homologue from rat (O35826) as MNKRAT and the MNK homologue from chicken (Q5F3U7) as MNKCHK. The other five sequences belong to bacterial sources and are ROK-family members. These are a glucokinase from *Enterococcus faecalis* (GCKFAE), a ManNAc kinase from *E. coli* (NAMKEC), the MLC protein from *E.coli* (MLCECO), a fructose kinase from *Bacillus subtillis* (FRKBSU), and the N-acetyl glucosamine (GlcNAc) kinase from *Thermotoga maritima* (NAGKTM). The sequence comparison was performed with the program CLUSTALW [111] and graphically represented with the program ESPript [112].

4.7. hMNK requires Zinc binding for structural stability and activity

Using anomalous difference electron density maps we could confirm the presence of a Zn^{2+} located between $\alpha4$ and $\alpha5$ and tetrahedrally coordinated by three cysteines (C579, C581 and C586) and one histidine (H569) arising from the loop between these two α-helices (4.10). The Zn^{2+}-S distances are 2.35 Å for C579, 2.33 Å for C581 and 2.26 Å for C586. The Zn^{2+}-ND distance measures 2.11 Å for Nε of H569. The four residues implied in the Zn^{2+} binding form part of the specific ROK-family motif signature as described in section 1.12. The Zn^{2+} binding site is close to the ManNAc binding site. Indeed, the NE2 of H569 is in hydrogen bond distance (2.74 Å) to the C1 hydroxyl group of ManNAc. Zn^{2+} is properly orientating the H569 side chain for sugar binding. The observed B factor for Zn^{2+} correlates with the B factor of the atoms in the surrounding space indicating full occupancy, although no zinc has been added during purification. This indicates the endogenous strong binding of Zn^{2+} and underlines its central role for MNK activity. Furthermore, no enzyme activity could be detected in presence of EDTA that had removed the Zn^{2+} from hMNK.
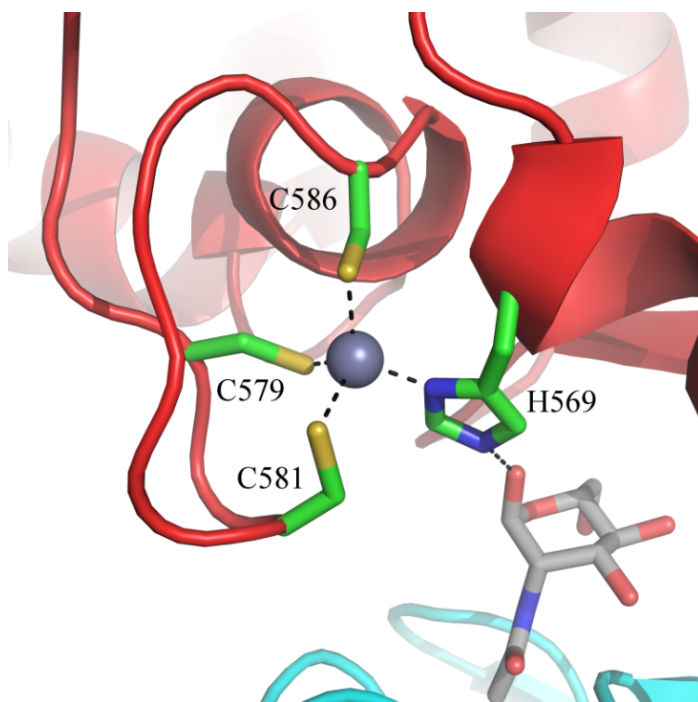

Figure 4.10 Zinc binding site. The tetrahedral coordination of the zinc atom (gray sphere) is performed by 3 Cysteine residues (sulfur atoms in yellow) and a single histidine (nitrogen in blue). Upon metal binding H569 adopts the right orientation for coordination with C1-OH of ManNAc.

4.8. The ManNAc binding site

One of the main goals of this work was to elucidate which residues are implied in ManNAc binding and which conformation ManNAc adopts when bound to hMNK. The co-crystallization of hMNK with ManNAc yielded crystals diffracting at 1.65 Å. After solving the structure by molecular replacement using the previously published MNK-apo-structure ([84], PDB code 3EO3) as search model, difference electron density maps clearly showed the position and conformation of ManNAc.

hMNK binds the α-anomeric form of N-acetyl mannosamine in $^4C_1$ chair conformation. The average B factor for the sugar molecule, 12.2 $Å^2$, is even lower than the average B factor for the main chain of hMNK (14.3 $Å^2$). This indicates that the sugar binding site is fully occupied.

All the polar sugar atoms are hydrogen bounded by the surrounding residues of hMNK. A total of eight amino acids and three water molecules are involved in the substrate binding network forming a total of 17 hydrogen bonds with the ligand. The N-terminal domain is the major contributor to this network with five amino acids (G476, R477, T489, N516 and D517). The other three residues belong to the C-terminal domain of hMNK (E566, H569 and E 588).

The ManNAc binding network is displayed in Figure 4.11, and all the interactions are summarized in Table 4.5. The hairpin β-sheet formed by $\beta5$ and $\beta6$ orientates three of these residues: G476 and R477 are situated in the loop connecting $\beta4$ with the hairpin and T489 is in the loop region located at the C-terminis of strand $\beta6$. The short loop connecting $\beta7$ and helix $\alpha3$ bears the other two residues, N516 and the presumed catalytic residue D517 that are located in the N-terminal domain and implied in sugar binding.

The active center residues of the C-terminal domain seem to be orientated by the Zn^{2+} binding motif. This is especially evident for H569, which directly coordinates both, the Zn^{2+} (ND1, 2.11 Å) and ManNAcO1 (over NE2, 2.74 Å). But E566 and E588, which are two of the Zn^{2+} binding residues, are also close to H569 and C586, respectively. These findings underline the central role of the Zn^{2+} binding motif for hMNK activity.
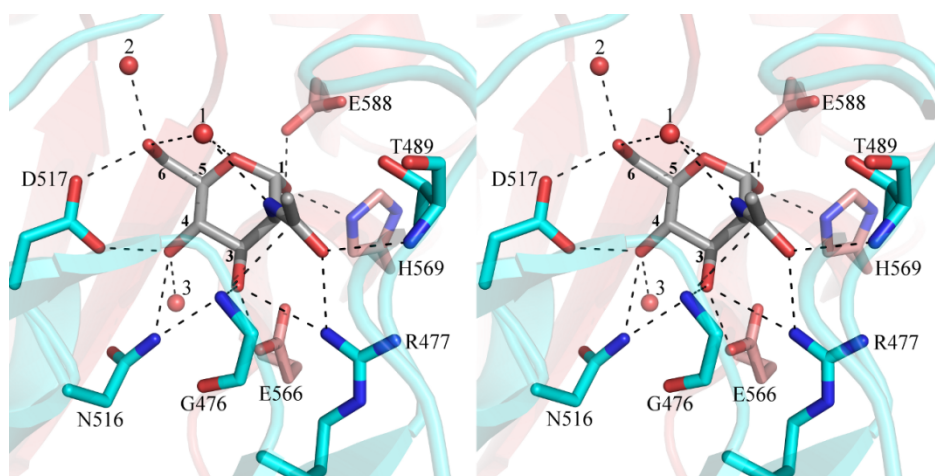
Figure 4.11. Stereo view of the ManNAc binding site. The colors of the secondary structures are consistent with Figure 4.8 A and B, indicating whether the residues arise from the N-terminal lobe or from the C-terminal one. The amino acids involved in sugar binding are represented as sticks. Oxygen and nitrogen atoms are displayed in red and blue, respectively. The 3 water molecules are shown as red spheres. Broken lines show the extensive hydrogen bond network engaged in ManNAc binding.

Number	Sugar atom / H2O	Protein atom / H2O	Distance (A)
1	ManNAc O1	H569 NE2	2.7
2		E588 OE1	2.6
3	ManNAc N2	H2O - 1	3.0
4	ManNAc O3	G476 N	2.9
5		R477 NH2	3.2
6		E566 OE2	2.6
7		N516 ND2	3.1
8	ManNAc O4	N516 ND2	3.2
9		H2O - 3	2.8
10		D517 OD2	2.6
11	ManNAc O6	D517 OD1	2.6
12		H2O - 2	2.7
13		H2O - 1	2.9
14	ManNAc O5	H2O - 1	3.2
15	ManNAc carbonyl	T489 N	2.9
16		R477 NH2	2.9
17	ManNAc C7	E476 N	3.2

Table 4.5. Direct and water mediated hydrogen bonds between MNK and its native substrate ManNAC

4.9. Domain movements upon ManNAc binding

A comparison of the apo-MNK structure [84] with the structure of the hMNK-ManNAc complex using DYNDOM [113] showed a clear conformational change of the V-shaped protein (Figure 4.12). Upon substrate binding, the N-terminal lobe (one of the legs of the V) rotates 12° toward the C-terminal lobe (the other leg of the V). This closure allows hMNK to embrace and tightly coordinate ManNAc. A close view of the sugar binding site at the inner bottom of the V is shown in Figure 4.11. Both lobes behave as rigid bodies, and the flexibility is conferred by a hinge region formed by two loops (amino acids 529-535 and 700-702) (Figure 4.8a and b).

Interestingly, the DYNDOM software suggests residues 516 and 517 (that belong to helix α-3) to form a third hinge. Both residues are directly implied in sugar binding (Figures 4.8b and 4.11). The orientation change of the side chains induced by ligand binding to apo-MNK might be the driving force for and trigger lobe movement. Notably, no significant lobe movements were observed upon ADP/ATP/AMPPCP binding. (see section 4.10 and further).
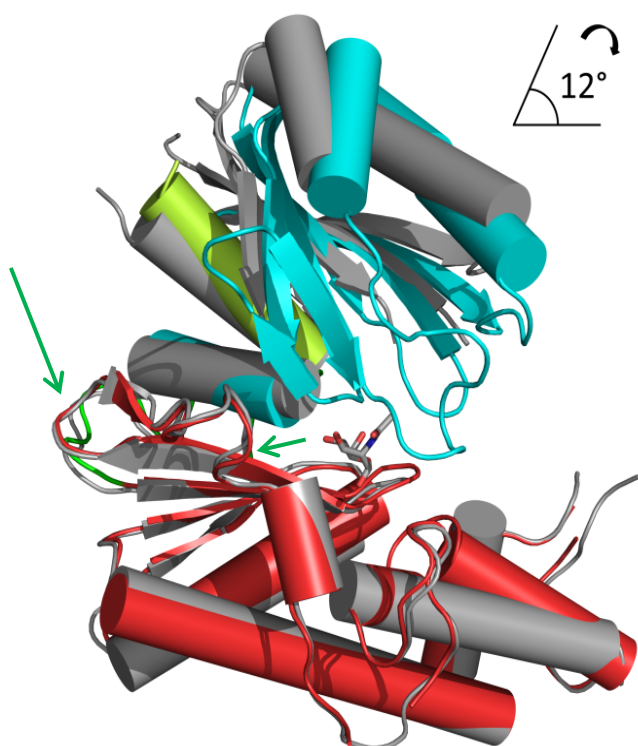
Figure 4.12. Superimposition of the C-terminal lobes from hMNK/ManNAc (red) and apo-MNK (gray, PDB code 3EO3) structures. The helices have been displayed as cylinders for clarity. Upon ManNAc binding, the N-lobe (blue and gray for MNK/ManNAc and apo-MNK, respectively) pivots 12° towards the C-lobe over the hinge region (green loops remarked with green arrows). Based on this adaptability we can clearly differentiate an open ligand-free conformation (gray) from a close ligand-bound conformation (blue and red).

4.10. Crystal structure of the ternary complexes hMNK/ManNAc/ADP, hMNK/ManNAc-6P/ADP and hMNK/ManNAc/AMPPCP

After the ManNAc binding site had been characterized, the next step necessary for understanding the activity of the kinase was to determine the structure of the ternary complex formed by hMNK, the sugar and the nucleotide (ADP or ATP or analogues). To this extent we first tried to co-crystallize the mentioned complexes, but numerous screenings failed to yield diffraction quality crystals. Therefore, we decided to soak hMNK/ManNAc crystals (4.3.2) with ATP, ADP or AMPPCP.

4.10.1. Soaking experiments

The soaking solution was prepared by mixing ADP, ATP or AMPPCP at final concentrations ranging between 5 mM and 20 mM with the cryo solution without calcium acetate. (0.1M sodium cacodylate pH 6.5 and 50 % PEG 300). Inclusion of calcium acetate in the mixture resulted in precipitation of the solution. The soaking solution was then stepwise added to the crystal containing drops and the mother liquor was slowly exchanged in this way. After replacement of the buffer, the crystals were incubated in the new solution for at least 30 minutes. This process externally damaged most crystals but some of them remained intact and were used for X-ray data collection. Since the soaking experiments were performed in a cryo solution, the crystals could be directly mounted and frozen for data collection.

4.10.2. Structure determination

X-ray data collection and processing was performed in the same way as for the hMNK/ManNAc structure (4.3.3). For the ternary complexes hMNK/ManNAc/ADP and hMNK/ManNAc-6P/ADP, the unit cell constants did not significantly vary and the space group remained $P4_12_12$. For the complex hMNK/ManNac/AMPPCP the soaking process damaged the crystals, and this resulted in a loss of symmetry and resolution. The new space group in this case is $P2_12_12_1$, and the unit cell constants are a=83.316, b=89.715, c=101.166, α=β=γ=90.000.

The structure of MNK in complex with ManNAc and ADP could be determined at 1.82 Å resolution. The electron density difference maps clearly showed the presence and

position of the α- and β-phosphates as well as of the magnesium cation necessary for catalysis. The ribose moiety was partially defined but no electron density was found for adenine, which is probably due to weak coordination of ATP and high flexibility of the nucleotide binding site.

	hMNK - ManNAc - ADP	hMNK – ManNAc6P - ADP	hMNK – ManNAc- AMPPCP
Data collection			
Beamline	BESSY MX 14.2	BESSY MX 14.2	BESSY MX 14.2
Space group	P 41 21 2	P 41 21 2	P 21 21 21
Unit Cell (Å)	a= b= 90.4; c= 101.2	a= b= 90.6; c= 101.4	a=83.3; b= 89.8; c= 101.1
	$\alpha= \beta= \gamma= 90°$	$\alpha= \beta= \gamma= 90°$	$\alpha= \beta= \gamma= 90°$
Nominal resolution (Å)	50.0 – 1.82	41.40 - 2.15	33.5 - 2.5
Outermost resolution shell (Å)	1.92-1.82	2.16 – 2.27	2.50 – 2.56
Unique reflections	38183(5567)	23574 (3484)	26261 (1937)
Completness (%)	100(100)	99.7 (100)	97.7 (99)
Redundancy	12.8 (12.9)	11.8 (3.9)	2.5 (4.0)
Rcryst	5.3 (69.4)	7.9 (64.7)	11.99 (65.4)
Rmrgd-F	6.0 (40.9)	9.3 (44.6)	15.7 (72.1)
Mean I/σ(I)	34.07 (4.40)	24.52 (4.0)	9.1 (2.2)
Refinement			
R / Rfree (%)	15.2/18.2	17.2 / 20.0	23.7 / 27.9
r.m.s.d. From ideal geometry			
Bond lengths (Å)	0.025	0.022	0.017
Bond angles (°)	2.097	1.788	1.858
Dihedral angles (°)	6.180	6.465	6.573
Chiral center restraints	0.128	0.108	0.133
Mean B-factor (Å2)			
Overall model	31.6	37.1	33.2
Protein atoms	30.8	37.0	32.0
Sugar	16.2	18.7 (ManNAc)	25.2 (in ChainA)
		23.4 (ManNAc-6P)	19.5 (in ChainD)
ADP	58.0	66.3	-
AMPPCP	-	-	86.4
PDB ID	2YHY	2YI1	-

Table 4.6 Data collection, refinement and Ramachandran plot statistics for the ternary complexes hMNK/ManNAc/ADP, hMNK/ManNAc-6P/ADP and hMNK/ManNAc/AMPPCP

After longer soaking of hMNK/ManNAc crystals with ATP the structure of the ternary complex hMNK/ManNAc-6P/ADP could be solved at 2.1 Å resolution. In this case, also no electron density could be found for the adenine moiety of ADP. The presence of additional electron density at ManNAc-O6 has been attributed to a phosphate at this position with about half occupancy. The formation of the complex hMNK/ManNAc-6P/ADP when soaking crystals of hMNK/ManNAc with ATP, however, indicates that ATP has entered the crystals and the active site harbouring ManNAc and the kinase reaction has taken place. Obviously, the binding of ATP was only transient but the reaction product ADP was bound tighter and permitted crystal structure determination. Data collection and refinement statistics for the three ternary complexes are shown in Table 4.6.

4.11.   The nucleotide binding site

The following description of the nucleotide binding site is based on the 1.88 Å hMNK/ManNAc/ADP ternary complex crystal structure. The β-phosphate of ADP is well stabilized by a total of eight interactions (see Figure 4.13 and Table 4.7). On the one side, the β-phosphate interacts with the backbone NH groups of T417, N418, and T544, as well as with $T544O_{\gamma 1}$. On the other side, the β-phosphate is stabilized by hydrogen bonds to 3 water molecules, H_2O-179, H_2O-192 and H_2O-195, that are further hydrogen bonded to ManNAc-O6H and the NH group of G545, D413O1 and D517O1 and to $R420N_{\eta 1}$, respectively.

We also found an octahedrally coordinated magnesium cation: the β-phosphate and the atom $D413-O_{\delta-2}$ coordinate Mg^{2+} axially whereas four water molecules (H2O192, H2O193, H2O194, H2O195) occupy the equatorial sites. The side-chain of D413 does not directly bind one of the oxygen of the β1-phosphate but is necessary for Mg^{2+} coordination, and consequently crucial for ATP binding.

The α-phosphate of ADP is mainly coordinated by the side-chains of $R420N_{\eta 2}$ and $N418N_{\delta 2}$ and further stabilized by 2 water-mediated hydrogen bonds.

All the amino acids involved in pyrophosphate coordination are located within strand β2 of the N-terminal lobe (T417, N418, R420) or in the loop connecting β8 and β9 of the C-terminal lobe (T544).

The electron density for the ribose is only partially defined (with the 2Fo-Fc map contoured at 1.0 σ), and no electron density was found for adenine. Nevertheless, we could fit the ribose according to the available electron density, and this model is consistent with the position and puckering of ribose of the recently published structure of the fructokinase YdhR from *Bacillus Subtilis* in complex with ADP [114]. The ribose is only stabilized by a single water mediated hydrogen bond. This water molecule (H2O196) is further coordinated by Q597 (OE1).

In the ternary complex hMNK/ManNAc-6P/ADP, the ribose engages in only one single water-mediated hydrogen bond of its O2'H with G593O and A624N. The adenine moiety was modeled in a hydrophobic pocket and is stacked between V670 and L625, again similar as in the above mentioned structure of fructokinase YdhR in complex with ADP.

Number	ADP atom / H2O	Protein atom / H2O	Distance (A)
1	β-phosphate O1	T417 N	3.0
2		N418 N	3.0
3	β-phosphate O2	T544 OG1	2.5
4		T544 N	2.8
5		H2O 179	2.8
6	β-phosphate O3	H2O 192	3.1
7		H2O 195	3.0
8		Mg	2.2
9	α-phosphate O1	R420 NH2	2.9
10		N418 ND2	2.8
11		H2O 195	2.9
12	α-phosphate O2	H2O 195	2.2
13		H2O 112	2.9
14	Ribose hydroxyl O2	H2O 196	2.7
15	H2O 196	Q597 OE	3.1

Table 4.7. Direct and water mediated hydrogen bonds between hMNK and ADP
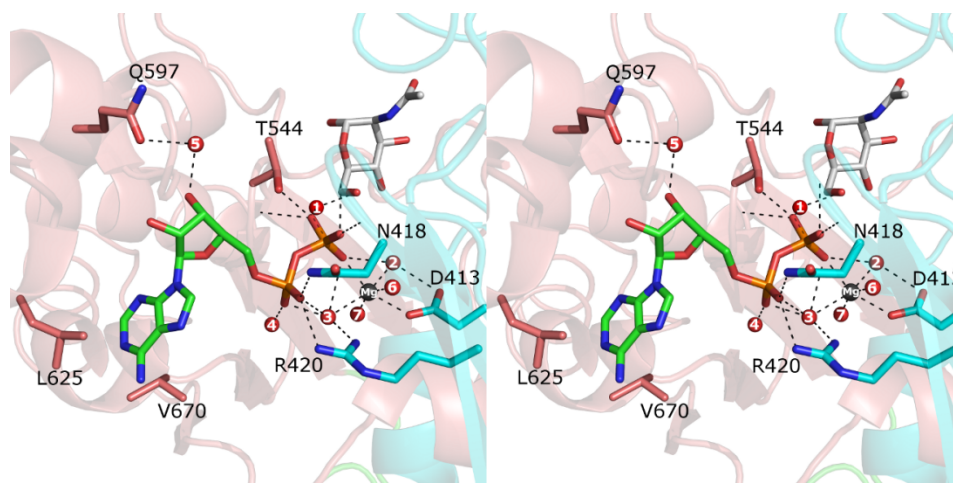
Figure 4.13. Stereo view of the ADP binding site. The colors of the secondary structure elements are consistent with Figure 4.8 (A), Figure 4.8 (B) and Figure 4.11. Oxygen and nitrogen atoms are displayed in red and blue respectively. The seven water molecules involved in ADP binding are displayed as red spheres and numbered in white. (1 corresponds to the water molecule number 179 in the PDB file with accession code 2YHY, 2 to 192, 3 to 195, 4 to 112, 5 to 196, 6 to 193 and 7 to 194). Broken lines show hydrogen bonds whose distances are omitted in the picture for clarity but can be found in Table 4.7. The ADP molecule is shown in green (adenine moiety and ribose) and orange (phosphates). The magnesium atom (gray sphere) is octahedrally coordinated, axially between D413 and the β–phosphate O3 and equatorially by four water molecules (2,3,6,7). This demonstrates its key importance for nucleotide binding and consequently for the catalytic activity of hMNK. Furthermore, the ManNAc molecule has also been displayed (white backbone), hydrogen bonded to water molecule 1. This gives a first impression of the distance separating the β-phosphate and the sugar phosphorylation site, the hydroxyl at the C-6 position.

4.12.   The MNK/ManNAc-6-P/ADP structure

As described in section 4.10, to solve the structure of the ternary complexes the hMNK/ManNAc crystals were soaked with different nucleotides for different periods of time. One of these trials was treated with ATP for almost one hour. Under these conditions most of the crystals were externally damaged, probably due to lack of calcium acetate in the soaking solution (4.10.1). Therefore we had to measure many crystals until we found one with good diffraction quality. The aim of such experiments was to find out whether the enzymatic reaction could take place in the crystal and to characterize the post-reaction state.

After data collection and refinement, additional electron density at the ManNAc-O6 end was found. However, after attribution of this density to a phosphate molecule with full occupancy and posterior refinement, the difference map (Fo-Fc) showed a clear negative peak at the phosphate position whereas the rest of the ligand (all ManNAc atoms) showed no peaks, clearly indicating, that, if the phosphate had been really transferred, the reaction was only partial. Since the electron density shown by the 2Fo-Fc map at this position was too big to be explained by a water molecule, a model with partially occupancy of both phosphorylated and unphosphorylated ManNAc was constructed. The final model contained a ManNAc molecule with 0.6 relative occupancy and a ManNAc-6P at 0.4 occupancy. The average RMSD, calculated considering only the common atoms of both modeled molecules (ManNAc and ManNAc-6P) has a value of 0.2492 Å. The major contributors to this divergence are the differences between the atoms of the C-6 position and the O-6 position with their respective homologs (0.26Å and 0.84Å respectively). A closer look at the surrounding space revealed an ideally suited coordination environment for the phosphate that is engaged in a total of 10 hydrogen bonds stabilize the transferred molecule (Figure 4.14 and Table 4.8).

The ADP molecule also shows some changes with respect to its orientation in the ternary complex structure hMNK/ManNAc/ADP. In detail, the orientation of adenosine was changed, whereas the pyrophosphate remained the same. The ribose in this structure was stabilized by three hydrogen bonds: the ribose-O3' interacts with T417OG1 and T544OG1 (2.85Å and 2.70Å) and the ribose-O2' with one water molecule (H_2O #141 in PDB 2YI1) further stabilized by Q597NE2. The adenine ring adopted a different configuration, too, and interacted with the two hydrophobic residues L625 and V670 via van der Waals contacts.
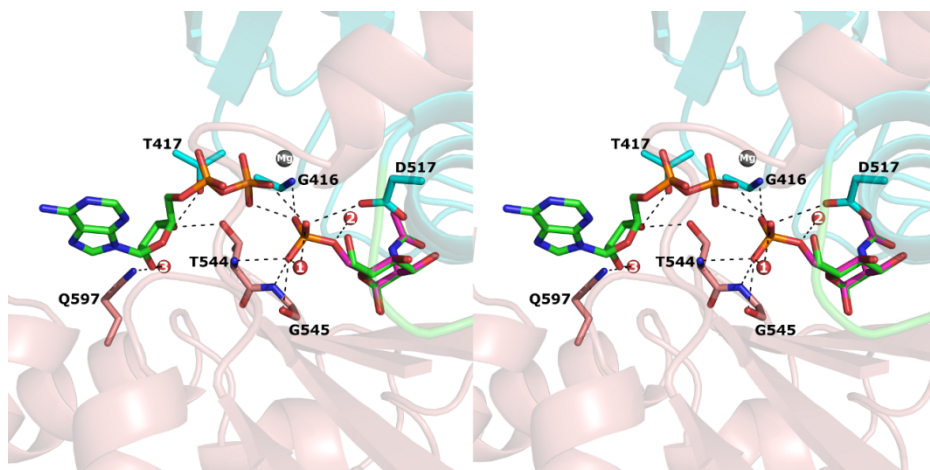
Figure 4.14 Stereo view of the ManNAc-6P phosphate moiety environment and coordination in sticks representation. The colors of the secondary structures are consistent with Figure 4.8 (A), Figure 4.8 (B) and Figure 4.11. Oxygen and nitrogen atoms are displayed in red and blue respectively. Water molecules involved are displayed as red spheres and numbered in white. (1 corresponds to 68 and 2 corresponds to 87 in the water nomenclature of the PDB file with accession code 2YI1). Broken lines show the dense hydrogen bond network surrounding the phosphate (orange) at the O-6 position. All distances (Å) can be found in Table 4.8. The ManNAc-6P molecule (0.4 occupancy in the model) is displayed with lila backbone. The unphosphorylated ManNAc molecule (0.6 occupancy) is displayed in green.

Number	Phosphate atom	Protein atom / H2O	Distance (A)
1	O17	T544N	3.0
2		G545N	3.0
3		G545O	2.5
4		H2O 68	2.8
5	O18	D517OD1	2.8
6		H2O 68	3.1
7		ADP O3B	3.0
8	O19	G416N	2.7
9		ADP O1B	2.9
10	ManNAc-O6	H2O 87	2.9

Table 4.8 Direct and water mediated hydrogen bonds between MNK and the phosphate moiety of the end product ManNAc-6P

4.13.　The MNK/ManNAc/AMPPCP complex

To characterize the catalytic event, it is important to trap the transition state of the enzymatic reaction. Addition of ATP to the MNK/ManNAc crystals ended up with the structure of the final product of the reaction as already presented (section 4.12) indicating the conservation of the enzymatic activity in the crystal. Therefore, the ATP-analogues, AMPPCP and AMPPNP, that mimic the ATP structure but are not hydrolysable, had been used in our trials to obtain the desired transition state complex.

Either the soaking process or the binding of AMPPCP provoked a loss of symmetry (from the original $P4_12_12$ to $P2_12_12_1$). In contrast to the other determined structures, there are two monomers in the asymmetric unit, forming a natural dimer. After structure refinement of the hMNK/ManNAc/AMPPCP crystal structure only one of the monomers (ChainA) was found to contain additional electron density at the nucleotide binding site that could be attributed to an AMPPCP molecule with occupancy of 0.8. However, the quality of the data and the corresponding electron density is not good enough to unambiguously attribute the atomic coordinates to the ATP-analogue. Further experiments and the consequent improvement of the X-ray data are necessary to really characterize the enzyme-substrate complex and the enzyme mechanism. The data presented in this section, should be therefore critically considered and not taken as a dogma.

The number of interactions stabilizing the AMPPCP molecule is significantly less than for the ADP in the hMNK/ManNAc/ADP structure or in the hMNK/ManNAc-6P/ADP complex as detailed in Table 4.9 and Figure 4.15. The average B factor for ChainA of hMNK is 31.9 Å^2, whereas the same values for the ligands ManNAc and AMPPCP are 25.2 Å^2 and 86.4 Å^2, respectively.

Number	ADP atom / H2O	Protein atom / H2O	Distance (A)
1	γ-phosphate-O1	G545-N	2.8
2		ManNAc-6OH	2.2
3	γ-phosphate-O2	G545-O	3.0
4	γ-phosphate-O3	ManNAc-6OH	2.8
5		D517-$O_{\delta 1}$	2.7
6		Mg^{2+}	2.7
7	γ-phosphate-P	ManNAc-6OH	2.8
8	α-phosphate O1	R420-$N_{\eta 1}$	2.6

Table 4.9 Hydrogen bond network for AMPPCPP
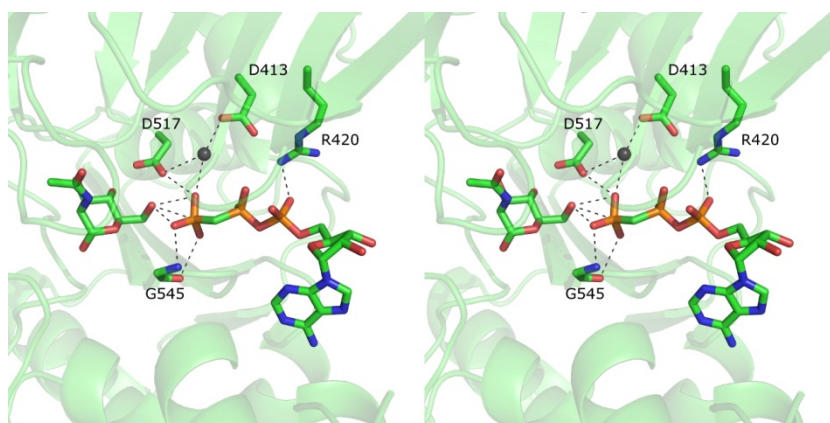
Figure 4.15 Stereo view of the active site for the ternary complex hMNK/ManNAc/AMPPCP. Oxygen, nitrogen, carbon and phosphor atoms are displayed in red, blue, green and orange, respectively. The data quality and resolution made not possible to clearly add water molecules. The gray sphere represents Mg2+. Broken lines show the hydrogen bond network surrounding AMPPCP. Only the γ-phosphate moiety of the AMPPCP (orange) is coordinated by an extensive hydrogen bond network.

4.14. Surface representation and electrostatic potential

The hMNK sugar and nucleotide binding sites have been described previously in sections 4.8 and 4.11, respectively, using cartoon and stick models to visualize them. In the present section, surface representations mapping the local electrostatic potential of the YdhR/ADP/fructose [114] (Figure 4.16a and b) and of the hMNK/ADP/ManNAc (Figure 4.16 c and d) monomer have been prepared.
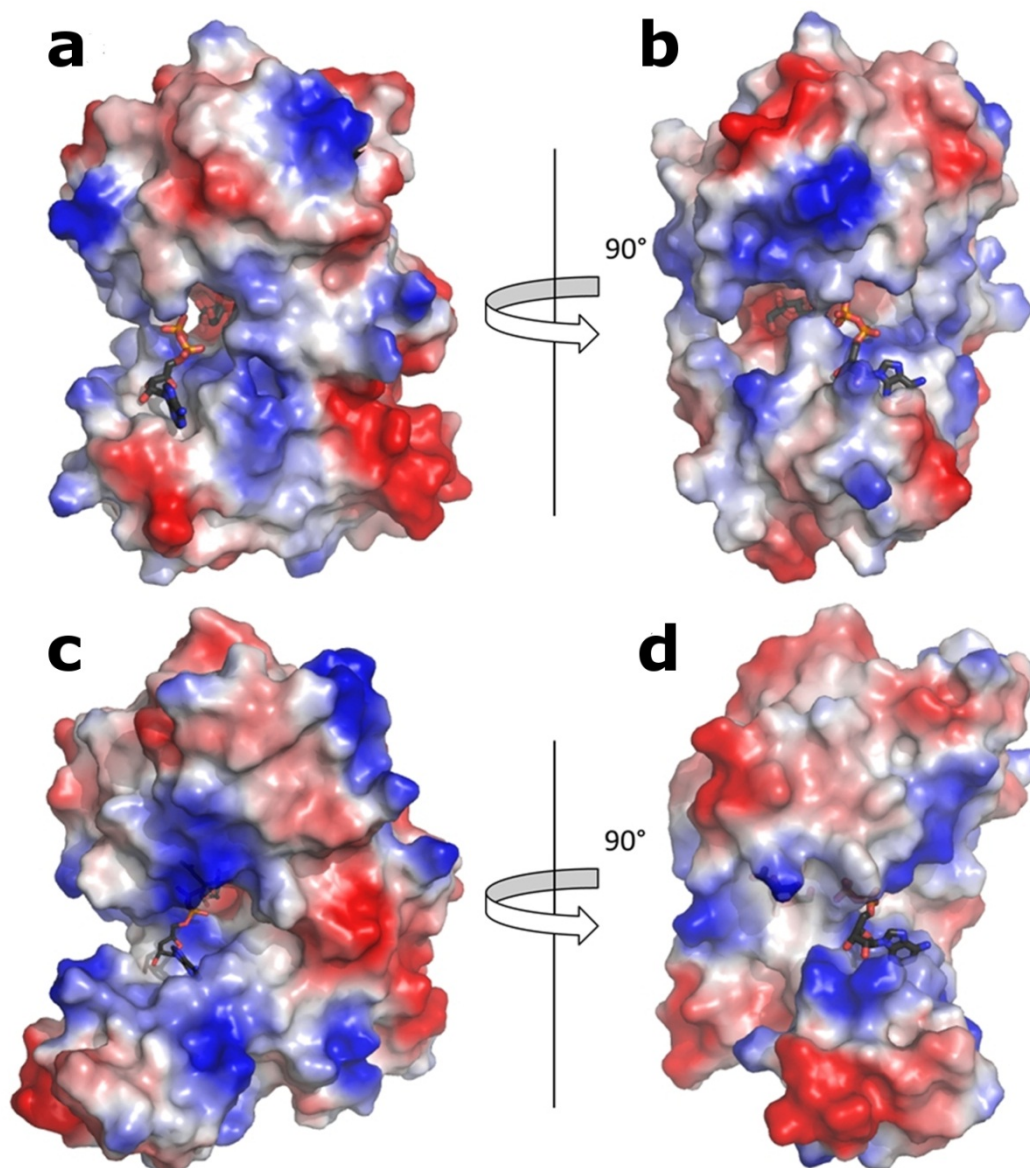
Figure 4.16 Surface representation mapping the electrostatic potentials of YdhR and hMNK. (a) and (c) are in the same orientation. Idem for **(b)** and **(d)**. As indicated by the arrow, rotation of **(a)** and **(c)** by 90° produces **(b)** and **(d)**, respectively. The electrostatic figures were calculated using Pymol. The positive and negative charge potentials at the +70 kTe^{-1} and -70dTe^{-1} scales are displayed in blue and red, respectively.

YdhR (Figure 4.16a and b), the only kinase of the ROK-family whose structure was solved in complex with its substrate, Fructose, reveals an open, solvent accessible sugar binding site whereas hMNK (Figures 4.16 c and d) shows a closer configuration, where the sugar moiety is completely buried and only the hydroxyl group at the C-6 position of ManNAc (the phosphorylation site) is accessible to solvent (Figure 4.17). Regarding the nucleotide binding, in both cases only the pyrophosphate is simultaneously interacting with both lobes, whereas the ribose and adenine moiety are just stacking in a groove present on the surface of the C-terminal lobe. All this, graphically explains the high affinity of hMNK for ManNAc and moderate for ATP.

Observation of the electrostatic potential mapping did not reveal any noticeable feature but the negative surface patch at the bottom of the sugar binding pocket of both YdhR and hMNK. Acidic, negatively charged residues are more likely to coordinate the hydroxyl moieties of sugars forming hydrogen bonds with them.
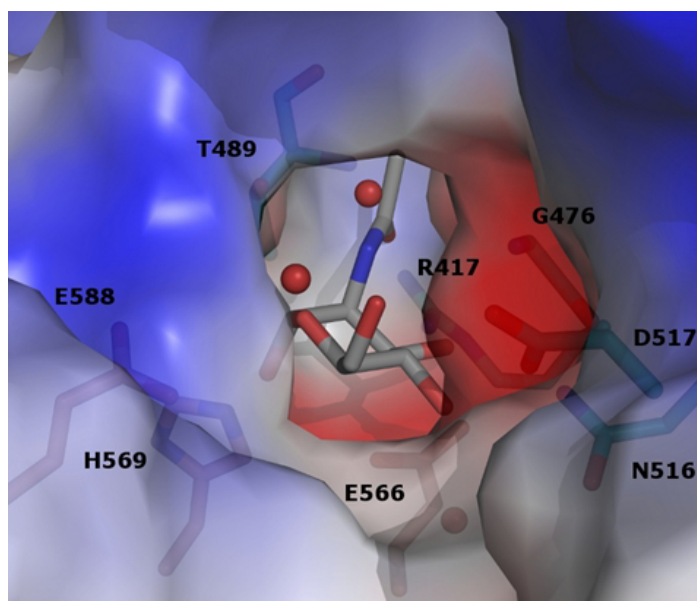

Figure 4.17 Closer view of the hMNK ManNAc binding site. The positive and negative charge potentials at the +70 kTe^{-1} and -70dTe^{-1} scales are displayed in blue and red, respectively.

4.15.   hMNK inhibition

Once the crystal structures presented in this work had been elucidated, it was possible to design hMNK inhibitors using molecular modelling techniques. Based on the geometry of the active center of hMNK, it has been concluded that modifications at the C-6 position of ManNAc could yield potential inhibitors. Enzyme activity assays were conducted with different putative inhibitors. GlcNProp and 3OMe-GlcNAc were described in previous studies to inhibit MNK activity in cell lysates [115, 116]. Using purified recombinant hMNK, these substances were found to weakly inhibit hMNK activity. With a final concentration of 5 mM inhibitor the activity of hMNK was decreased 17% and 26%, respectively. As a first approach to find an enhanced inhibitor, ManNAc-6OAc has been synthesized and has shown significantly stronger inhibitory effects (60% at 5 mM). Since an acetyl modification would not work *in vivo* due to unspecific esterase activities in cells, it is necessary to look for other modifications in search for an efficient inhibitor.

5. DISCUSSION

The biosynthesis of sialic acids (Sias) and the subsequent incorporation of them to cell membrane surfaces and glycoproteins, is essential for cell development and defense in front of pathogens. GNE is the key enzyme of the Sias biosynthetic pathway and the conversion that catalyzes ,UDP-GlcNAc to ManNAc, is considered the bottleneck for Sias production. Therefore, regulating the enzymatic activity of GNE would imply the possibility to control the numerous processes that are dependent on Sias production, the major exponent of these being the abnormally accelerated cell growth and metastatic potential of cancer cells, whose universal feature is an increased level of Sias on their cell surface. Given this situation, it is understandable that GNE has been a matter of interest over the last years and especially its structure, due to the inherent relationship between structure and function. However, despite of all the efforts put on structural determination, no success has been achieved thus far. An alternative approach was offered by the bifunctional character of GNE. On this basis, the structures of its two enzymatic domains, an epimerase and a kinase, were tried to solve separately.

During this thesis, the structures of the kinase domain of GNE (hMNK) have been solved in complex with its native substrate ManNAc and as ternary complexes with ManNAc and ATP, ADP or AMPPCP. The overall fold and specific structural features for the cited structures has been descriptively presented in the results section (4). Returning to the original motivation of this thesis (1.13), the structural information will be used in this chapter to discuss possible mechanism of the enzyme and to establish a relationship between the substrate specificity and the architecture of the binding site. Furthermore, the significance of an inhibitor of hMNK and the usefulness of the presented findings to design and inhibitor as well as the relationships between the HIBM mutations and the disease will be discussed.

5.1. The catalytic mechanism

5.1.1. General considerations (based on [117])

Phosphoryl transfer reactions are essential in many fundamental biochemical processes like gene regulation, signal transduction and metabolism. Nucleotiside di- and triphosphates act as phosphoryl donors and the phosphoryl moiety is transferred to a protein, a small molecule or another nucleotide. Phosphoryl moieties are excellent leaving groups, which makes them well suited for substitution chemistry. Moreover, the phosphoanhydrides used as phosphoryl donors are metastable, which means that they possess a very large negative free energy of hydrolysis (Table 5.1) but this hydrolysis is kinetically so slow that in the context of the biological "life times" it practically does not occur. This kinetic slowness is related to the high energy barrier necessary for the activation of the reaction (Figure 5.1).

The regulation of biological processes is crucial for life since these processes cost energy and should be only activated when they are required. A metastable reaction offers a simple mechanism for regulation. These reactions only take place if catalyzed by kinases, a group of ubiquitous enzymes that can dramatically accelerate the rate of phosphoryl transfer by lowering the activation energy barrier, the cause of the slow reaction turnover rate. The hydrolysis of methyl phosphate can be used as an illustrative example of the acceleration rate achieved by kinases. The uncatalyzed reaction has a half-life of more than one trillion years [118]. However, in presence of the enzyme alkaline phosphatase this hydrolysis can reach acceleration rates of more than 10^{27}-fold [117].

The mechanism of the phosphoryl-transfer reaction has been a matter of discussion over the last 30 years. It seemed to be clear that all phosphoryl transfer reactions with an ATP molecule as donor are initiated by a nucleophilic attack at the electropositive phosphorous of ATP. However, it was controversial wether these reactions proceeded though stable intermediate species or employed a concerted mechanism. At this point it is important to note the thermodynamical difference within a transition state and a reaction intermediate: a transition state is a local energy maximum along a reaction coordinate while an intermediate describes any local energy minimum along the reaction pathway as graphically illustrated in Figure 5.1a.
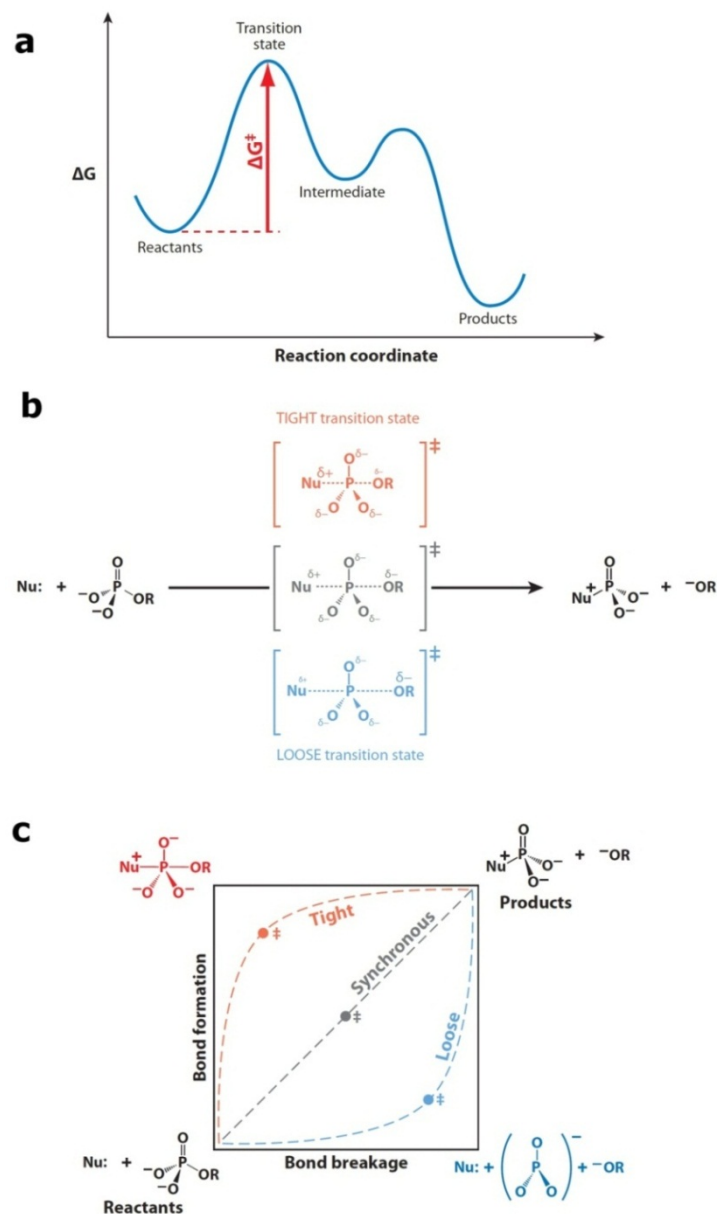
Figure 5.1 (a) Reaction coordinate diagram. The energetic pathway for a hypothetical phosphoryl transfer reaction is shown as a blue curve. The conceptual difference within a transition state (local energy maximum along the reaction coordinate) and an intermediate (local minimum) are graphically represented. **(b) range of possible concerted transition states.** "Tight" and "loose" transition states are indicated by shorter and longer Nu….P….OR distances, respectively and **(c) two-dimensional reaction coordinate diagram.** At the top left (in red) and at the bottom right (in blue) we find the two extremes for an associative stepwise reaction occurring over a pentacovalent phosphorane intermediate and for a dissociative stepwise reaction occurring over a metaphosphate intermediate, respectively. The dashed lines show the diverse ranges of concerted reactions displayed in (b). The gray line is an ideal synchronous reaction, whereas the red line is a single step reaction with a tight transition state (close to a phosphorane) and the blue line is a loose transition state (close to a metaphosphate). Figure extracted from [117].

The stepwise reactions occur via an intermediate, and it is possible to distinguish between an associative mechamism (addition-elimination, SN2-like) where a pentacoordinate phosphorane intermediate is formed (in red in Figure 5c) and a dissociative mechanism (elimination-addition, SN1-like) where a trivalent metaphosphate intermediate is created (in blue in Figure 5c). In contrast, a coordinated reaction may occur in a single step, and therefore no thermodynamically stable intermediate is formed. Analogously, in concerted reactions we can distinguish between tight transition states (SN2-like, in red in Figure 5.1b) and loose transition states (SN1-like, in blue in Figure 5.1b). The available experimental data support that phosphoryl transfer reactions proceed generally trough concerted processes [117].

The main principle of the rate acceleration achieved by enzymes is their ability to stabilize transition states relative to the substrates [119]. Two of the strategies employed by kinases to enhance the rate of phosphoryl transfer are:

- Activation of the nucleophile: as stated before, all phosphoryl transfer reactions are initiated by a nucleophilic attack. Kinases bind their substrates and align them so that the phosphorus atom and the leaving group are in the optimum orientation for an in-line nucleophilic attack, where the attacking nucleophile and the leaving group are in apical positions of the trigonal bipyramidal transition state. By fixing the two substrates relative to each other, the translational and rotational degrees of freedom are reduced, which increases the velocity of the reaction. Additionally, the reactivity of the nucleophile can be increased by removing a proton of the attacking nucleophile with a general base or by metal activation.

- Stabilization of the leaving group: during the transfer reaction a rearrangement of the charge distribution occurs relative to the ground state. The stabilization by coordination of the developing negative charge between the phosphoryl group being transferred and the leaving group contributes to the catalytic effect.

5.1.2. Proposed catalytic mechamism for the ManNAc kinase

5.1.2.1. D517 has a catalytic role in hMNK

Based on the hMNK/ManNAc structure D517 was presumed to exert a catalytic role, due to its proximity to the ManNAc-6OH and to its high conservation among homologous sugar kinases (Figure 4.9 and Table 5.1). To validate this hypothesis the variants D517A and D517N were prepared, and their enzymatic activity was tested. In both cases, no activity could be detected (4.2.3). These results are consistent with the observation made for human hexokinase I, where all residues involved in sugar binding were mutated to alanine, revealing that D657A (structurally equivalent to D517 of hMNK) showed the biggest activity reduction to a level of less than 1% relative to the wild-type [120].

PDB code	Source organism	Function	% Seq Id	Amino acids					
2yhw	*Human*	ManNAc Kinase	100	N516	D517	R477	E566	H569	E588
2qm1	*E. faecalis*	Glucokinase (Put)	27	N113	D114	-	E163	H166	E185
2aa4	*E. coli*	ManNAc Kinase (Put)	26	N104	D105	I66	H153	H156	E175
3r8e	*CHU 1875*	Sugar kinase (Put)	23	N107	D108	L68	E157	H160	E170
2hoe	*TM 1224*	GlcNAc Kinase (Put)	20	N184	D185	P147	E232	Y235	E248
3lm9	*B. subtilis*	Fructokinase (YdhR)	22	T102	D103	P60	E150	H153	E176
1z05	*E. coli*	MLC-like Repressor	23	N192	D193	L155	E242	H245	E264
1woq	*Arthrobacter sp.*	Glucomannokinase (GMK)	25	N122	D123	I85	E168	H171	E180
1bdg	*Schistosoma M.*	Hexokinase I	19	N208	D209	P157	E260	G262	E294
1bg3	*Rat*	Hexokinase I	20	N656	D657	P605	E708	A711	E742
1cza	*Human*	Hexokinase I	16	N656	D657	P605	E708	A711	E742
2ch5	*Human*	GlcNAc kinase	18	T106	D107	-	-	-	D152

Table 5.1 Conservation of amino acids in the sugar binding site of different sugar kinases. The three dimensional structures of twelve sugar kinases from different organisms and with different substrate specificity were superimposed and the structural conservation of the amino acids implied in sugar binding was compared. The structure of hMNK in complex with ManNac (PDB code 2yhw, top line) has been taken as reference and the 6 amino acids whose side chains are implied in ManNAc binding have been listed. The columns under each of these amino acids list the corresponding structurally equivalent residues for each of the compared structures. The not conserved amino acids have been highlighted in yellow. A dash indicates that no structurally comparable amino acid has been found. The sequence identity has been given relative to hMNK and the kinase function has been listed. For structures with a putative annotated function but without biochemical data available (Put) has been included. (-) means that no structurally homologous residue has been found.

Further, to elucidate whether the MNK inactivation was due to a missense folding induced by the point mutations, the secondary structure content was analyzed by CD-spectra (4.2.1). No major differences were found for the variant D517N, whereas D517A showed a small yet insignificant increase for the random coil content with respect to the wild type (38% vs. 40%). A closer observation of Table 4.2 reveals that of all the variants, D517A and D517N show the smallest secondary structure content variation with respect to the wild-type. These data suggest that the loss of activity for the D517 variants (Table 4.3) is rather related to the specific catalytic role of this amino acid than to the effect of this single point mutation on the overall fold of the enzyme.

Since D517 is also involved in ManNAc coordination, it was important to find out whether the enzyme inactivation was caused by an impairment of the sugar binding ability or by the mutation of the catalytic residue. The dissociation constants (K_D) for wild type (wt)-hMNK/ManNAc (2.5 μM) and D517N/ManNAc (259 μM) were determined by isothermal titration calorimetry (4.2.2). D517N shows 100-fold lower binding affinity compared to wt-hMNK, but this binding affinity would still be sufficient for normal enzyme activity. All other variants tested in this study (including D517A) showed a weaker binding, and no K_D could be evaluated by ITC. Here again, it is important to consider that all variants have at least partial enzymatic activity except D517N and D517A. In contrast, the binding affinity for the natural substrate ManNAc is considerable higher for D517N than for all HIBM variants tested in the present work (4.2.2 and 4.2.3).

5.1.2.2. The phosphorylation of ManNAc proceeds by an associative SN2-like mechanism

The expected chemical mechanism implies a nucleophilic attack of the O6 atom of the substrate N-acetyl mannosamine on the γ-phosphorous atom of the ATP molecule (Figure 5.2), which possesses a partial electropositive charge (P_δ=+1.166 and O_δ=-0.776) [121]. The nucleophilicity of the O6 atom from the alcohol group at the C6 atom is increased by deprotonation. For this purpose, the catalytic residue D517 acts as a general base. D517-$O_{\delta 1}$ and ManNAc-O6 are in hydrogen bond distance (2.6Å) and well oriented with respect to each other. D517 is otherwise hydrogen bonded to the O4 atom of ManNAc (Figure 4.11, Table 4.5).
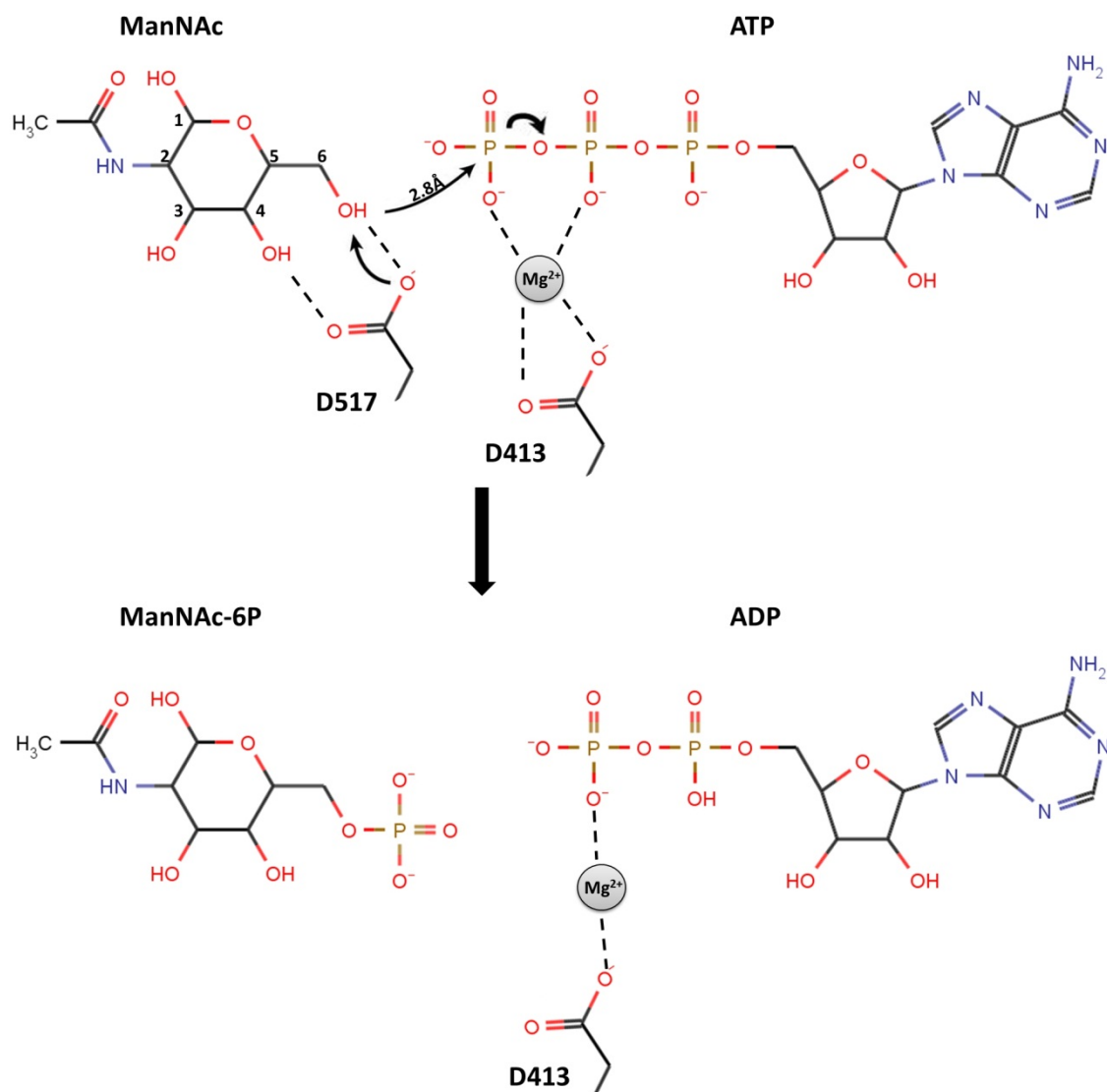
Figure 5.2 Schematic representation of the phosphoryl transfer mechanism of hMNK. N-Acetyl mannosamine (ManNAc) reacts with ATP to produce ManNAc-6P and ADP. The model was created with the program Marvinsketch (Chemaxon).

A relevant issue is the position of the γ-phosphate of ATP relative to the nucleophilic ManNAc-6O atom in the ground state complex. For the hMNK/ManNAc/ADP structure (4.11) and the hMNK/ManNAc-6P/ADP complex (4.12), the position of the pyrophosphate (α and β phosphates) is well defined by the electron density and plausible from the coordination point of view. An alignment of the ManNAc atoms in the hMNK/ManNAc/ADP structure with the glucose atoms of the crystal structure of human glucokinase in complex with glucose and AMPPNP (PDB code 3FGU) has been performed (Figure 5.3) revealing that the positions of the α and β phosphates for the

two structures overlap (rmsd is less than 1 Å). The structure of the complex hMNK/ManNAc-6P/ADP has been also superimposed in Figure 5.3 revealing that the γ-phosphate of the AMPPNP molecule in glucokinase complex occupies the same position as the phosphate moiety of the product ManNAc-6P in the hMNK/ManNAc-6P/ADP structure. Furthermore, the same position is occupied by a water molecule in the hMNK/ManNAc/ADP structure (#1 in Figure 4.13 and 5.3), which strongly suggests that this is the position occupied by the γ-phosphate in the ground state complex hMNK/ManNAc/ATP. In this thesis, the structure with an ATP analogue like AMPPCP has been solved. As described in section 4.13, a structure could be obtained but the quality of the data is not good enough to unambiguously model the nucleotide. Nevertheless, the position of the γ-phosphate for the hMNK/ManNAc/AMPPCP structure correlates with the position described in Figure 5.3.
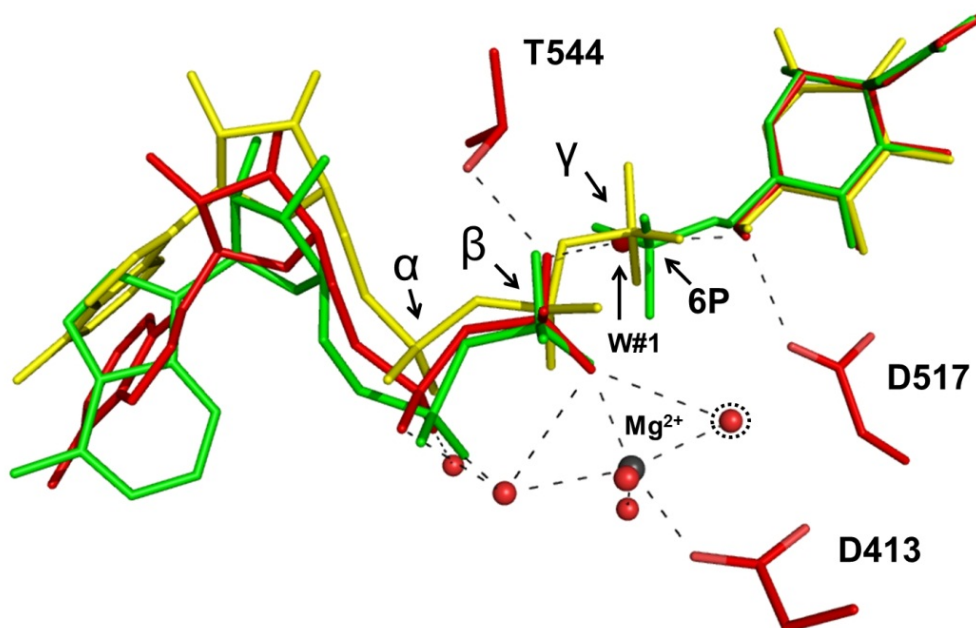
Figure 5.3 Comparison of the nucleotide binding site. The crystal structures of the human glucokinase in complex with AMPPNP and glucose (yellow, PDB 3FGU), hMNK in complex with ADP and ManNAc-6P (green- 2YI1) and hMNK in complex with ADP and ManNAc (red- 2YHY) have been superimposed on their respective pyranoses. Only the relevant side chains of hMNK have been shown for clarity. Magnesium is represented as a gray sphere and water molecules as red spheres. The water in the dotted circle (corresponding to #2 in Figure 4.13) represents an alternative magnesium position (see 5.1.2.3), and the water #1 shown with an arrow occupies the position of the γ-phosphate in the hMNK/ManNAc/ADP structure.

The distance between the ManNAc-6O atom and the γ-phosphate is 2.8 Å. A transition state is considered to have an associative character if the distance separating the nucleophile and the γ-phosphorous atom is less than 4.9 Å (the sum of a P-O van der Waals contact and a P-O single bond) [122]. Therefore, the reaction proceeds over a tight transition state (5.1.1), whereby the enzyme aligns the β- and γ- phosphates with the attacking nucleophile for an in-line transfer reaction.

Finally, some authors suggested that kinases could bind ATP with the oxygen atoms of the β and γ phosphates in a high energy eclipsed conformation which increases the electrostatic repulsion between the β and γ phosphoryl groups and can accelerate the reaction [122, 123]. This could not be observed for hMNK, since the positions of the AMPPCP atoms in the hMNK/ManNAc/AMPPCP structure are not well defined. However, the crystal structure of the human glucokinase in complex with AMPPNP shown in Figure 5.3 shows this feature, suggesting that ATP could bind to hMNK in an eclipsed conformation.

5.1.2.3.   hMNK is a magnesium dependent kinase

Kinase activity tests (3.4.1) have shown that recombinant hMNK requires magnesium for its enzymatic activity. If the reaction buffer contains no magnesium the reaction rate is lowered by one order of magnitude. Addition of EDTA results in inactivation of the reaction. As described for other magnesium dependent phosphoryl transfer enzymes and based on the structural findings presented here, it can be inferred that magnesium plays an important role for catalysis at three different levels [123]:

-   Mg^{2+} facilitates ATP binding to the enzyme. In the hMNK/ManNAc/ADP structure, Mg^{2+} is axially coordinated by D413 and the β phosphate of the ADP molecule (Figures 5.2 and 5.3) as a bridge between the protein and the nucleotide. For the ground state complex formed by hMNK, ATP and ManNAc, Mg^{2+} is expected to occupy a position between the β and γ phosphates and D413. This position is occupied by a water molecule in the hMNK/ManNAc/ADP crystal structure (numbered as 2 in Figure 4.13 and encircled in Figure 5.3).
-   Mg^{2+} activates the γ-phosphate of ATP. Acting as a Lewis acid, Mg^{2+} polarizes one of the P-O bonds of the γ-phosphate, which results in an increase of the electrophilicity of P_γ atom and a consequently higher susceptibility for a nucleophilic attack at the ManNAc-6O.

- Mg^{2+} neutralizes negative charges: in the ground state it neutralizes electrostatic repulsions between the negatively charged oxygen atoms of the β and γ phosphates. This allows the enzyme to bind ATP in an extended form with the oxygen atoms of the β and γ phosphates in an eclipsed conformation, which mimics the transition state conformation of ATP and lowers therefore the free energy of activation (5.1.1) for phosphoryl transfer reactions. Furthermore, by adopting this conformation the γ-phosphoryl group is positioned in-line with the nucleophile. During the transition state, the nucleophilic attack of ManNAc-O6 on the γ-phosphate produces an increase of electron density on the breaking bond between the β and γ phosphate moieties. Mg^{2+} contributes to stabilize this developing charge, thereby reducing the free energy of activation and accelerating the reaction.

5.1.2.4. hMNK needs a conformational rearrangement upon ManNAc binding for catalysis

In section 4.9 it has been described how upon ManNAc binding the N-terminal domain of hMNK rotates against the C-terminal domain by 12°. A similar global conformational change had been previously described for other sugar kinases like glucokinases and hexokinases [124, 125]. In some ATP-dependent glucokinases like rat liver hexokinase I, ATP can only bind after the rearrangement induced by the binding of glucose [126], which underlines the importance of this domain dynamics to form a catalytically competent enzyme.

Figure 5.4 shows a superimposition of the C-terminal domain of the apo-hMNK structure (PDB code 3EO3- green) and the hMNK/ManNac structure (2YHY- red). In the apo-structure the amino acids of the N-terminal domain involved in ManNAc binding are too far away (D517) or in an unsuitable orientation (N516) to perform the necessary substrate binding for the catalytic event. The conformational change induced by the binding of ManNAc is also important for ATP binding. The loop containing T417 (in yellow for the apo-structure and in orange for the ManNAc-bound structure), an amino acid involved in nucleotide binding, differs by 5 Å within both structures.

The conformational change induced by substrate binding varies within kinases. Indeed, time-resolved fluorescence studies on adenylate kinase suggested that there is not only an open and a close conformation but that substrate binding contributes to trap the

protein in a so called "close" conformation, which otherwise exists also in solution [127]. Apart from orientating the side chains to bind the substrates, these conformational changes prevent the enzyme from unnecessary waste of ATP in absence of substrate.
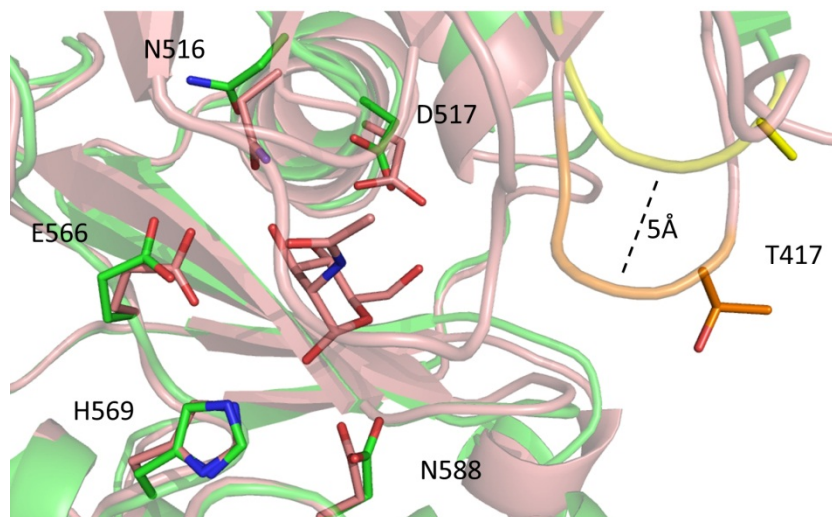

Figure 5.4 Structural local changes produced by domain dynamics. The C-terminal lobes of the apo-form (green) and sugar bound form (magenta) of hMNK have been superimposed. A careful exploration reveals relevant changes in the amino acids orientation. Also some major global changes can be observed like the difference between the loops containing T417 (in yellow for the apo-form and orange for the ManNAc bound form).

5.2. hMNK specificity

The term glucose kinases is generally used to define enzymes that catalyze the phosphorylation of glucoses and other hexoses by phosphoryl donors ATP, ADP or inorganic polyphosphate [Poly(P)]. Glucose kinases are further divided into the hexokinase family and the ribokinase family. Further, based on their primary structures, the memebers of the hexokinase family can be classified into the group A, B or HK. The primary sequences of the ROK-family kinases are homologous to those of the B group hexokinases and therefore ROK-kinases are classified as B group hexokinases [128]. One of the features of hexokinases is that they can catalyze the phosphorylation of a broad range of monosaccharides like glucose, fructose, mannose and galactose if present in high concentrations [129, 130]. In contrast, glucokinases and fructokinases that belong to the ribokinase family are highly specific for glucose and fructose, respectively [114].

The specificity of hMNK for ManNAc has been tested by comparing the enzymatic activity of hMNK for different substrates at the same concentration (4.2.3). hMNK showed a low promiscuity level (ManNAc (100%), ManNProp (30%), ManNBut (4%), GlcNac (6%)).

The substrate binding site has been superimposed with ROK-fructokinase YdhR [114] and glucomannokinase (GMK) from *Arthrobacter sp.*, a group B hexokinase [131] (Figure 5.5). All residues involved in sugar binding are structurally conserved but R477 and N516 (in hMNK nomenclature). N516 is conserved between hMNK and glucomannokinase but YdhR has a threonine in this position. YdhR specifically catalyzes the phosphorylation of fructose but cannot phosphorylate glucose. Since N516 is highly conserved among the hexokinase family (Table 5.1), it seems clear that this mutation obeys the necessity of YdhR to specifically distinguish between both isomers.

R477 is not conserved among hexokinases (Table 5.1) and it is therefore likely to be a specific feature of hMNK. Its implication in the binding of the N-acetyl moiety of ManNAc is also in line with this idea. Furthermore, the loop containing R477 (marked with an arrow in Figure 5.5) is implied in sugar binding in all three compared structures but the amino acids in this loop are not conserved within the relevant enzymes, which suggests that this loop could regulate the affinity of the enzymes for a certain substrate.
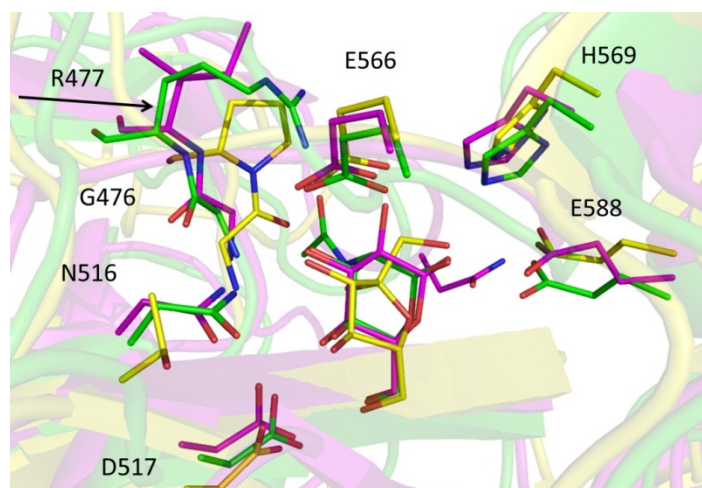
Figure 5.5 Superimposition of active site pockets. hMNK (green), YdhR (yellow-PDB code 3LM9) and GMK (magenta- 1WOQ) have been superimposed based on their respective sugars. The figure shows the high sequential and structural conservation of the residues involved in sugar binding and the presumed specificity regulating of the loop indicated by an arrow. The residues have been numbered corresponding to the hMNK structure, for the residue numbers for YdhR and GMK see Table 5.1.

The sturctures of the complexes hMNK/ManNAc/ADP and hMNK/ManNAc-6P/ADP showed clear electron density for the pyrophosphate moiety but poor density for the rest of the nucleotide. To elucidate if this phenomenon was due to an unspecificity of hMKN for ATP, the enzymatic test was repeated with GTP, CTP and UTP as phosphoryl donors (data not shown). However, compared to ATP, only GTP showed some residual activity, indicating that hMNK preferentially binds ATP as a donor. Interestingly, some glucose kinases belonging to the B group like GMK from *Arthrobacter sp.*[131], use [Poly(P)] (a polymer of orthophosphate residues) as phosphoryl donor. The high structural homology of hMNK with GMK (Figure 5.5 and Table 5.1) and the low coordination environment found for ribose and adenine moieties (4.11) appears to suggest that hMNK evolved from a [Poly(P)]-using ancestor and its affinity for ATP is based on triphosphate binding.

5.3. Structural Mapping of HIBM related mutations

HIBM is an autosomal recessive muscle disorder in humans caused by mutations of the GNE/MNK enzyme. Among both enzymatic domains there are more than 60 HIBM-associated mutations described to date [132]. The activity of both domains is affected independent of the localization of the mutation [83]. An extensive structural mapping of these disease-associated mutations has been performed previously [84, 132], based on the apo-hMNK structure (PDB 3EO3). However, the newly gained structural information concerning sugar and ATP binding sites makes possible to remap some of these mutations, based this time on tangible data instead of putative information. It is necessary to reveal at this point that crystallization trials were performed for three of the variants (M712T, A631T and N519S) but unfortunately no crystal were obtained for any one of them. There are more than 50 described point mutations causing HIBM. It is not the aim of this thesis to make an extensive analysis of all of them but to show the value of the presented data as a basis for understanding the relationship between the disease and the mutations that cause it. Here, only the mutants cloned, expressed and enzymatically tested in this work (the most common occurring ones- see Table 4.1) have been analysed.

As a first general statement, it is understandable, that in a highly compact folded structure such as hMNK many single point mutations are prone to disrupt hMNK architecture. **N519** is located on α3 and N519-$N_{\delta 2}$ is hydrogen bonded to D515-$O_{\delta 1}$,

thereby orienting N516 and D517, two of the sugar binding residues. A mutation to serine (N519S) alters this interaction and consequently the binding affinity of the sugar. **F528** is located at the very C-terminus of α3 in a hydrophobic contact interface with β11. The exchange of the bulky phenylalanine to a small polar residue might disrupt this interaction and affect the orientation of the sugar binding residues at the C-terminal part of α3. **I587** is buried and inaccessible to solvent. Its location between C586 (Zn^{2+}-binding) and E588 (sugar-binding) suggests that a change of I587 to a polar residue like Thr will disturb the binding of both, Zn^{2+} and ManNAc. The impairment of I587T to bind Zn^{2+} could explain why this variant is present only as a monomer, since Zn^{2+} is a very important structural element of dimeric hMNK. **A631** is located at the C-terminus of α7 in an area of poorly defined electron density, making the conformation of alanine unreliable. Nevertheless, A631 is far away from the sugar binding site, and a mutation of this residue is likely to rather impair ATP binding, which fits with the low enzymatic activity observed for the two variants, A631T and A631V (4.2.3), and the conservation of the specificity for ManNAc. **M712** stabilizes β4 and β7 by hydrophobic interactions. β4 and β7 bear four of the sugar binding residues in two loops at their respective C-terminus (G476, R477 for β4 and N516, D517 for β7). Thr is shorter than Met and unable to make these interactions, which explains the consequences of this mutation.

5.4. The search for an hMNK inhibitor

The introduction of this thesis describes the relevance of sialic acids and its biosynthetic pathway for life processes (1). Given the bottleneck role of GNE in sialic acid biosynthesis, there have been several attempts to obtain an inhibitor for this bifunctional enzyme, since it would be a valuable tool for GNE and sialic acid research and could offer a novel approach to counterbalance the increased sialylation in tumors and metastatic cells (1.6). Many UDP-GlcNAc analogs and transition state analogs for the epimerase domain of the GNE were synthesized and tested to date [133]. However, none of the inhibitors designed so far proved to be effective in cellular systems. The ManNAc kinase domain (MNK) of GNE can be an equally valuable target for inhibition studies. The crystal structure of hMNK in complex with its native substrate ManNAc revealed that ManNAc is tightly bound by hMNK and only the ManNAc-6OH position is solvent accessible (4.8 and Figure 4.16). On this basis it was postulated that ManNAc modifications at the C-6 position with a relative polar group could yield potential inhibitors. In our first approach to verify this idea, ManNAc-6OAc was

synthesized and found to competitively inhibit hMNK stronger than all other previously published inhibitors of hMNK (4.15). Even though the acetylation of the ManNAc-O6 atom would not be stable *in vivo* due to the presence of unspecific esterase activities, the modification at this specific position is clearly one possible and potent strategy in the search for an efficient hMNK inhibitor.

Some hexokinases from mammals and lower organisms present an allosteric inhibition by the final product glucose-6P (G6P). The allosteric site overlaps with the ATP binding site: the phosphate moiety of G6P binds in the same site as the β-phosphate from ATP and the pyranose ring at the Mg^{2+} position [134]. A superimposition of hMNK/ManNAc with the human brain hexokinase-I in complex with glucose and G6P reveals that the allosteric site is structurally conserved in hMNK and occupied by water molecules. No evidence of hMNK inhibition by ManNAc-6P has been demonstrated to date and the existence of G6P insensitive yeast hexokinases with high sequential and structural homology to G6P sensitive hexokinases [135] suggest that hMNK may not be allosterically regulated. However, this knowledge offers an interesting alternative for the production of an inhibitor. The affinity of hMNK for ManNAc is three orders of magnitude higher than for ATP (4.2.3). Therefore, it is expected that creating an inhibitor that competes for the ATP binding site could be advantageous over creating one that competes for the ManNAc binding site.

6. SUMMARY

Sialic acids are essential components of membrane glycoconjugates. They are responsible for the interaction, structure and functionality of all deuterostome cells and have major functions in cellular processes and diseases. The key enzyme of the biosynthesis of sialic acid is the bifunctional UDP-*N*-acetylglucosamine-2-epimerase/*N*-acetylmannosamine kinase (GNE) that transforms UDP-*N*-acetylglucosamine to *N*-acetylmannosamine-6-phosphate and has a direct impact on the sialylation of the cell surface. In this thesis three high resolution crystal structures of the recombinant human acetylmannosamine kinase domain (hMNK) from GNE are presented. hMNK converts *N*-acetylmannosamine to *N*-acetylmannosamine-6-phosphate, a precursor of sialic acid, and has a direct impact on the sialylation of the cell surface, which is of medical interest because sialylation of tumor cell surface glycans is at a higher level than that of healthy cells. The complexes formed by hMNK with its substrate N-acetylmannosamine (ManNAc), with ManNAc and ADP, and with ManNAc-6-phosphate and ADP, show structural details of reaction educt and product. hMNK belongs to the ROK family of proteins, and this study presents the first human member of this family in complex with its cognate substrate. The interactions between hMNK and ManNAc explain the high substrate specificity of hMNK and suggest a key active site residue, Asp517, that was mutated and shown to be crucial for enzymatic activity. Since the structure of the complex formed between hMNK and ManNAc also indicated the structural properties of a possible inhibitor, we synthesized ManNAc-6-O-acetate that proved to be a modest inhibitor and may be taken as lead for more potent inhibitors that could open novel ways for sialic acid research, glycan bioengineering and cancer therapy.

6. ZUSAMMENFASSUNG

Sialinsäuren (Sias) sind essentielle Komponenten der Membran-Glycokonjugate. Sias sind zuständig für die Interaktion, Struktur und Funktionalität aller Deuterostomia-Zellen und spielen eine wichtige Rolle bei zahlreichen zellulären Prozessen und Krankheiten. Das Schlüsselenzym der Sialinsäurebiosynthese ist die bifunktionelle UDP-*N*-Acetylglukosamin-2-Epimerase/*N*-Acetylmannosamin Kinase (GNE), die UDP-*N*-Acetylglucosamin in *N*-Acetylmannosamin-6-phosphate umwandelt und einen direkten Impakt auf der Sialylierung der Zelloberfläche hat. Dies ist von medizinischem Interesse, denn Tumorzellen weisen eine höhere Sialylierung der Zelloberflächeglykane im Vergleich zu gesunden Zellen auf. In der vorliegenden Dissertation, werden drei hochaufgelöste Kristallstrukturen der rekombinanten menschlichen N-acetyl Mannosamine Kinase Domäne (hMNK) von GNE präsentiert. hMNK wandelt *N*-Acetylmannosamin in *N*-Acetylmannosamin-6-Phosphat (eine Vorläufersubstanz von Sias) um. Die Komplexe zwischen hMNK und ihrem natürlichen Substrate N-Acetylmannosamin (ManNAc), zwischen hMNK, ManNAc und ADP und zwischen hMNK, ManNAc-6-Phosphat and ADP zeigen strukturelle Details von Reaktions-edukt und –produkt. hMNK gehört zur ROK Proteinfamilie und diese Arbeit präsentiert die erste Struktur eines menschlichen Proteins dieser Familie im Komplex mit seinem Substrat. Die Interaktionen zwischen hMNK und ManNAc erklären die hohe Substratspezifität von hMNK und schlagen einen aktiven Aminosäuren Rest vor, Asp517, der mutiert wurde und eine entscheidende Rolle für die Katalyse zeigte. Da die Struktur des Komplexes hMNK/ManNAc die strukturellen Eigenschaften von einem möglichen Inhibitor vorgeschlagen hatte, wurde ManNAc-6-O-Acetat synthetisiert und zeigte eine schwache Inhibition. Diese Verbindung kann daher genommen werden als Startpunkt für die Herstellung von neuen und besseren hMNK- Inhibitoren, die guten Alternativen, sowohl für Sialinsäure Forschung, als auch für Glykan Bioengineering und die Krebs Therapie bieten sollten.

7. BIBLIOGRAPHY

1. Crick, F., *Central dogma of molecular biology.* Nature, 1970. **227**(5258): p. 561-3.
2. in *Essentials of Glycobiology*, A. Varki, et al., Editors. 2009: Cold Spring Harbor (NY).
3. IHGSC, *Finishing the euchromatic sequence of the human genome.* Nature, 2004. **431**(7011): p. 931-45.
4. Bertozzi, C.R. and L.L. Kiessling, *Chemical glycobiology.* Science, 2001. **291**(5512): p. 2357-64.
5. Campbell, C.T. and K.J. Yarema, *Large-scale approaches for glycobiology.* Genome biology, 2005. **6**(11): p. 236.
6. Buchner, P., et al., *Characterization of a tissue-specific and developmentally regulated beta-1,3-glucanase gene in pea (Pisum sativum).* Plant molecular biology, 2002. **49**(2): p. 171-86.
7. Varki, N.M. and A. Varki, *Diversity in cell surface sialic acid presentations: implications for biology and disease.* Laboratory investigation; a journal of technical methods and pathology, 2007. **87**(9): p. 851-7.
8. Varki, A., *Glycan-based interactions involving vertebrate sialic-acid-recognizing proteins.* Nature, 2007. **446**(7139): p. 1023-9.
9. G, B., *Über die Kohlenhydratgruppen des Submaxillarismucins.* Hoppe-Seyler´s Z Physiol Chem 1936(240): p. 43-54.
10. E, K., *Neuraminsäure, das Spaltprodukt eines neuen Gehirn-lipoids.* Hoppe-Seyler´s Z Physiologische Chemie, 1941. **268**(1-2): p. 50-58.
11. Blix, F.G., A. Gottschalk, and E. Klenk, *Proposed nomenclature in the field of neuraminic and sialic acids.* Nature, 1957. **179**(4569): p. 1088.
12. Gottschalk, A., *The chemistry and biology of sialic acids and related substances.* University press, Cambridge, 1960.
13. Inoue, S., K. Kitajima, and Y. Inoue, *Identification of 2-keto-3-deoxy-D-glycero--galactonon99onic acid (KDN, deaminoneuraminic acid) residues in mammalian tissues and human lung carcinoma cells. Chemical evidence of the occurrence of KDN glycoconjugates in mammals.* The Journal of biological chemistry, 1996. **271**(40): p. 24341-4.
14. Angata, T., et al., *Biosynthesis of KDN (2-keto-3-deoxy-D-glycero-D-galacto-nononic acid). Identification and characterization of a KDN-9-phosphate synthetase activity from trout testis.* The Journal of biological chemistry, 1999. **274**(33): p. 22949-56.
15. Angata, T. and A. Varki, *Chemical diversity in the sialic acids and related alpha-keto acids: an evolutionary perspective.* Chemical reviews, 2002. **102**(2): p. 439-69.
16. Saito, M., H. Kitamura, and K. Sugiyama, *Occurrence of gangliosides in the common squid and pacific octopus among protostomia.* Biochimica et biophysica acta, 2001. **1511**(2): p. 271-80.
17. Kim, K., et al., *Expression of a functional Drosophila melanogaster N-acetylneuraminic acid (Neu5Ac) phosphate synthase gene: evidence for endogenous sialic acid biosynthetic ability in insects.* Glycobiology, 2002. **12**(2): p. 73-83.
18. Schauer, R., *Sialic acids as regulators of molecular and cellular interactions.* Current opinion in structural biology, 2009. **19**(5): p. 507-14.
19. Prives, J.M. and K. Olden, *Carbohydrate requirement for expression and stability of acetylcholine receptor on the surface of embryonic muscle cells in culture.* Proceedings

of the National Academy of Sciences of the United States of America, 1980. **77**(9): p. 5263-7.

20. Egrie, J.C. and J.K. Browne, *Development and characterization of novel erythropoiesis stimulating protein (NESP).* British journal of cancer, 2001. **84 Suppl 1**: p. 3-10.

21. Ganss, B. and W. Hoffmann, *Calcium binding to sialic acids and its effect on the conformation of ependymins.* European journal of biochemistry / FEBS, 1993. **217**(1): p. 275-80.

22. Saladini, M., L. Menabue, and E. Ferrari, *Binding ability of sialic acid towards biological and toxic metal ions. NMR, potentiometric and spectroscopic study.* Journal of inorganic biochemistry, 2002. **88**(1): p. 61-8.

23. Veerman, E.C., M. Valentijn-Benz, and A.V. Nieuw Amerongen, *Viscosity of human salivary mucins: effect of pH and ionic strength and role of sialic acid.* Journal de biologie buccale, 1989. **17**(4): p. 297-306.

24. Raju, T.S. and E.A. Davidson, *Role of sialic acid on the viscosity of canine tracheal mucin glycoprotein.* Biochemical and biophysical research communications, 1994. **205**(1): p. 402-9.

25. Iijima, R., et al., *Novel biological function of sialic acid (N-acetylneuraminic acid) as a hydrogen peroxide scavenger.* FEBS letters, 2004. **561**(1-3): p. 163-6.

26. Ogasawara, Y., et al., *Sialic acid is an essential moiety of mucin as a hydroxyl radical scavenger.* FEBS letters, 2007. **581**(13): p. 2473-7.

27. Rens-Domiano, S. and T. Reisine, *Structural analysis and functional role of the carbohydrate component of somatostatin receptors.* The Journal of biological chemistry, 1991. **266**(30): p. 20094-102.

28. Woronowicz, A., et al., *Dependence of neurotrophic factor activation of Trk tyrosine kinase receptors on cellular sialidase.* Glycobiology, 2007. **17**(1): p. 10-24.

29. Lehmann, F., E. Tiralongo, and J. Tiralongo, *Sialic acid-specific lectins: occurrence, specificity and function.* Cellular and molecular life sciences : CMLS, 2006. **63**(12): p. 1331-54.

30. Schauer, R., ed. *The diversity of sialic acids and their interplay with lectins.* Glycobiology2007, Edited by Sansom C, Markman O. Bloxham: Cion Publ. Ltd. 136-149.

31. Ashwell, G. and A.G. Morell, *The role of surface carbohydrates in the hepatic recognition and transport of circulating glycoproteins.* Advances in enzymology and related areas of molecular biology, 1974. **41**(0): p. 99-128.

32. Janicik, J.M., et al., *Sequestration of neuraminidase-treated erythrocytes. Studies on its topographic, morphologic and immunologic aspects.* Cell and tissue research, 1978. **186**(2): p. 209-26.

33. Fischer, C., et al., *Reversible binding of sialidase-treated rat lymphocytes by homologous peritoneal macrophages.* Carbohydrate research, 1991. **213**: p. 263-73.

34. Bratosin, D., et al., *Flow cytofluorimetric analysis of young and senescent human erythrocytes probed with lectins. Evidence that sialic acids control their life span.* Glycoconjugate journal, 1995. **12**(3): p. 258-67.

35. Laidler, P. and A. Litynska, *Tumor cell N-glycans in metastasis.* Acta biochimica Polonica, 1997. **44**(2): p. 343-57.

36. Varki, A., *Sialic acids in human health and disease.* Trends in molecular medicine, 2008. **14**(8): p. 351-60.

37. Alper, J., *Glycobiology. Turning sweet on cancer.* Science, 2003. **301**(5630): p. 159-60.

38. Schwarzkopf, M., et al., *Sialylation is essential for early development in mice.* Proceedings of the National Academy of Sciences of the United States of America, 2002. **99**(8): p. 5267-70.

39. Hirst, G.K., *Adsorption of Influenza Hemagglutinins and Virus by Red Blood Cells.* The Journal of experimental medicine, 1942. **76**(2): p. 195-209.

40. Pangburn, M.K., *Host recognition and target differentiation by factor H, a regulator of the alternative pathway of complement.* Immunopharmacology, 2000. **49**(1-2): p. 149-57.

41. Pangburn, M.K. and H.J. Muller-Eberhard, *Complement C3 convertase: cell surface restriction of beta1H control and generation of restriction on neuraminidase-treated cells.* Proceedings of the National Academy of Sciences of the United States of America, 1978. **75**(5): p. 2416-20.

42. Ram, S., et al., *A novel sialic acid binding site on factor H mediates serum resistance of sialylated Neisseria gonorrhoeae.* The Journal of experimental medicine, 1998. **187**(5): p. 743-52.

43. McEver, R.P., *Selectins: lectins that initiate cell adhesion under flow.* Current opinion in cell biology, 2002. **14**(5): p. 581-6.

44. Varki, A., *Selectin ligands.* Proceedings of the National Academy of Sciences of the United States of America, 1994. **91**(16): p. 7390-7.

45. Rosen, S.D., et al., *Involvement of sialic acid on endothelial cells in organ-specific lymphocyte recirculation.* Science, 1985. **228**(4702): p. 1005-7.

46. Tyrrell, D., et al., *Structural requirements for the carbohydrate ligand of E-selectin.* Proceedings of the National Academy of Sciences of the United States of America, 1991. **88**(22): p. 10372-6.

47. Johnston, G.I., R.G. Cook, and R.P. McEver, *Cloning of GMP-140, a granule membrane protein of platelets and endothelium: sequence similarity to proteins involved in cell adhesion and inflammation.* Cell, 1989. **56**(6): p. 1033-44.

48. Handa, K., et al., *Selectin GMP-140 (CD62; PADGEM) binds to sialosyl-Le(a) and sialosyl-Le(x), and sulfated glycans modulate this binding.* Biochemical and biophysical research communications, 1991. **181**(3): p. 1223-30.

49. Crocker, P.R., et al., *Siglecs: a family of sialic-acid binding lectins.* Glycobiology, 1998. **8**(2): p. v.

50. Crocker, P.R. and A. Varki, *Siglecs, sialic acids and innate immunity.* Trends in immunology, 2001. **22**(6): p. 337-42.

51. Ghosh, S., et al., *Glucosamine metabolism. V. Enzymatic synthesis of glucosamine 6-phosphate.* The Journal of biological chemistry, 1960. **235**: p. 1265-73.

52. Reinke, S.O., et al., *Regulation and pathophysiological implications of UDP-GlcNAc 2-epimerase/ManNAc kinase (GNE) as the key enzyme of sialic acid biosynthesis.* Biological chemistry, 2009. **390**(7): p. 591-9.

53. Allen, M.B. and D.G. Walker, *Kinetic characterization of N-acetyl-D-glucosamine kinase from rat liver and kidney.* The Biochemical journal, 1980. **185**(3): p. 577-82.

54. Strominger, J.L. and M.S. Smith, *Uridine diphosphoacetylglucosamine pyrophosphorylase.* The Journal of biological chemistry, 1959. **234**(7): p. 1822-7.

55. Hinderlich, S., et al., *A bifunctional enzyme catalyzes the first two steps in N-acetylneuraminic acid biosynthesis of rat liver. Purification and characterization of UDP-N-acetylglucosamine 2-epimerase/N-acetylmannosamine kinase.* The Journal of biological chemistry, 1997. **272**(39): p. 24313-8.

56. Chou, W.K., et al., *Sialic acid biosynthesis: stereochemistry and mechanism of the reaction catalyzed by the mammalian UDP-N-acetylglucosamine 2-epimerase.* Journal of the American Chemical Society, 2003. **125**(9): p. 2455-61.

57. Roseman, S., et al., *Enzymatic synthesis of sialic acid 9-phosphates.* Proceedings of the National Academy of Sciences of the United States of America, 1961. **47**: p. 958-61.

58.   Maliekal, P., et al., *Identification of the sequence encoding N-acetylneuraminate-9-phosphate phosphatase.* Glycobiology, 2006. **16**(2): p. 165-72.

59.   Munster-Kuhnel, A.K., et al., *Structure and function of vertebrate CMP-sialic acid synthetases.* Glycobiology, 2004. **14**(10): p. 43R-51R.

60.   Kean, E.L., *Nuclear cytidine 5'-monophosphosialic acid synthetase.* The Journal of biological chemistry, 1970. **245**(9): p. 2301-8.

61.   Eckhardt, M., et al., *Expression cloning of the Golgi CMP-sialic acid transporter.* Proceedings of the National Academy of Sciences of the United States of America, 1996. **93**(15): p. 7572-6.

62.   Iwersen, M., V. Vandamme-Feldhaus, and R. Schauer, *Enzymatic 4-O-acetylation of N-acetylneuraminic acid in guinea-pig liver.* Glycoconjugate journal, 1998. **15**(9): p. 895-904.

63.   Tanner, M.E., *The enzymes of sialic acid biosynthesis.* Bioorganic chemistry, 2005. **33**(3): p. 216-28.

64.   Watts, G.D., et al., *Clinical and genetic heterogeneity in chromosome 9p associated hereditary inclusion body myopathy: exclusion of GNE and three other candidate genes.* Neuromuscular disorders : NMD, 2003. **13**(7-8): p. 559-67.

65.   Reinke, S.O., et al., *Biochemical characterization of human and murine isoforms of UDP-N-acetylglucosamine 2-epimerase/N-acetylmannosamine kinase (GNE).* Glycoconjugate journal, 2009. **26**(4): p. 415-22.

66.   Comb, D.G. and S. Roseman, *Enzymic synthesis of N-acetyl-D-mannosamine.* Biochimica et biophysica acta, 1958. **29**(3): p. 653-4.

67.   Ghosh, S. and S. Roseman, *Enzymatic phosphorylation of N-acetyl-D-mannosamine.* Proceedings of the National Academy of Sciences of the United States of America, 1961. **47**: p. 955-8.

68.   Van Rinsum, J., et al., *Subcellular localization and tissue distribution of sialic acid precursor-forming enzymes.* The Biochemical journal, 1983. **210**(1): p. 21-8.

69.   Ghaderi, D., et al., *Evidence for dynamic interplay of different oligomeric states of UDP-N-acetylglucosamine 2-epimerase/N-acetylmannosamine kinase by biophysical methods.* Journal of molecular biology, 2007. **369**(3): p. 746-58.

70.   Kornfeld, S., et al., *The Feedback Control of Sugar Nucleotide Biosynthesis in Liver.* Proceedings of the National Academy of Sciences of the United States of America, 1964. **52**: p. 371-9.

71.   Horstkorte, R., et al., *Protein kinase C phosphorylates and regulates UDP-N-acetylglucosamine-2-epimerase/N-acetylmannosamine kinase.* FEBS letters, 2000. **470**(3): p. 315-8.

72.   Oetke, C., et al., *Epigenetically mediated loss of UDP-GlcNAc 2-epimerase/ManNAc kinase expression in hyposialylated cell lines.* Biochemical and biophysical research communications, 2003. **308**(4): p. 892-8.

73.   Giordanengo, V., et al., *Epigenetic reprogramming of UDP-N-acetylglucosamine 2-epimerase/N-acetylmannosamine kinase (GNE) in HIV-1-infected CEM T cells.* The FASEB journal : official publication of the Federation of American Societies for Experimental Biology, 2004. **18**(15): p. 1961-3.

74.   Jay, C.M., et al., *Hereditary Inclusion Body Myopathy (HIBM2).* Gene regulation and systems biology, 2009. **3**: p. 181-90.

75.   Krause, S., et al., *Localization of UDP-GlcNAc 2-epimerase/ManAc kinase (GNE) in the Golgi complex and the nucleus of mammalian cells.* Experimental cell research, 2005. **304**(2): p. 365-79.

76.   Weidemann, W., et al., *The collapsin response mediator protein 1 (CRMP-1) and the promyelocytic leukemia zinc finger protein (PLZF) bind to UDP-N-acetylglucosamine 2-*

epimerase/N-acetylmannosamine kinase (GNE), the key enzyme of sialic acid biosynthesis. FEBS letters, 2006. **580**(28-29): p. 6649-54.

77. Wang, Z., et al., *Roles for UDP-GlcNAc 2-epimerase/ManNAc 6-kinase outside of sialic acid biosynthesis: modulation of sialyltransferase and BiP expression, GM3 and GD3 biosynthesis, proliferation, and apoptosis, and ERK1/2 phosphorylation.* The Journal of biological chemistry, 2006. **281**(37): p. 27016-28.

78. Weiss, P., et al., *Identification of the metabolic defect in sialuria.* The Journal of biological chemistry, 1989. **264**(30): p. 17635-6.

79. Enns, G.M., et al., *Clinical course and biochemistry of sialuria.* Journal of inherited metabolic disease, 2001. **24**(3): p. 328-36.

80. Leroy, J.G., et al., *Dominant inheritance of sialuria, an inborn error of feedback inhibition.* American journal of human genetics, 2001. **68**(6): p. 1419-27.

81. Eisenberg, I., et al., *The UDP-N-acetylglucosamine 2-epimerase/N-acetylmannosamine kinase gene is mutated in recessive hereditary inclusion body myopathy.* Nature genetics, 2001. **29**(1): p. 83-7.

82. Argov, Z. and S. Mitrani-Rosenbaum, *The hereditary inclusion body myopathy enigma and its future therapy.* Neurotherapeutics : the journal of the American Society for Experimental NeuroTherapeutics, 2008. **5**(4): p. 633-7.

83. Penner, J., et al., *Influence of UDP-GlcNAc 2-epimerase/ManNAc kinase mutant proteins on hereditary inclusion body myopathy.* Biochemistry, 2006. **45**(9): p. 2968-77.

84. Tong, Y., et al., *Crystal structure of the N-acetylmannosamine kinase domain of GNE.* PloS one, 2009. **4**(10): p. e7165.

85. Kurochkina, N., T. Yardeni, and M. Huizing, *Molecular modeling of the bifunctional enzyme UDP-GlcNAc 2-epimerase/ManNAc kinase and predictions of structural effects of mutations associated with HIBM and sialuria.* Glycobiology, 2010. **20**(3): p. 322-37.

86. Titgemeyer, F., et al., *Evolutionary relationships between sugar kinases and transcriptional repressors in bacteria.* Microbiology, 1994. **140 (Pt 9)**: p. 2349-54.

87. Hansen, T., et al., *The first archaeal ATP-dependent glucokinase, from the hyperthermophilic crenarchaeon Aeropyrum pernix, represents a monomeric, extremely thermophilic ROK glucokinase with broad hexose specificity.* Journal of bacteriology, 2002. **184**(21): p. 5955-65.

88. Schiefner, A., et al., *The crystal structure of Mlc, a global regulator of sugar metabolism in Escherichia coli.* The Journal of biological chemistry, 2005. **280**(32): p. 29073-9.

89. Dennis, J.W. and S. Laferte, *Tumor cell surface carbohydrate and the metastatic phenotype.* Cancer metastasis reviews, 1987. **5**(3): p. 185-204.

90. Keppler, O.T., et al., *UDP-GlcNAc 2-epimerase: a regulator of cell surface sialylation.* Science, 1999. **284**(5418): p. 1372-6.

91. Hinderlich, S., et al., *The homozygous M712T mutation of UDP-N-acetylglucosamine 2-epimerase/N-acetylmannosamine kinase results in reduced enzyme activities but not in altered overall cellular sialylation in hereditary inclusion body myopathy.* FEBS letters, 2004. **566**(1-3): p. 105-9.

92. Bradford, M.M., *A rapid and sensitive method for the quantitation of microgram quantities of protein utilizing the principle of protein-dye binding.* Analytical biochemistry, 1976. **72**: p. 248-54.

93. Winter, R.N., F. , *Methoden der Biophysikalischen Chemie*1988, Stuttgart

Teubner Studienbücher Chemie.

94.   Sreerama, N. and R.W. Woody, *Estimation of protein secondary structure from circular dichroism spectra: comparison of CONTIN, SELCON, and CDSSTR methods with an expanded reference set.* Analytical biochemistry, 2000. **287**(2): p. 252-60.

95.   Whitmore, L. and B.A. Wallace, *DICHROWEB, an online server for protein secondary structure analyses from circular dichroism spectroscopic data.* Nucleic acids research, 2004. **32**(Web Server issue): p. W668-73.

96.   Ducruix, A. and R. Giegé, *Crystallization of nucleic acids and proteins : a practical approach*. [2nd ed. The practical approach series1999, Oxford ; New York: Oxford University Press. xxii, 435 p.

97.   AGW, L., *Recent changes to the MOSFLM package for processing film and*

image plate data. Joint CCP4 + ESF-EAMCB Newsletter on Protein Crystallography, 1992. **26.**

98.   Kabsch, W., *Xds.* Acta crystallographica. Section D, Biological crystallography, 2010. **66**(Pt 2): p. 125-32.

99.   Vagin, A. and A. Teplyakov, *Molecular replacement with MOLREP.* Acta Crystallogr D Biol Crystallogr. **66**(Pt 1): p. 22-5.

100.   Murshudov, G.N., A.A. Vagin, and E.J. Dodson, *Refinement of macromolecular structures by the maximum-likelihood method.* Acta Crystallogr D Biol Crystallogr, 1997. **53**(Pt 3): p. 240-55.

101.   Emsley, P. and K. Cowtan, *Coot: model-building tools for molecular graphics.* Acta crystallographica. Section D, Biological crystallography, 2004. **60**(Pt 12 Pt 1): p. 2126-32.

102.   Chen, V.B., et al., *MolProbity: all-atom structure validation for macromolecular crystallography.* Acta crystallographica. Section D, Biological crystallography, 2010. **66**(Pt 1): p. 12-21.

103.   Holm, L. and P. Rosenstrom, *Dali server: conservation mapping in 3D.* Nucleic acids research, 2010. **38**(Web Server issue): p. W545-9.

104.   *The PyMOL Molecular Graphics System* Schrödinger, LLC.

105.   McCoy, A.J., et al., *Phaser crystallographic software.* Journal of applied crystallography, 2007. **40**(Pt 4): p. 658-674.

106.   Murshudov, G.N., A.A. Vagin, and E.J. Dodson, *Refinement of macromolecular structures by the maximum-likelihood method.* Acta crystallographica. Section D, Biological crystallography, 1997. **53**(Pt 3): p. 240-55.

107.   Laskowski, R.A., D.S. Moss, and J.M. Thornton, *Main-chain bond lengths and bond angles in protein structures.* Journal of molecular biology, 1993. **231**(4): p. 1049-67.

108.   Diederichs, K. and P.A. Karplus, *Improved R-factors for diffraction data analysis in macromolecular crystallography.* Nature structural biology, 1997. **4**(4): p. 269-75.

109.   Krissinel, E. and K. Henrick, *Inference of macromolecular assemblies from crystalline state.* Journal of molecular biology, 2007. **372**(3): p. 774-97.

110.   Bork, P., C. Sander, and A. Valencia, *An ATPase domain common to prokaryotic cell cycle proteins, sugar kinases, actin, and hsp70 heat shock proteins.* Proceedings of the National Academy of Sciences of the United States of America, 1992. **89**(16): p. 7290-4.

111.   Goujon, M., et al., *A new bioinformatics analysis tools framework at EMBL-EBI.* Nucleic acids research, 2010. **38**(Web Server issue): p. W695-9.

112.   Gouet, P., et al., *ESPript: analysis of multiple sequence alignments in PostScript.* Bioinformatics, 1999. **15**(4): p. 305-8.

113.   Hayward, S. and R.A. Lee, *Improvements in the analysis of domain motions in proteins from conformational change: DynDom version 1.50.* J Mol Graph Model, 2002. **21**(3): p. 181-3.

114. Nocek, B., et al., *Structural studies of ROK fructokinase YdhR from Bacillus subtilis: insights into substrate binding and fructose specificity.* Journal of molecular biology, 2011. **406**(2): p. 325-42.

115. Grunholz, H.J., et al., *Inhibition of in vitro biosynthesis of N-acetylneuraminic acid by N-acyl- and N-alkyl-2-amino-2-deoxyhexoses.* Carbohydrate research, 1981. **96**(2): p. 259-70.

116. Zeitler, R., et al., *Inhibition of N-acetylglucosamine kinase and N-acetylmannosamine kinase by 3-O-methyl-N-acetyl-D-glucosamine in vitro.* European journal of biochemistry / FEBS, 1992. **204**(3): p. 1165-8.

117. Lassila, J.K., J.G. Zalatan, and D. Herschlag, *Biological phosphoryl-transfer reactions: understanding mechanism and catalysis.* Annual review of biochemistry, 2011. **80**: p. 669-702.

118. Lad, C., N.H. Williams, and R. Wolfenden, *The rate of hydrolysis of phosphomonoester dianions and the exceptional catalytic proficiencies of protein and inositol phosphatases.* Proceedings of the National Academy of Sciences of the United States of America, 2003. **100**(10): p. 5607-10.

119. Lienhard, G.E., *Enzymatic catalysis and transition-state theory.* Science, 1973. **180**(82): p. 149-54.

120. Arora, K.K., C.R. Filburn, and P.L. Pedersen, *Glucose phosphorylation. Site-directed mutations which impair the catalytic function of hexokinase.* The Journal of biological chemistry, 1991. **266**(9): p. 5359-62.

121. Cornell, W.D., et al., *A Second Generation Force Field for the Simulation of Proteins, Nucleic Acids, and Organic Molecules.* Journal of the American Chemical Society, 1995. **117**(19): p. 5179-5197.

122. Matte, A., L.W. Tari, and L.T. Delbaere, *How do kinases transfer phosphoryl groups?* Structure, 1998. **6**(4): p. 413-9.

123. Tari, L.W., et al., *Mg(2+)-Mn2+ clusters in enzyme-catalyzed phosphoryl-transfer reactions.* Nature structural biology, 1997. **4**(12): p. 990-4.

124. Steitz, T.A., M. Shoham, and W.S. Bennett, Jr., *Structural dynamics of yeast hexokinase during catalysis.* Philosophical transactions of the Royal Society of London. Series B, Biological sciences, 1981. **293**(1063): p. 43-52.

125. Kamata, K., et al., *Structural basis for allosteric regulation of the monomeric allosteric enzyme human glucokinase.* Structure, 2004. **12**(3): p. 429-38.

126. Monasterio, O. and M.L. Cardenas, *Kinetic studies of rat liver hexokinase D ('glucokinase') in non-co-operative conditions show an ordered mechanism with MgADP as the last product to be released.* The Biochemical journal, 2003. **371**(Pt 1): p. 29-38.

127. Sinev, M.A., et al., *Domain closure in adenylate kinase.* Biochemistry, 1996. **35**(20): p. 6425-37.

128. Kawai, S., et al., *Hypothesis: structures, evolution, and ancestor of glucose kinases in the hexokinase family.* Journal of bioscience and bioengineering, 2005. **99**(4): p. 320-30.

129. Cardenas, M.L., A. Cornish-Bowden, and T. Ureta, *Evolution and regulatory role of the hexokinases.* Biochimica et biophysica acta, 1998. **1401**(3): p. 242-64.

130. Middleton, R.J., *Hexokinases and glucokinases.* Biochemical Society transactions, 1990. **18**(2): p. 180-3.

131. Mukai, T., et al., *Crystal structure of bacterial inorganic polyphosphate/ATP-glucomannokinase. Insights into kinase evolution.* The Journal of biological chemistry, 2004. **279**(48): p. 50591-600.

132.   Huizing, M. and D.M. Krasnewich, *Hereditary inclusion body myopathy: a decade of progress.* Biochim Biophys Acta, 2009. **1792**(9): p. 881-7.
133.   Stolz, F., et al., *Novel UDP-glycal derivatives as transition state analogue inhibitors of UDP-GlcNAc 2-epimerase.* J Org Chem, 2004. **69**(3): p. 665-79.
134.   Mulichak, A.M., et al., *The structure of mammalian hexokinase-1.* Nature structural biology, 1998. **5**(7): p. 555-60.
135.   Wilson, J.E., *Hexokinases.* Reviews of physiology, biochemistry and pharmacology, 1995. **126**: p. 65-198.

Curriculum vitae

2008-2011   Dissertation bei Prof. Dr. Saenger, Freie Universität Berlin

2007   Diplomarbeit mit Titel „Das Cop Operon und die Kupfer Homeostasis in Enterococcus Hirae. Überexpression, Reinigung und Kristallisation der Kupfer-Repressoren CopY und CopR", AG Saenger, Freie Universität Berlin

2005   Chemie Diplom, Universitat Autònoma de Barcelona, Barcelona, Spanien

1999   Abitur, Gymnasium Escola La Farga, Sant Cugat del Vallès, Spanien

Publikationen

Regulation and structure of YahD, a copper-inducible alpha/beta serine hydrolase of Lactococcus lactis IL1403.
Martinez J, Mancini S,Tauberger E, Weise C, Saenger W, Solioz M
(2011)*FEMS microbiology letters **314**(1): 57-66.*
PMID: 21059179

Crystal structures of *N*-acetylmannosamine kinase provide insights into enzyme activity and inhibition.
Martinez J, Nguyen L, Hinderlich S, Zimmer R, Tauberger E, Reutter W, Saenger W, Fan H, Moniot S (Submitted)

HemW is a novel heme chaperone required for cytochrome *bd* maturation.
Abicht H, Martinez J, Layer G, Jahn D, Solioz M (Submitted)

Präsentationen

2011   Poster Präsentation beim IUCR meeting in Madrid
2010   Poster Präsentation beim 2e HZB-Joint User's Meeting in Berlin
2010   Poster Präsentation beim SFB 449 International Meeting in Berlin
2009   Poster Präsentation beim 1e HZB-Joint User's Meeting in Berlin